AD-A098 673   HUGHES RESEARCH LABS MALIBU CA   F/G 20/5
                OPTICAL-MICROWAVE INTERACTIONS IN SEMICONDUCTOR DEVICES.(U)
   MAR 81 L FIGUEROA, C W SLAYMAN, H W YEN   N00173-78-C-0192
UNCLASSIFIED   NL

A867

LEVEL $\overline{I\mathcal{U}}$ $\mathcal{C}$ $\mathcal{P}\mathcal{U}$
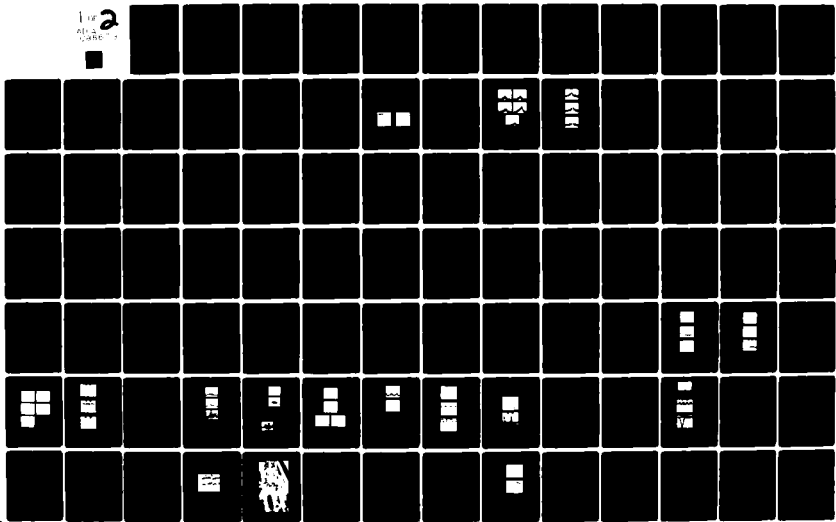
ARPA 690

OPTICAL–MICROWAVE INTERACTIONS IN SEMICONDUCTOR DEVICES

L. Figueroa , C.W. Slayman and H.W. Yen

Hughes Research Laboratories
3011 Malibu Canyon Road
Malibu, CA 90265

March 1981

DTIC
ELECTE
MAY 8 1981
C

Approved for public release; distribution unlimited.

AD A098673

DTIC FILE COPY

X

81 5 04 169

UNCLASSIFIED

SECURITY CLASSIFICATION OF THIS PAGE (When Data Entered)

REPORT DOCUMENTATION PAGE		READ INSTRUCTIONS BEFORE COMPLETING FORM
1. REPORT NUMBER	2. GOVT ACCESSION NO.	3. RECIPIENT'S CATALOG NUMBER
4. TITLE (and Subtitle) OPTICAL-MICROWAVE INTERACTIONS IN SEMICONDUCTOR DEVICES		5. TYPE OF REPORT & PERIOD COVERED Final Report 30 June 1978— 31 Dec 1980
		6. PERFORMING ORG. REPORT NUMBER
7. AUTHOR(s) L. Figueroa, C.W. Slayman, H.W. Yen		8. CONTRACT OR GRANT NUMBER(s) N00173-78-C-0192
9. PERFORMING ORGANIZATION NAME AND ADDRESS Hughes Research Laboratories 3011 Malibu Canyon Road Malibu, California 90265		10. PROGRAM ELEMENT, PROJECT, TASK AREA & WORK UNIT NUMBERS
11. CONTROLLING OFFICE NAME AND ADDRESS Defense Advanced Research Project Agency Arlington, Virginia 22209		12. REPORT DATE March 1981
		13. NUMBER OF PAGES
14. MONITORING AGENCY NAME & ADDRESS(if different from Controlling Office) Naval Research Laboratory Washington, D.C. 20375		15. SECURITY CLASS. (of this report)
		15a. DECLASSIFICATION DOWNGRADING SCHEDULE

16. DISTRIBUTION STATEMENT (of this Report)

Approved for public release; distribution unlimited.

17. DISTRIBUTION STATEMENT (of the abstract entered in Block 20, if different from Report)

18. SUPPLEMENTARY NOTES

19. KEY WORDS (Continue on reverse side if necessary and identify by block number)

AR coating analog modulation, detector optical response, optical cavity, Gunn Diode, IMPATT Diodes, Interdigital Photoconductor, MESFET modelocking, optical cavity, p-n junction, self-pulations, time multiplexing, traps.

20. ABSTRACT (Continue on reverse side if necessary and identify by block number)

The results of an extensive characterization of microwave-optical devices is presented. The study has concentrated in the optical injection locking of IMPATT oscillators, high-speed analog modulation of (GaAl)As injection laser, mode-locking of (GaAl)As injection laser, and high-speed optical detectors.

DD FORM 1473 EDITION OF 1 NOV 65 IS OBSOLETE

UNCLASSIFIED
SECURITY CLASSIFICATION OF THIS PAGE (When Data Entered)

Commerical X-band IMPATT oscillators were injection-locked using a modulated (GaAl)As laser beam. Locking bandwidths greater than 10 MHz were obtained. Theoretical calculations indicate a locking bandwidth of 100 MHz when light is efficiently coupled into the active region of the IMPATT. Optical injection locking can also be used to reduce side band noise. A 13 dB reduction in sideband noise was observed. Extension into millimeter wave frequencies appears theoretically possible. However, new IMPATT structures with optical waveguides and optical sources that can be modulated beyond 10 GHz must be developed.

Commercial (GaAl)As injection lasers have been efficiently modulated up to 5 GHz. The 5 GHz value represents a practical upper limit to the modulation bandwidth of existing commercial lasers. The frequency response is limited by laser geometry, self-pulsations, and junction parasitics.

A theoretical and experimental study of mode-locking in (GaAl)As injection lasers was performed. Our results indicate that the mode-locking of (GaAl)As injection lasers is related to either saturable absorbing or electron-trap defects within the active region of the laser. These defects are also responsible for self-pulsations in injection lasers. "Good" mode locking is achieved only in lasers having a high density of these defects. We have achieved detector-limited mode-locked pulses (less 60 psec full width at half-maximum) with repetition rates from 400 MHz to 1.5 GHz and 100% modulation depth. We have also been able to time multiplex the mode-locked pulses to double the pulse repetion rate. A mode-locked laser unit with multiplexer and dc power supply has been delivered to the Naval Research Laboratory in Washington, D.C.

High-speed optical detectors were characterized, and we found that some commercial p-n junction can respond to optical pulses with 50 psec half-width. However, the sensitivity and difficult laser alignemnt are severe handicaps. We characterized the optical response of GaAs MESFETs and found that they can respond to 80 to 100 psec half-width optical pulses and analog-modulated optical signals at frequencies beyond 4 GHz.

Waveguide heterostructure MESFET and Gunn diodes were fabricated and characterized. The rf optical response of the MESFET showed a bandwidth greater than 4 GHz. However, the sensitivity was 10 to 20 dB lower than existing p-n junction detectors. Significant improvements in the waveguide detectors could be made by optimizing the geometry and using a P-I-N or APD detector. Such detectors will have the ultimate high-speed response.

A novel interdigital photoconductive detector was developed and characterized. The detector had an optical pulse response of 50 to 60 psec and sensitivity comparable or better than the best commercial high-speed detectors.

PREFACE

The following personnel contributed to the research reported here:
L. Figueroa, C.W. Slayman, H.W. Yen, C. Krumm, J.H. Myer, C. Mohr R.K. Kain,
D. Pierson, and D.F. Lewis.

TABLE OF CONTENTS

LIST OF ILLUSTRATIONS

5

LIST OF ILLUSTRATIONS

7

SECTION 1

INTRODUCTION AND SUMMARY

In this program, "Optical Microwave Interactions in Semiconductor Devices," one of our primary goals is the use of microwave-modulated optical signals to control microwave semiconductor devices, so that various functions such as injection locking and switching of oscillators, mixing, and detection of microwave-modulated optical signals can be achieved. A second goal is to combine microwave and optical devices for use in microwave signal processing systems. To perform such functions, we must develop methods and devices that can provide modulation and detection of optical beams at microwave frequencies.

During the past 18 months, our efforts were concentrated in the following areas: optical injection locking of IMPATT oscillators, direct current modulation and characterization of (GaAl)As injection lasers at gigahertz frequencies, mode-locking of (GaAl)As injection lasers, and fabrication and characterization of high-speed optical detectors.

Optical injection locking of IMPATT oscillators was investigated both theoretically and experimentally. The injection-locking characteristics of X-band Si IMPATT oscillators was investigated by measuring the locking range as a function of locking gain. Subharmonic locking was used with a frequency ratio ranging from 3:1 to 8:1. A locking range of several megahertz was achieved with an oscillator of 8.11 GHz. Even subharmonic locking was preferable to odd harmonic locking for our oscillators. A reduction of the IMPATT oscillator sideband noise was observed when using optical locking. Sideband noise reduction of $\sim$13 dB was obtained.

The feasibility of achieving optical injection locking of millimeter-wave IMPATT oscillators was investigated by calculating the efficiency of subharmonic optical locking of IMPATT oscillators. The calculations were carried out by adding a time-varying reverse saturation current term, which was generated by the incident optical signal, to the IMPATT avalanche equation. Solving the equation yielded a diode external current component related to the injection signal. This current was then taken as the injection source in the oscillator equivalent circuit to calculate

9

the locking range. The results indicated that the locking range is proportional to the optically generated current and is inversely proportional to the circuit Q and the dc bias current. These conclusions are in agreement with the experimental observations. A locking range on the order of 100 MHz could be achieved in X-band IMPATT oscillators if modulated optical signal was converted into rf photocurrent efficiently. Our results show no inherent physical limitation on the optical-injection locking at millimeter-wave frequencies. However, novel IMPATT structures, such as those incorporating an optical waveguide, will have to be fabricated and characterized. In addition, efficient modulation of semiconductor laser sources at frequencies in excess of 10 GHz will be required.

To modulate the optical beam at gigahertz rates, we studied the modulation capability of (GaAl)As injection lasers. The simplest technique involves the direct modulation of the laser current. An understanding of the capabilities and limitations of existing laser structures is an essential prerequisite to progress toward improving their ultimate performance. Our results indicate that efficient modulation of commercial (GaAl)As injection lasers is limited by the relaxation oscillation frequency of the laser, laser junction parasitics, and self-pulsations. These constraints set a practical upper limit of $\sim$5 GHz. We have observed a wide variation in the amplitude and frequency of the relaxation oscillation resonance. The wide variation results from the different laser geometries and the tendency of some lasers to self-pulse at high drive currents. An experimental determination of the laser equivalent circuit at frequencies from 0.1 to 6 GHz was performed. Our results indicate that the product of laser shunt resistance, R_d, and shunt capacitance, C_d is $\sim 10^{-10}$ sec, and plays a significant role in the laser frequency response at gigahertz rates.

One of our main conclusions is that the frequency response of the laser can be significantly increased by reducing the diode cavity length. A frequency response greater than 10 GHz is predicted by reducing the cavity length to 75 μm.

Mode locking of (GaAl)As injection lasers was studied both theoretically and experimentally. Mode locking is a technique that pulse modulates the light output and can produce an output with large peak powers and very rich

harmonic content, making it directly applicable to the phase-locking of microwave semiconductor devices. We found, as originally speculated, that mode locking in various commerical (GaAl)As injection lasers is strongly influenced by the type of laser structure used. In particular, we found that lasers having a high density of saturable absorbing defects are most susceptible to mode locking. One of our key findings is the direct correlation between the phenomenon of self-pulsation and "good" mode locking. Our results imply that mode locking in (GaAl)As injection lasers is very similar to mode locking in dye lasers. Our most recent results have produced pulses with 60 psec pulse width (detector limited) operating at frequencies greater than 1 GHz. The peak power was greater than 20 mW. The pulse train obtained is relatively free of frequency jitter, and thus has enabled us to time multiplex the light output and obtain 2 GHz repetition rates. We have delivered as part of this program a workable mode-locked laser unit, multiplexer, and dc power supply to the Naval Research Laboratory in Washington, D.C.

Our theoretical calculations predict the dependence of pulse amplitude on dc injection level and external cavity length. We find a resonant behavior for the amplitude. Furthermore, our calculations indicate that the pulse amplitude will be a strong function of the saturable absorbing center density, the geometry of the laser, and the absorption losses. We find that the pulse width is inversely related to the saturable absorbing density and directly related to the absorption losses in the cavity. A reduction of the laser volume leads to an increase in the pulsewidth. The optimum frequency of the mode-locked pulses can be controlled by varying the spontaneous and cavity lifetimes. Higher frequencies are obtained by reducing these parameters.

Of primary concern to this program and to future microwave signal processing systems, such as optical-fiber delay lines, is a high-speed optical detector. Although, not all the work related to high speed detetectors was funded by the present contract, we have included it for completeness.

Commerically available high-speed detectors were characterized. This characterization is an important step in redesigning detectors for improved high-frequency performance. We find that no commercial

detector can respond to pulses less than 50 psec. Furthermore, the relatively low sensitivity and difficulty in aligning such detectors are distinct disadvantages in fiber optics systems.

We performed theoretical calculations and experimental measurements on the high frequency optical characteristics of GaAs MESFETs. The results obtained using HAC MESFETs provided the first extensive characterization of this type of detector. We have characterized both the pulse and analog responses of the devices using analog modulation of (GaAl)As injection lasers, mode-locked (GaAl)As injection laser ($\lambda = 0.83\,\mu m$) and a mode-locked dye laser ($\lambda = 0.57\,\mu m$). We have observed a flat analog response for frequencies up to, and probably beyond, 4 GHz. The pulse response shows that it is possible to detect optical pulses with a 80 to 100 psec half-width using one-half micron gate MESFET's. The observed results were interpreted using a theoretical model which assumes a photoconductive mode of operation in conjunction with a voltage-dependent carrier recombination-time. Calculations and experimental results were in qualitative agreement.

A novel heterostructure MESFET was monolithically integrated with an optical waveguide. The device pinch-off voltage was typically less than 3V. The analog response of the device was greater than 4 GHz. However, a poor waveguide coupling efficiency, combined with an unoptimized FET geometry, led to relatively poor sensitivities. Typical sensitivities were 10 to 20 dB below state-of-the-art detectors. By using a detector with a uniform electric field (APD or PIN) and integrating it with an optical waveguide, the ultimate high-speed detector could be obtained.

Novel heterostructure Gunn diodes were fabricated and characterized. We fabricated Gunn diodes ranging in length from 30 to 120 μm in 30 μm steps. Typical current drop-back efficiencies ranged from 20 to 30%. We obtained oscillation at frequencies as high as 9 GHz by using an appropriate strip-line circuit. These diodes have potential importance in electro-absorption modulators. However, because of their poor thermal stability, we could not make any measurements related to their optical-microwave characteristics.

12

Lastly, we have developed and characterized using internal IR&D funding
a novel interdigital photoconducting detector with 50 to 60 psec rise and
fall time and a high-speed sensitivity $\sim$0.1 - 0.8 mA/mW. The simplicity and
performance characteristics of the device make it a potentially important
element in future opto-electronic devices. This work is being included for
completeness.

For completeness we have included a copy of the final report of
July 1978 in the Appendix. This report describes the earlier work on
optical-microwave interactions in semiconductor devices and gives some
of the motivation behind the present work.

SECTION 2

INJECTION LOCKING OF IMPATT OSCILLATORS

One of the primary objectives of this program has been to study the physics of microwave and millimeter-wave semiconductor devices under optical illumination. Such studies are important to assess the potential applications of microwave-optical devices in microwave signal processing systems such as phased-array radars. In this section we present our results relating to the injection locking of X-band silicon IMPATT oscillators and theoretical calculations which give insight on the ultimate limits of optical injection locking.

A. INJECTION LOCKING OF X-BAND SILICON IMPATT OSCILLATORS

Optical injection locking of oscillators is, in principle, identical to electrical injection locking.[1] The only difference is in the way the locking signal is introduced into the oscillator circuit. In the optical approach, the key is to obtain efficient laser modulation and efficient optical coupling into the active element of the oscillator. The feasibility of optical injection locking was first demonstrated using silicon bi-polar transistor oscillators[2]; this technique was subsequently extended to include other microwave devices such as GaAs FET oscillators[3] and silicon IMPATT oscillators.[4-6]

As with electrical injection locking, optical injection locking can take place at the fundamental frequency and at various subharmonics. In this section we describe the results of our experimental study on optical injection of Silicon IMPATT oscillators.

Figure 1 shows the experimental setup used to study the optical injection locking of IMPATT oscillators. The IMPATT diodes used were packaged commercial devices from Hewlett-Packard (HP5082-0435). The operation frequency was 8 to 12 GHz with an operating voltage of $\sim$90 V and operating current of $\sim$30 mA. The diodes were mounted in a microwave package and hermetically sealed in a ceramic sleeve with metallic contacts on each end. To expose

15

the diode chip for illumination, we cut a small groove in the ceramic sleeve using a wire saw. The diode package was then mounted in an X-band microwave cavity with a waveguide tuning short on one side and an output coupling probe on the other. A small hole was drilled in the side of the cavity to permit the output of the modulated injection laser to be coupled to the IMPATT chip via a piece of optical fiber or by direct beam focusing. The optical coupling efficiency to the IMPATT was inhibited because of a protective coating that surrounds the chip to prevent edge leakage and breakdown. For example, with 3mW of optical power at 0.83 µm from a (GaAl)As laser (Hitachi HLP-1400) focused onto the IMPATT diode, a photocurrent of only 40 µA was generated (see Figure 2). A typical microwave modulation depth of the laser output was estimated to be about 30%.

It has been shown that the most significant contribution of optical illumination in an IMPATT diode is the drastic increase in its reverse saturation current I_s.[7] Under normal operating conditions, I_s results from thermally generated carriers and is negligible compared with the avalanche current. However, with sufficient optical illumination, I_s must be included in the dynamic equations that govern the operation of the device (discussed in Section 2-B). As a result, the output microwave frequency and power of an IMPATT oscillator will vary with the illuminating optical intensity. If the incident optical signal is modulated at a frequency close to that of the IMPATT oscillator, phase locking can occur.

One of the methods of examining the injection locking process is to display the frequency content of the oscillator output on a spectrum analyzer. From the evolution of the frequency content one can determine whether the oscillator is synchronized with the injection source. Another method is to use a microwave network analyzer. With this instrument one can display the relative phase and magnitude between the locked oscillator output and the injection signal. Since the injection signal frequency is being swept constantly, depending on the signal power level, there will be a certain frequency range called the locking band around the oscillator free-running

16

5733-1
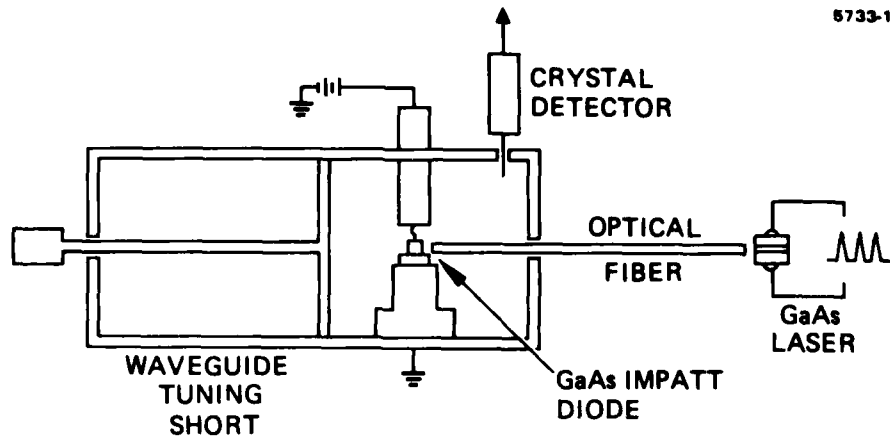
Figure 1. Experimental setup for optical phase-locking of
IMPATT oscillators.

5733-2
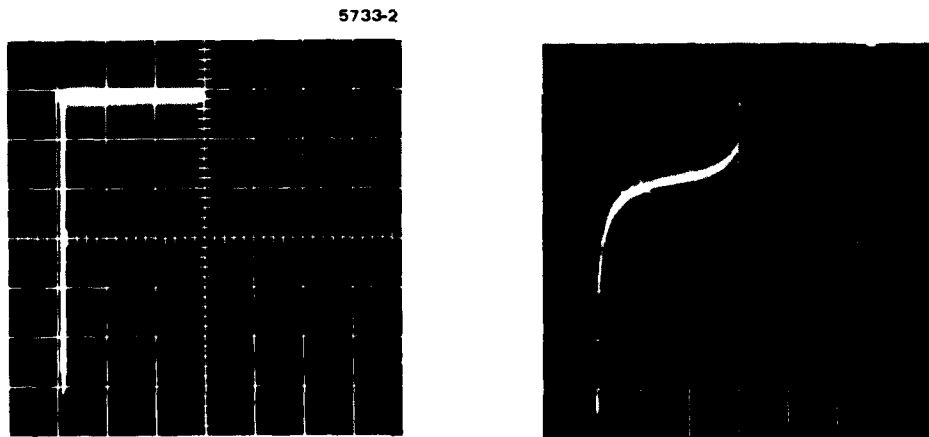
(a) Without laser light   (b) With laser light
     illumination.   illumination.

Figure 2. IMPATT diode I-V characteristics. (Horizontal scale
10 V/div., vertical scale 50 µA/div.)

17

frequency so that injection locking occurs. Within the locking band, the oscillator output frequency tracks that of the injection signal and the oscillator output power remains relatively constant. We have used both techniques in the experiments to obtain locking-gain and locking-band information.

The injection locking characteristics of IMPATT oscillators were found to depend heavily on the cavity tuning conditions. If the cavity was tuned so that the IMPATT oscillated with a high Q factor (i.e., narrow spectral width, minimum sideband noise), the locking range typically was very small (a few hundred kilohertz). However, if the cavity was tuned such that a low-Q situation existed then the locking process became very efficient. This observation agrees well with theoretical calculations (discussed in Section 2-B). Another factor that affected the injection locking process was the dc bias of the IMPATT diode. Depending on the bias condition of the diode, one could observe different amounts of IMPATT oscillator frequency shift for a fixed dc optical illumination. Under certain conditions, the frequency shift was positive, and for a different combination of circuit tuning and dc bias, the frequency shift could be negative as well. In general, a large locking band was obtained if the oscillator frequency shift caused by optical illumination was large, and vice versa.

One of the IMPATT oscillators when biased at 28 mA and tuned to 8.116 GHz could be optically injection locked to several different orders of subharmonics. Figure 3 shows the oscillator spectrum at five different injection signal power levels. From 3(a) to 3(d) the injection signal level was raised from -20 to +10 dBm in 10-dBm steps. As shown in Figure 3(a) the oscillator output was initially at 8.111 GHz, while the injection signal was about one-sixth of 8.1146 GHz, (or 1.3524 GHz). However, as shown in Figure 3(e), when injection locking finally took place, the oscillator frequency was pulled in and locked to the sixth harmonic of the injected signal frequency.

During the experiments we found that reduction of IMPATT oscillator sideband noise can be achieved through optical illumination. In Figure 4 we display the spectrum of an IMPATT oscillator under three different situations: Figure 4(a) is the free-running oscillator output at 8.113 GHz. Figure 4(b)

18

8241-4
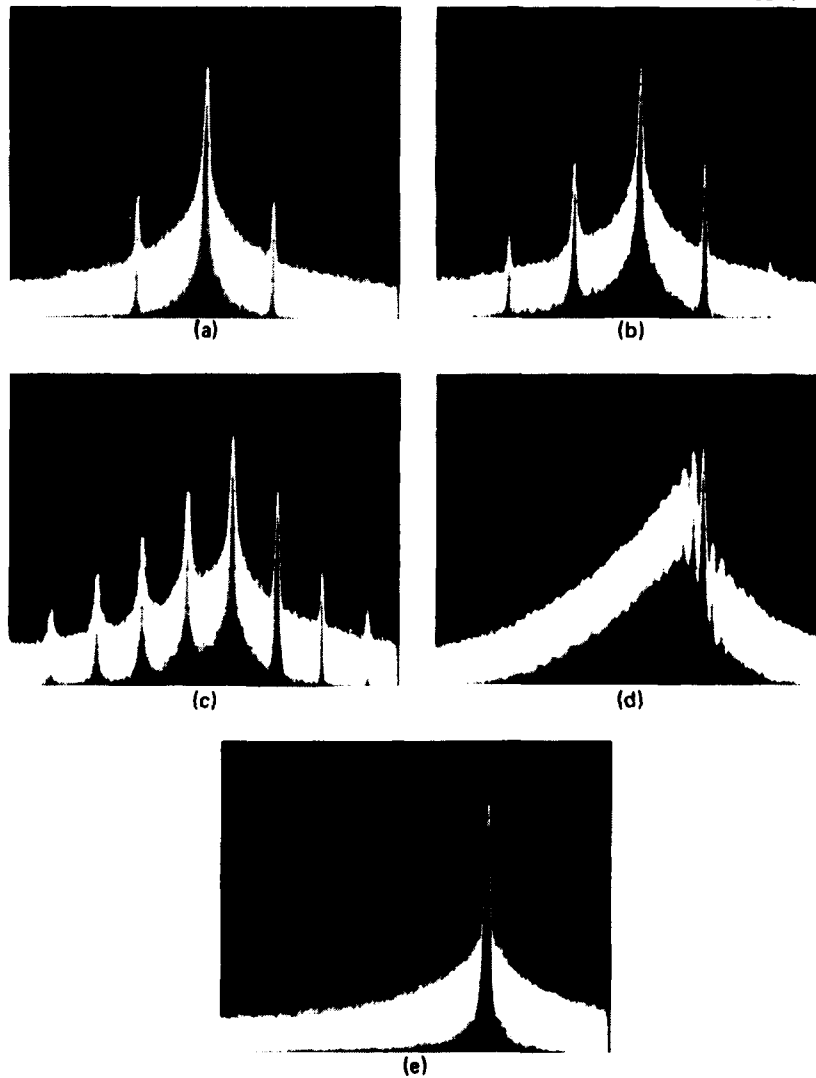
Figure 3. Spectra of an injection-locked IMPATT oscil-
lator at various injection signal levels.
IMPATT oscillation frequency: 8.111 GHz
Injection signal frequency: 1.352 GHz
Horizontal scale: 2 MHz/div
Vertical scale: 10 dB/div
Reference level: 30 dBm.

19
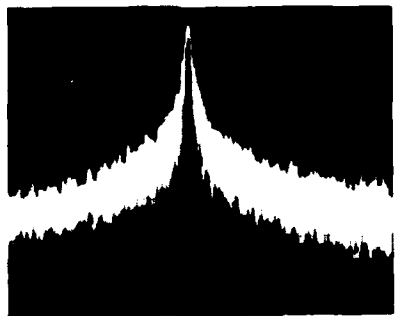
FREE RUNNING
(a)
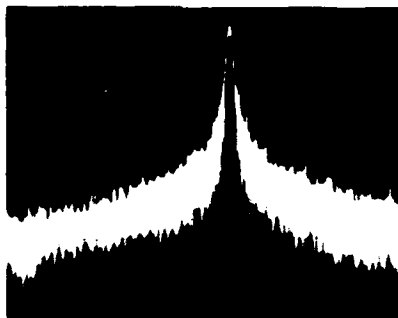
ILLUMINATED
(b)
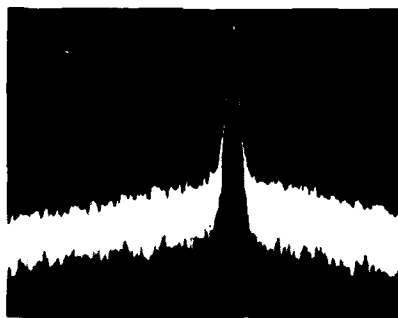
OPTICALLY
INJECTION LOCKED
(c)

(f = 8.11 GHz, VERTICAL: 10 dB/div, HORIZONTAL: 100 KHz/div)

Figure 4.   IMPATT oscillator output spectrum under three
             different conditions.

is the spectrum of the same oscillator under optical illumination with constant
intensity. There is an upward frequency shift of about 80 kHz and a sub-
stantial sideband noise reduction (about 8 dB) around the oscillation frequency.
Figure 4(c) is the output spectrum of the oscillator phase locked to a source
at 2.704 GHz through third-harmonic optical injection locking. There is a
further reduction of sideband noise by 5 dB. Thus an overall sideband noise
improvement of 13 dB is accomplished by the optical injection locking process
in IMPATT oscillators. The additional noise reduction resulting from dc
illumination can be attributed to the result of fine optical tuning of the
oscillator as well as the clamping of the background carrier level in the
IMPATT diode.

Figure 5 is a locking band versus locking gain plot of an IMPATT
oscillator for several different subharmonic orders. The IMPATT oscillation
frequency was at 8.116 GHz. It is seen that a frequency ratio as high as
8:1 was used (i.e., the injection signal was running at 1.014 GHz) to achieve
injection locking. The locking gain was defined as the ratio of the IMPATT
oscillator output power and the microwave power used to modulate the injection
laser. Therefore, the locking-band-locking-gain plot actually contains
modulation-response information for the injection laser as well. For instance,
the modulation depth of the laser at 2.03 GHz (4:1 frequency ratio) was
not as large as that at 1.35 GHz (6:1 frequency ratio); therefore, the
injection locking efficiency of 6:1 subharmonic became better than that of
4:1 subharmonic when the locking gain was greater than 8 dB. It is also
interesting to note that in this oscillator the even order of subharmonics
are preferred over the odd order of subharmonics as far as the injection
locking efficiency is concerned. We believe this is a result of the particular
cavity tuning. Further studies are needed to clarify this point.

B. CALCULATIONS AND DISCUSSIONS ON OPTICAL INJECTION LOCKING OF IMPATT
OSCILLATORS

In a previous quarterly report[8] we described the process of optical
injection locking. In this subsection we summarize those results and make
projections on the ultimate limits of this technology.
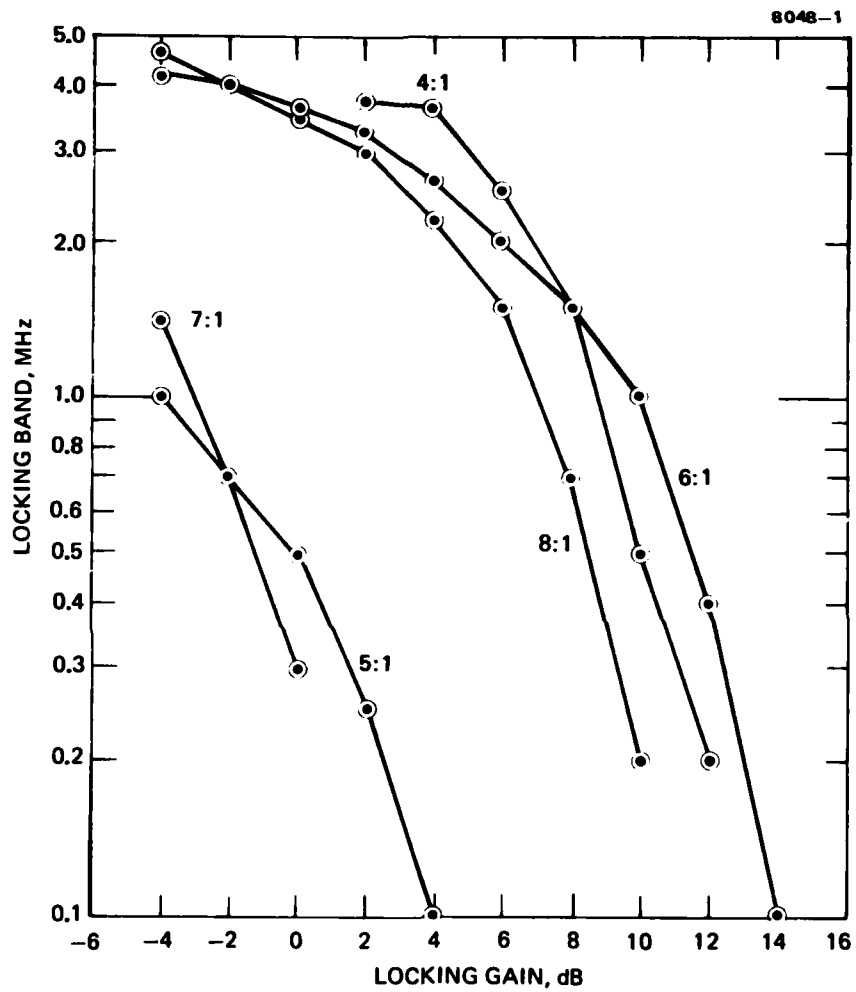
Figure 5. Locking band versus locking gain of a subharmonically optically injection-locked IMPATT oscillator.

The equation that describes the avalanche current density, J, of an IMPATT diode is given by[9]

$$\frac{\tau_a}{2} \frac{dJ}{dt} = J \left[\int_0^{\ell_a} \alpha \ dx - 1 \right] + J_s \ ,$$ (1)

where

$\tau_a = \ell_a/v$ is the avalanche zone transit time

ℓ_a is the avalanche zone length

α is the impact ionization coefficient

J_s is the reverse saturation current density

v is the saturated carrier velocity.

The ionization coefficient α is a function of the electric field in the avalanche region and can be approximated by the following expression:

$$\alpha = \alpha_o \left(\frac{E}{E_o} \right)^m \quad \left(m \approx 6 \text{ for Si} \right) \quad .$$ (2)

Assuming that the electric field distribution inside the IMPATT diode is as shown in Figure 6, where the field varies from its peak E_p, down to the drift region valve, E_d, with dE/dx constant, then, it follows that

$$\int_0^{\ell_a} \alpha \ dx \cong \left(\frac{E_p}{E_{p_o}} \right)^{m+1} \ ,$$ (3)

where E_{p_o} is the peak field at breakdown under dc conditions

(i.e. when $\int_0^{\ell_a} \alpha \, dx = 1$).

23
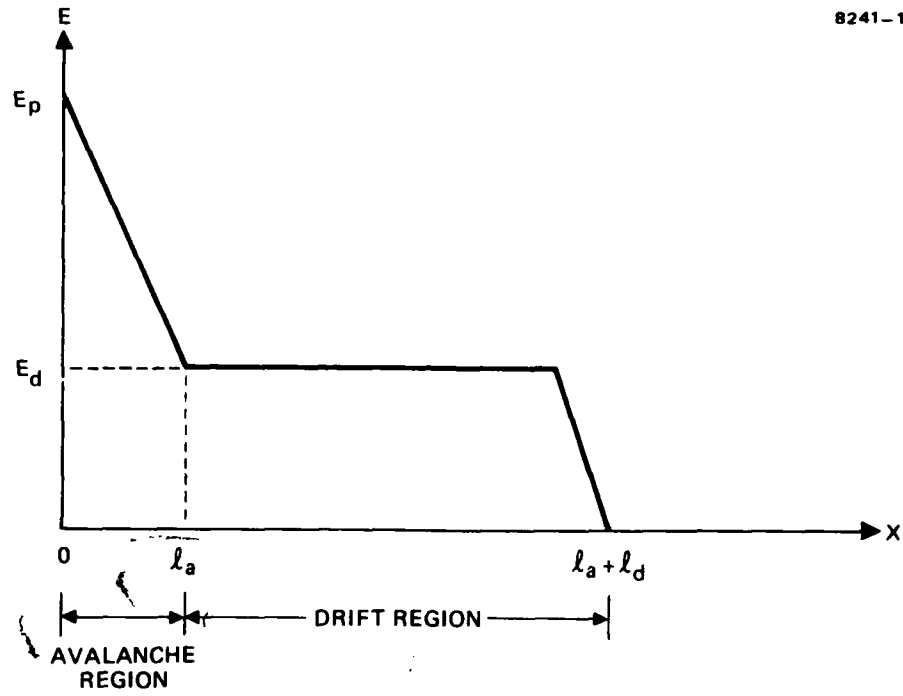
Figure 6.   Electric field distribution inside an IMPATT diode.

The peak electric field, E_p, can be written as

$$E_p(t) = E_{p_0} - E_b + E_a \sin \omega t - \frac{1}{\epsilon \tau_d} \int_{t-\tau_d}^{t} (\tau_d - t + t') J(t') dt' \quad , \qquad (4)$$

where E_b is a constant, $E_a \sin \omega t$ is the field from the applied rf voltage, τ_d is the drift zone transit time, and

$$- \frac{1}{\epsilon \tau_d} \int_{t-\tau_d}^{t} (\tau_d - t + t') J(t') dt'$$

is a field resulting from the so-called space-charge effect. As an approximation, the effects of E_b and the space-charge field can be treated by assuming that the carrier generation rate is sinusoidal but has a zero at $\pi - \delta$ instead of π.[10] Therefore, Eq. (4) becomes

$$E(t) = E_{p_0} + E_a \sin(\omega t + \delta) \quad , \qquad (5)$$

and Eq. (1) can be reduced to

$$\frac{dJ}{dt} = \frac{2(m+1)}{\tau_a} J \frac{E_a}{E_{p_0}} \sin(\omega t + \delta) + \frac{2}{\tau_a} J_s \quad , \qquad (6)$$

where only the first term of the expansion $\left(E_p / E_{p_0} \right)^{m+1} - 1$ was kept.

With these preliminary calculations we can begin to study the effects of subharmonic locking. We first consider the case of fundamental injection

25

locking. Our previous calculations[2] have shown that the dominant effect of optical illumination is to increase the reverse saturation current. Thus we assume that the IMPATT diode is illuminated by an optical signal modulated at frequency ω; then J_s can be written as

$$J_s = J_{s_0} + J_{s_1} \sin(\omega t + \delta + \phi) \quad . \tag{7}$$

Our goal is to find the value of the current density J. Since the mathematics is straighforward, but tedious, we will just quote the final result. The interested reader is referred to Ref. 8.

We find that the fundamental component of the current density J, which we denote as $J_{(1)}$, can be written as

$$J_{(1)} = -2J_{dc} \frac{I_1(x)}{I_0(x)} \cos(\omega t + \delta_2) + 2J_{s_1} K(x) \cos(\omega t + \delta + \phi) \quad , \tag{8}$$

where

$$J_{dc} = J_0 I_0(x) \text{ is the dc current of the IMPATT Diode.}$$

$I_0, I_1 I_2 \doteq$ modified Bessel functions of order 0, 1, and 2.

$$\delta_s \simeq \sin^{-1}\left\{ \left(\frac{J_{s_0}}{J_{dc}} \frac{I_0 \left[2 I_0(x) - 3 I_2(x) \right]}{\omega \tau_a} \right) + \delta \right\}$$

$$K(x) = \frac{4I_2^2(x) + 3I_1^2(x) - 6I_0^2(x)}{6\omega \tau_a} \quad .$$

Physically, we believe the injection-locking process results from the modification of the electric field distribution by the optically generated carriers within the avalanche region.   It is clear from Eq. (2) that the ionization coefficient, and thus the IMPATT current density, are a strong nonlinear function of the electric field strength. This strong nonlinearity can lead to subharmonic injection locking.

The locking bandwidth can be obtained by using the IMPATT diode in the resonant circuit shown in Figure 7. We find that the maximum locking band-width is given by

$$(2\Delta\omega)_{max} = \left[\frac{-K(x)I_0(x)}{I_1(x)}\right] \frac{\omega\, I_{s_1}}{Q\, I_{dc}} \; , \qquad \text{(a).} \qquad (9)$$

where Q is the quality factor of the resonant circuit and is given by

$$Q = \left(\frac{\omega\, C_d}{G_1}\right)^{-1} = (\omega\, C_d\, R)^{-1} \quad . \qquad \text{(b).}$$

Thus Eq. (9) shows that the locking range is proportional to the optically generated rf current I_{s_1}, and is inversely proportional to the circuit Q and the bias dc current. These predictions are in qualitative agreement with the results described in Section 2-A. It is worthwhile to consider a simple numerical example in order to get a feeling of what the maximum locking bandwidth can be. We consider the following example:

I_{dc} = 25 mA, ℓ_a = 1 μm, ℓ_d = 4 μm, $E_{P_o} \sim 2 \times 10^7$ V/m, v = 1 x 10^5 m/sec,

A = $10^{-8}/m^2$, V_1 = 10V (the magnitude of the rf voltage) I_{s_1} = 20 μA,

Q = 20, m = 6, and f = 10 GHz.

These numbers correspond approximately to the experimental conditions described in Section 2-A. Using Eq. (9) we find $(2\Delta f)_{max} \sim 4.0$ MHz. If we take V_1 = 15 V rather than 10 V then $(2\Delta f)_{max} \sim 14.7$ MHz.

8241-2

IMPATT
Y_I

LOAD
Y_L
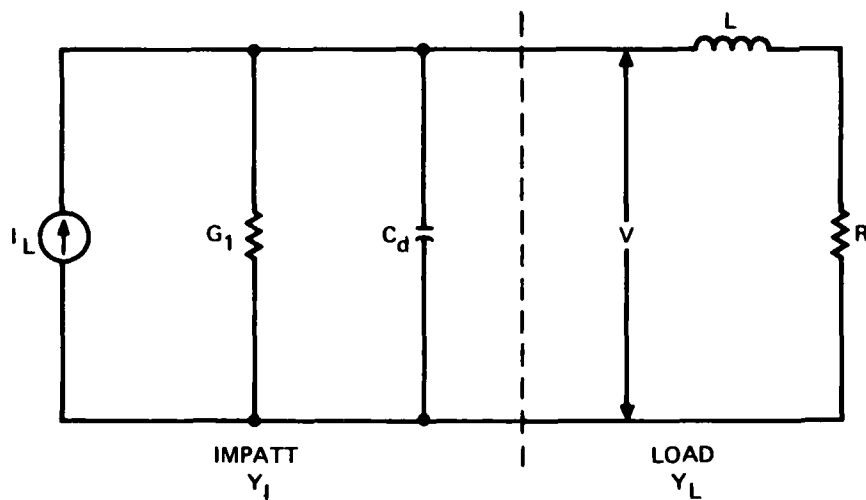
Figure 7. Equivalent circuit of an IMPATT oscillator used for injection locking calculations.

The previous analysis can be carried to the more interesting case of subharmonic optic injection locking. However, we shall note that the analysis becomes increasingly tedious for higher order injection locking. The reader is referred to reference 8 for further details.

C.   CONCLUSIONS

The conclusions derived from the previous calculations, ref. 8, and experimental results, are the importance of maximizing the following parameters:

$$x = \frac{2(m+1)E_a}{\omega \tau_a E_{p_o}}$$

$$y = \frac{2(m+1)\ n\ J_{1/n\ o}\ \tau d}{\omega \tau_a\ E_{p_o}\ 2\epsilon}$$

$$E_a = V_{1/\ell}$$

where E_a is the rf electric field in the diode and $J_{1/n\ o}$ is the component of the current density corresponding to the nth subharmonic. Therefore, in a short diode, E_a is larger for a given V_1. On the other hand, the optimum oscillation frequency (ω) of a shorter diode is higher. Thus, the optimal situation seems to be to operate the diode in the lower portion of its frequency band. Our limited experimental results seem to indicate that this is the case. The best way to increase y is to have a large optically generated current. A simple calculation reveals that 1 mW of optical power at rf frequency can generate up to 660 μA of rf photocurrent under ideal conditions. This would mean a locking range of 250 MHz for the case $\omega_{osc} : \omega_{inj} = 3:1$. Therefore, it is important to investigate means of generating efficient, high frequency modulated optical sources. In sections 3 and 4 we describe our efforts in this area.

Our preliminary experiments (described in Section 2-A) on subharmonic optical injection locking of X-band Si IMPATT oscillators have shown a locking range of close to 7 MHz with a 4 to 1 frequency ratio. The amplitude of the rf photocurrent in these experiments is estimated to be only 5 μA. However, the actual numerical parameters of the diodes used are not available to permit an accurate comparison with analytical results.

Our analysis involved several approximations, and the result is accurate only for moderate rf voltage swings and photocurrents. Also, the effect of circuit tuning is completely neglected. We believe that in a real oscillator the interaction of the device and the circuit can play a major role in determining the injection locking efficiency.

It is interesting to note that injection locking with an input signal proportional to sin 2/3 ωt is also possible. Similarly, any multiples of the subharmonics are also possible injection-locking signals.

In concluding this section, we have shown that subharmonic optical injection locking of Si IMPATT oscillators can have a locking range of ∿100 MHz if modulated optical signals can be efficiently converted into rf photocurrent. In view of the experimental results obtained so far (more than 5 MHz locking range with less than 5 μA of rf optical current), we feel that the calculated results underestimate the locking range, although the experimental device parameters are not known well enough to permit careful comparison. We believe that there are no fundamental reasons this scheme will not work at millimeter-wave frequencies.[8] However, there are several problems to be overcome. First, a suitable modulation scheme for the optical source must be found. Alternative approaches are 1) direct modulation of injection lasers using a suitably modified laser structure, 2) mode-locking of injection lasers, and 3) the use of an external travelling-wave modulator. Second, high-frequency IMPATTs have a very small transit time and a correspondingly small active region thickness. Thus a significant portion of the absorbed light will not interact with the electric field region. Thus, we believe that millimeter wave IMPATT will have to incorporate some form of waveguide structure. Our attempts in the fabrication of waveguide structures utilizing active devices will be discussed in Section 5.

SECTION 3

ANALOG MODULATION OF (GaAl)As INJECTION LASERS

This section describes the important parameters affecting the direct-current
modulation of (GaAl)As injection lasers at gigahertz rates. Extensive
experimental results on the high-frequency characteristics of commercial
(GaAl)As injection lasers is presented.

A. DIRECT-CURRENT MODULATION OF (GaAl)As INJECTION LASERS AT GIGAHERTZ
   RATES

The easiest way to modulate an injection laser is to modulate the laser
current directly. The frequency response of the laser can be analyzed using
a pair of simple rate equations for a single longitudinal mode[11]:

$$\frac{dn}{dt} = \frac{J}{ed} - Gns - \frac{n}{\tau_s} \tag{11a}$$

$$\frac{ds}{dt} = Gns - \frac{s}{\tau_p} + \frac{\beta n}{\tau_s} \quad , \tag{11b}$$

where n is the electron inversion density, s is the photon density, J is the
laser driving current, e is the electronic charge, d is the thickness of the
laser active region, G is a constant related to the stimulated emission
process, τ_s is the spontaneous lifetime of the electrons, τ_p is the photon
lifetime in the laser cavity, and β is the spontaneous emission factor. This
last factor gives us the percentage of the total spontaneous emission that
goes into the lasing mode. The above equations neglect transverse optical
confinement, current spreading, lateral out-diffusion of injected carriers,
and the effects of circuit parasitics. Since this set of equations is non-
linear, exact analytical solutions are difficult to obtain. However, approxi-
mations can be used to calculate the small-signal response of the laser. We

first simplify the equations by using an appropriate normalization procedure which we define as:

$$t \equiv \frac{t}{\tau_s}$$

$$n_e \equiv G\tau_p n$$

$$s_p \equiv G\tau_s s$$

$$j \equiv G\tau_s\tau_p \left(\frac{J}{ed}\right)$$

$$C \equiv \frac{\tau_s}{\tau_p} \quad .$$

Using these definitions, Eq. (11) can be rewritten as

$$\frac{dn_e}{dt} = j - s_p n_e - n_e$$

(12)

$$\frac{ds_p}{dt} = C \left[s_p (n_e - 1) + \beta n_e\right]$$

To calculate the small-signal response, we use a perturbation technique. The relevant quantities are

$$j = j^{(0)} + j^{(1)}$$

$$n_e = n_e^{(0)} + n_e^{(1)} + n_e^{(2)}$$

(13)

$$s_p = s_p^{(0)} + s_p^{(1)} + s_p^{(2)} \quad .$$

32

The steady-state solutions, $n_e^{(0)}$ and $s_p^{(0)}$, are caused by the dc current $j^{(0)}$. If we define a normalized modulation depth $F(\omega)$ as $s_p^{(1)}(\omega)/j^{(1)}(\omega)$, then $F(\omega)$ can be shown to be

$$F(\omega) = \frac{C(s_p^{(0)} + \beta)}{(i\omega\tau_s + s_p^{(0)} + 1)\left[i\omega\tau_s - C(n_e^{(0)} - 1) + C(s_p^{(0)} + \beta)(n_e^{(0)})\right]} \quad . \quad (14)$$

For the simplest case, we assume $\beta = 0$ and Eq. (14) reduces to

$$F(\omega) = \frac{Cs_p^{(0)}}{(Cs_p^{(0)} - \omega\tau_s^2) + i\omega\tau_s(s_p^{(0)} + 1)} \quad . \quad (15)$$

We can define a frequency ω_0 where $F(\omega)$ has a resonance:

$$\omega_0 = \left(\frac{1}{\tau_p\tau_s}\right)^{1/2} (s_p^{(0)})^{1/2} \quad . \quad (16)$$

Since $s_p^{(0)}$ is the normalized dc photon value, we can write

$$s_p^{(0)} = (j_o - 1) \quad . \quad (17)$$

Thus, Eq. (16) reduces to

$$\omega_o = \left(\frac{1}{\tau_s\tau_p}\right)^{1/2} (j_o - 1)^{1/2} \quad . \quad (18)$$

Equations (17) and (18) are based on the fact that the normalized threshold current density J_{th} is equal to 1 in the case considered.

33

Figure 8 is a plot of the calculated magnitude of $F(\omega)$ for various values of I/I_{th} (I/I_{th} is equivalent to j_0) and assuming $\beta = 0$. Figure 9 shows the effect of a finite β. Note that increasing β reduces the amplitude of the resonance response. This result is expected since β is a measure of the amount of damping in the system. Furthermore, β is inversely proportional to the laser volume since we have a higher spontaneous emission rate for a small active region volume, in a manner similar to the increased stimulated emission rate. Thus, one conclusion is that injection lasers with a small active region volume should have a flatter modulation response.

B. CIRCUIT CONSIDERATIONS

In the previous subsection, we discussed the modulation response of the injection laser. However, the simple rate equations do not include the effects of circuit parasitics. Figure 10 is a schematic for an idealized equivalent circuit that represents the diode laser and package. C_p is the package shunt capacitance; L_s is the series inductance of the bond wire; and R_j and C_j are the forward-biased junction resistance and capacitance, respectively. It is the forward current flowing through R_j that causes lasing. Current flowing through C_p and C_j will not give rise to photon generation.

Figures 11 and 12 are plots of laser impedance from 100 MHz to 10 GHz in 100-MHz steps for the Hitachi buried-heterostructure (BH) and channeled-substrate-planar (CSP) lasers. Table 1 lists the values obtained for the circuit parameters shown in Figure 10. These values were obtained using a circuit analysis computer program to calculate the values by using a least-squares fit to the data of Figures 11 and 12. The values obtained in Table 1 fit the data of Figures 11 and 12 with an accuracy of 10% for frequencies between 100 MHz and 6 GHz. The reflection coefficient of the laser is

$$\Gamma = \frac{Z_L - Z_0}{Z_L + Z_0} \quad , \tag{19}$$

34

10298−8
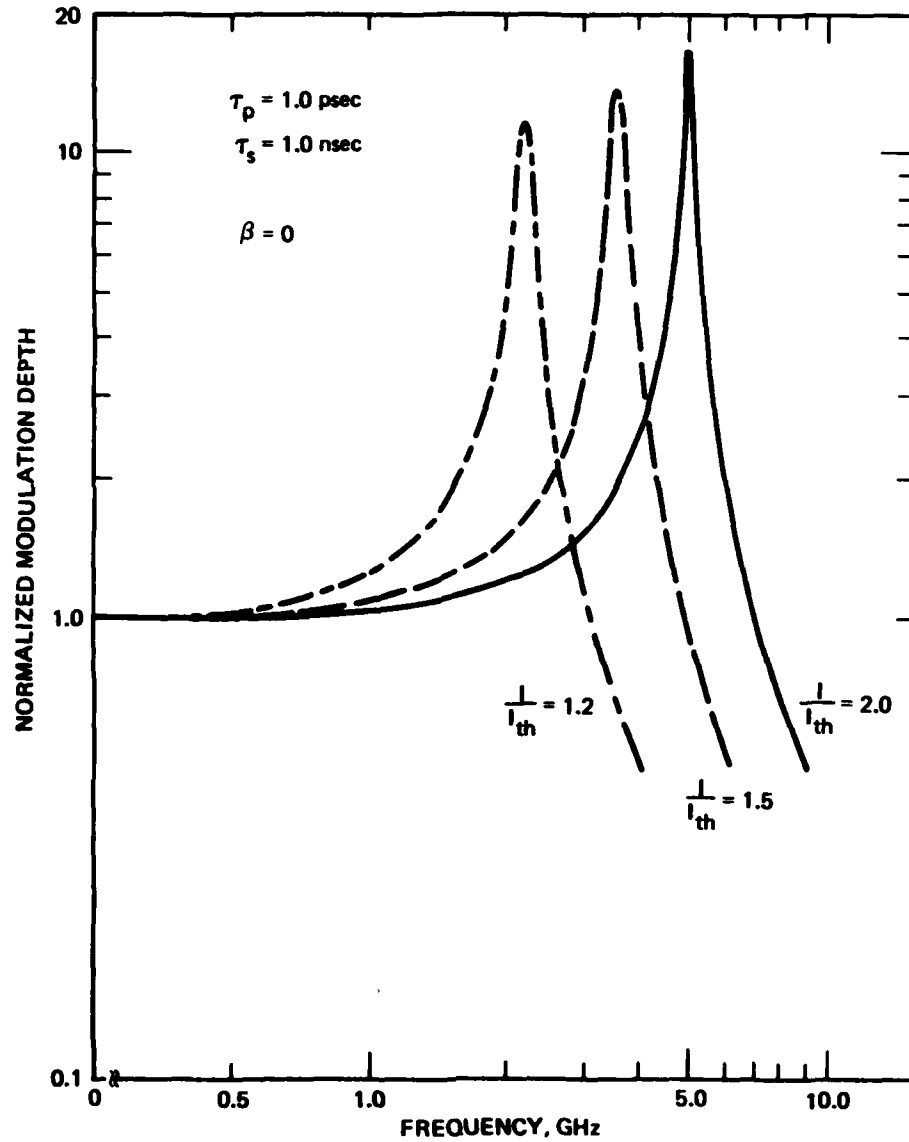
Figure 8. Frequency dependence of the normalized modulation depth of an injection laser. The spontaneous emission factor, β, is equal to zero.

35
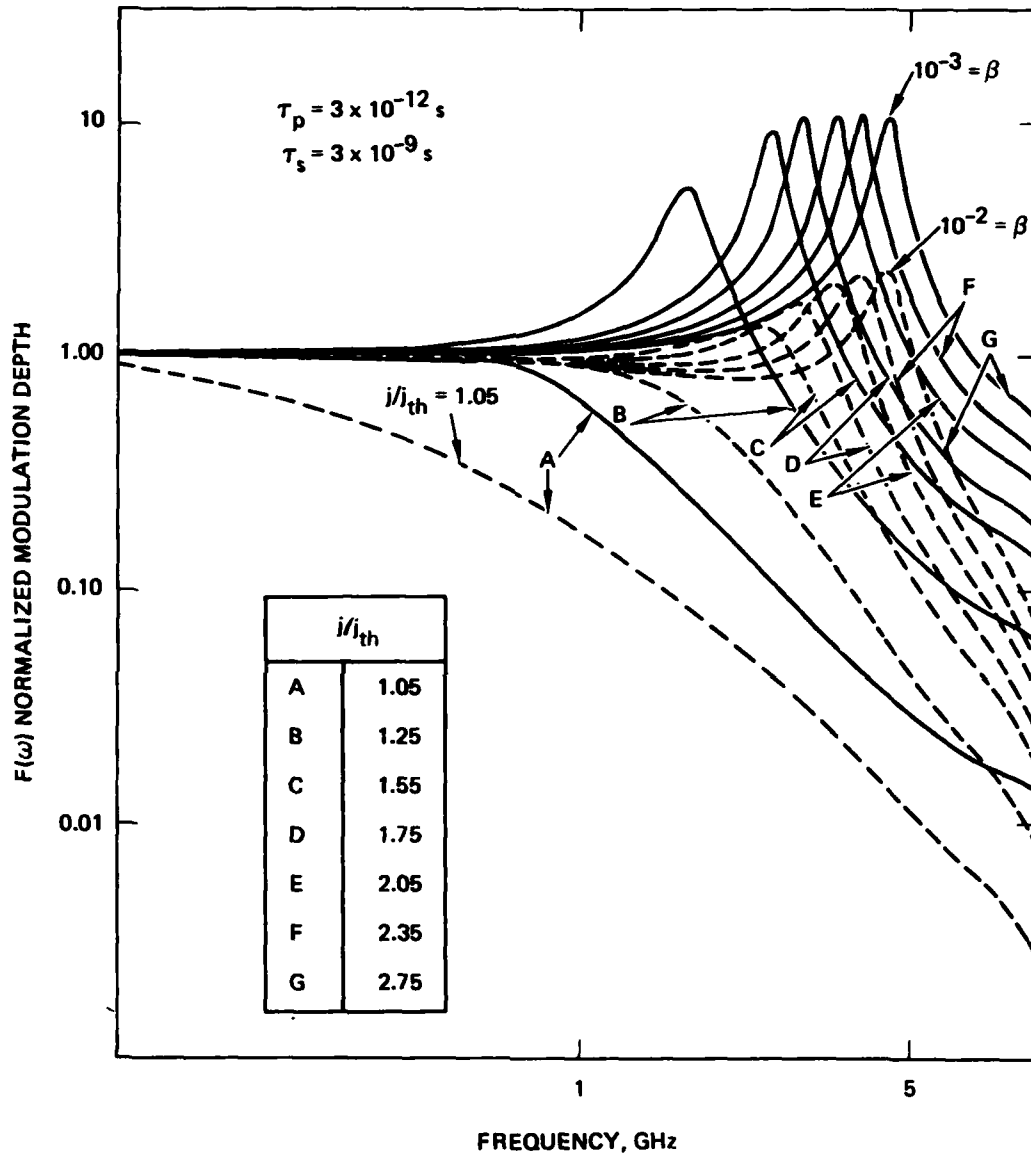
Figure 9. Frequency dependence of the normalized modulation
depth of an injection laser where the spontaneous
factor, β, is not zero.

10298-2
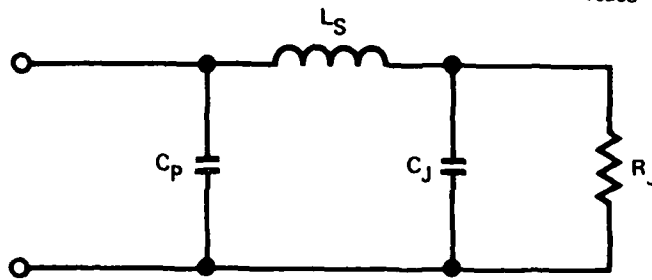
Figure 10. Equivalent circuit of the (GaAl)As
injection laser.
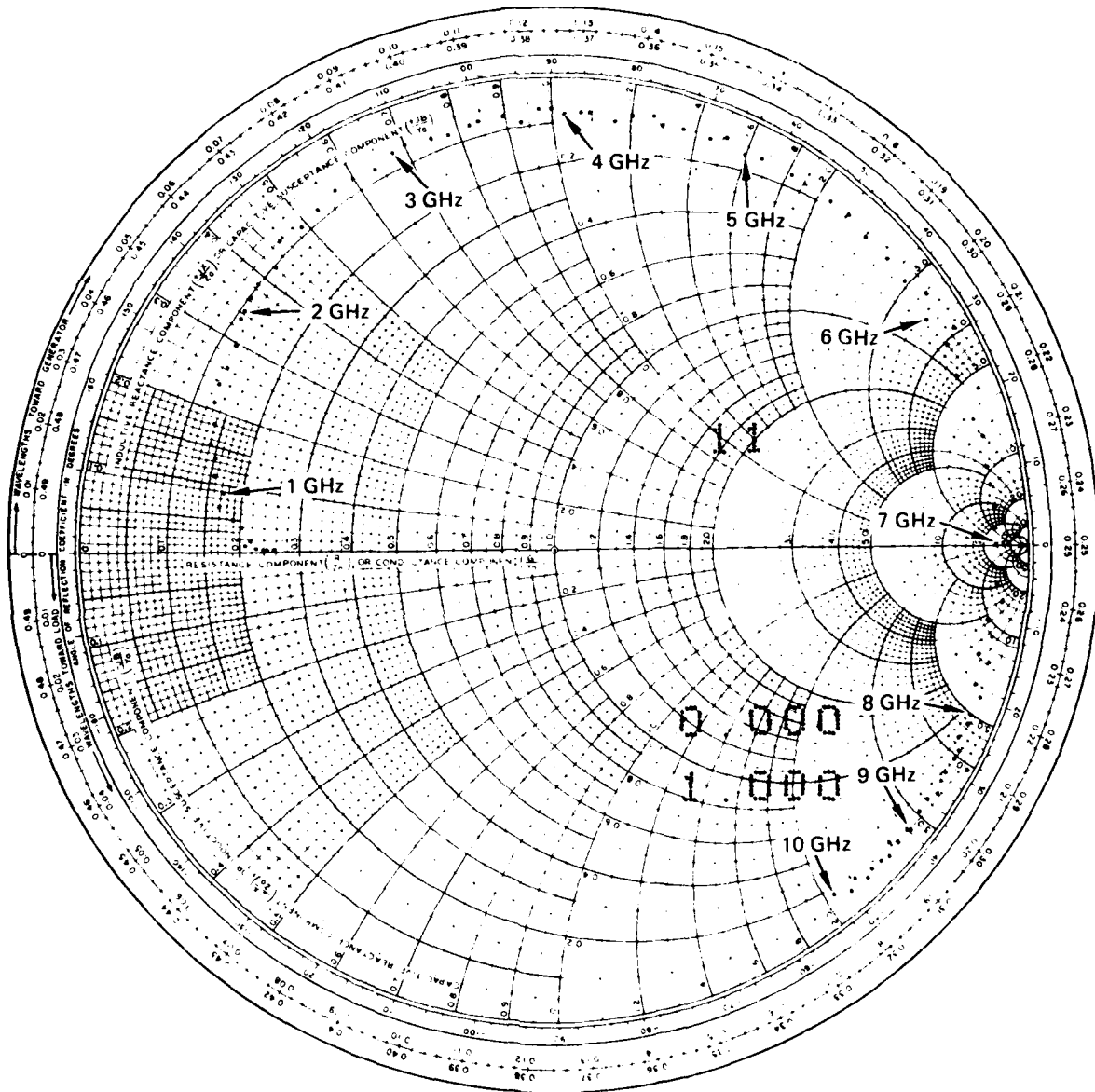
Figure 11. Hitachi BH laser (HLP 2400U) impedance from 100 MHz to 10 GHz in 100-MHz steps. Smith chart is normalized to 50 Ω.

38
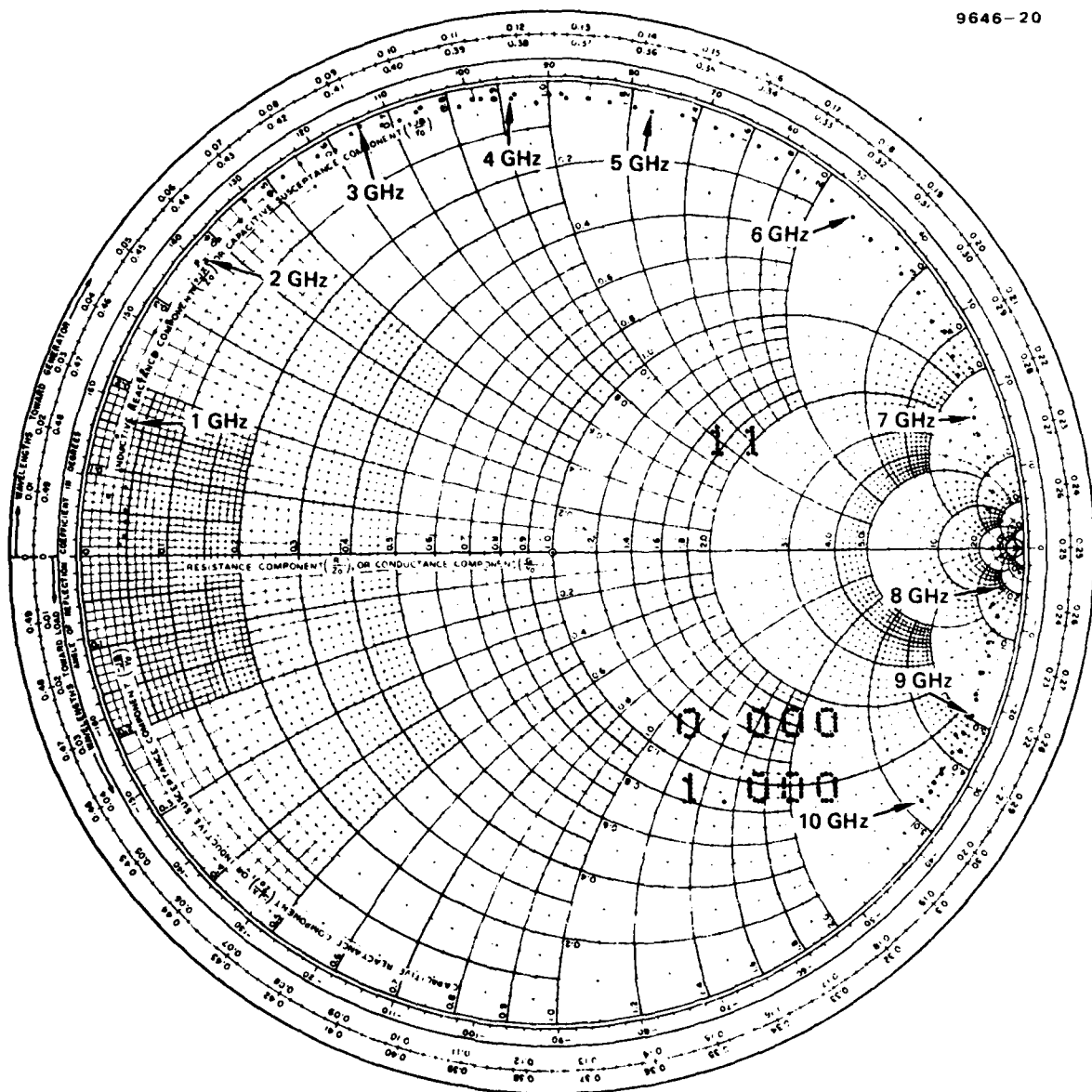
Figure 12. Hitachi CSP laser (HLP 1400) impedance from 100 MHz to 10 GHz in 100-MHz steps. Smith chart is normalized to 50 Ω.

Table 1. Equivalent Circuit Parameters

Laser Type	C_p, F	L_p, H	C_j, F	R_j, Ω
CSP	0.348×10^{-12}	1.5×10^{-9}	10×10^{-12}	10
BH	0.315×10^{-12}	1.318×10^{-9}	40×10^{-12}	2

T7429

where Z_L is the laser impedance, and Z_0 is the characteristic impedance
of the system (typically, Z_0 = 50 Ω). The magnitude of the current flowing
through the laser package is

$$i = i_0 \left| 1 - \Gamma \right| , \tag{20}$$

where i_0 is the magnitude of current from the rf source into a matched load.
Figure 13 shows $\left| 1 - \Gamma \right|$ as a function of frequency for the BH and CSP lasers.
Note that not all the current flowing into the package will flow through the
junction. Therefore, Eq. 20 represents the maximum possible current going
into photon generation.

To maintain a flat frequency response, a matching circuit can be used to
compensate for the frequency dependence of Γ. The conventional technique is
to reduce Γ to zero (i.e., power match). However, laser response is a func-
tion of the current going through (and not of the power delivered to) the
diode. If the laser appeared as a short circuit across the frequency band of
interest, twice as much current would flow compared to the case of a matched
load. Thus, the optical output of the laser would be 3 dB greater in the
short-circuit case. However, this 3 dB increase would be at the cost of an
infinite VSWR. In our experiments, no matching techniques were used. The
error produced by reflections was quite small since the reflection coefficient
is relatively independent of frequency at frequencies below 5 to 6 GHz.

40
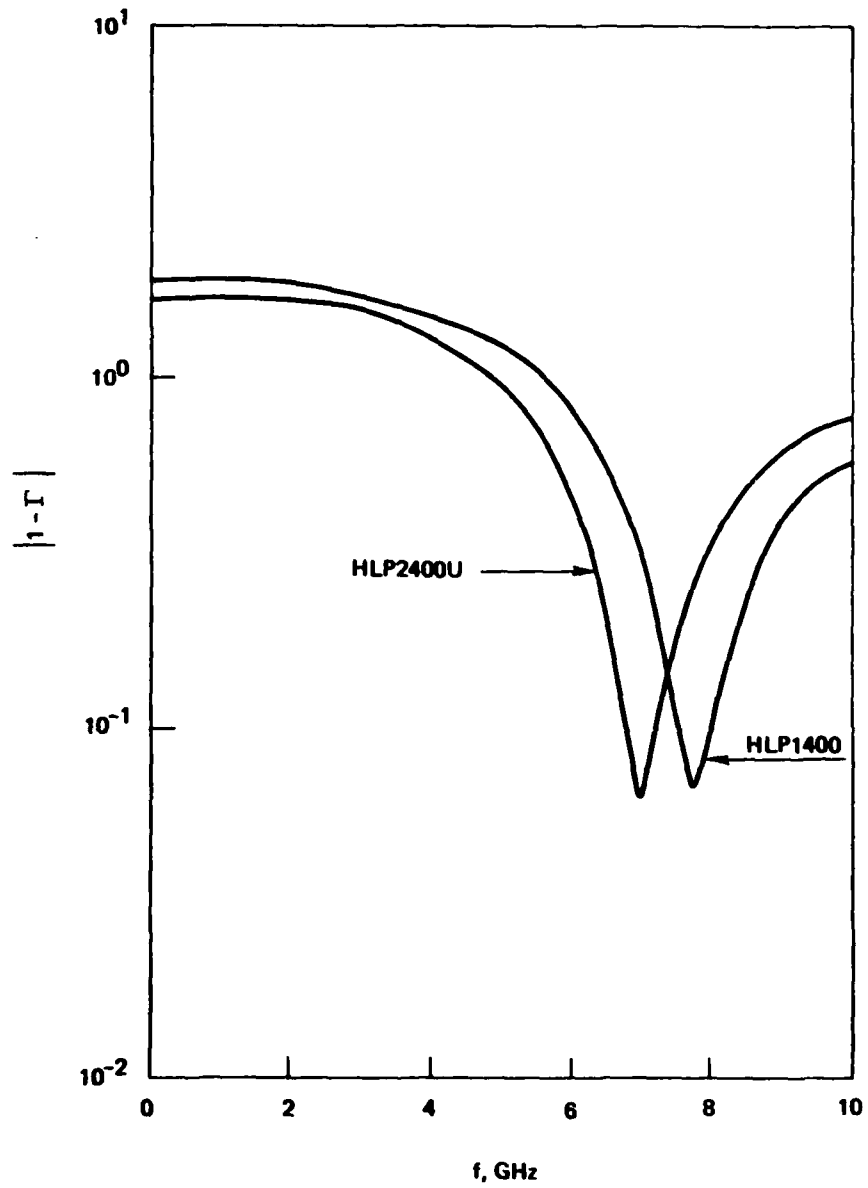
Figure 13. $|1 - \Gamma|$ as a function of frequency.

41

C. EXPERIMENTAL RESULTS

Several GaAs/GaAlAs lasers were characterized to determine their
suitability using direct current modulation. Because $|1 - \Gamma|$ was found to be
relatively flat for the BH and CSP lasers, no attempt was made to match to
the laser impedance. Each laser was mounted at the end of a microstrip
fabricated from Au-plated alumina. The rf power was coupled via an APC-7
microstrip launcher. The optical signal was demodulated by a Rockwell
GaAs/GaAlAs heterostructure photodiode. A Hewlett Packard network analyzer
system HP-8410 (harmonic converter/S-parameter test set/phase magnitude dis-
play, and rf sweep generator) was used to characterize the frequency response
of the laser-photodiode pair. Figure 14 is a block diagram of the frequency
response experiment. Figure 15 shows the optics used to couple the laser
radiation to the photodiode. A variable neutral density (ND) filter (or
optical attenuator) was used to prevent excess optical power from damaging
the photodiode.

Figures 16 and 17 show typical results for L(f) as a function of frequency
for the Hitachi BH and the General Optronics proton-bombarded stripe laser.
The absolute value of L for each laser/photodiode combination is relative
because different values of attenuation were used. The dc insertion loss was
measured by plotting the change in detector current as a function of laser
current.

The relaxation oscillation resonance can be seen in all of the lasers.
Self-pulsations, which could have resulted from the excessive drive level
used, probably caused the strong resonance in the General Optronics laser.
(Because of its importance, the problem of self-pulsation will be treated in
Section 4.) The laser structures studied differed vastly in resonance
behavior. This behavior can be qualitatively explained by considering the
spontaneous emission factor of the laser and using Figure 9. For example, the
CSP and the General Optronics lasers have a relatively wide stripe width (i.e.,
the width over which the current flows). Typical stripe widths are 6 to
15 um, which leads to a $\beta \simeq 10^{-3}$. On the other hand, the BH and TJS lasers
have relatively narrow stripe widths (~ 1 μm) and thus have a $\beta \simeq 10^{-2}$.
Therefore, we expect the CSP and the General Optronics lasers to have a more
pronounced resonance behavior than the BH and TJS lasers. A comparison of
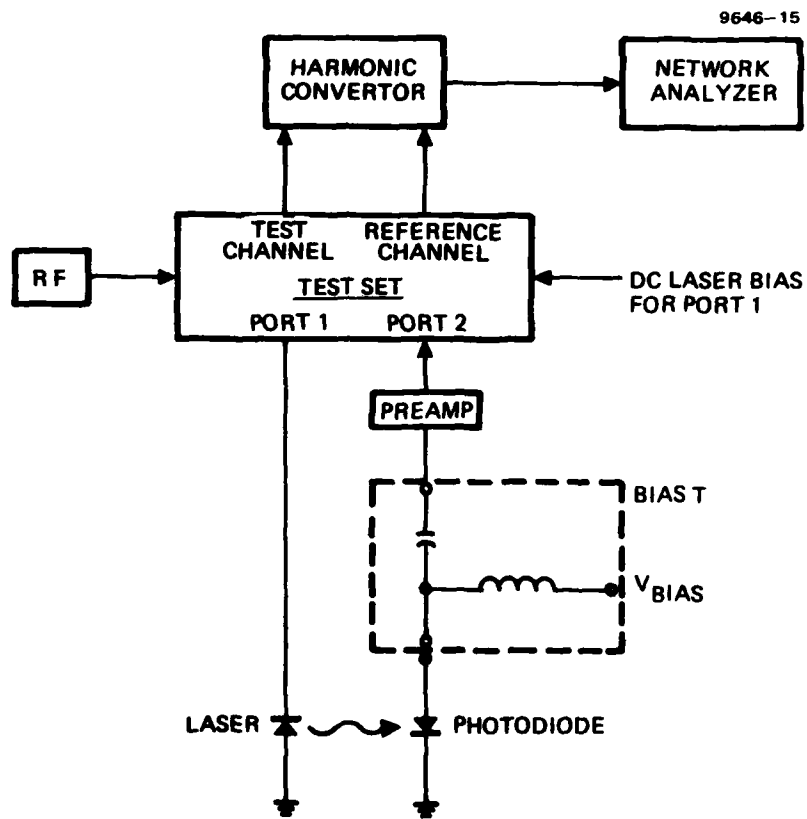
Figure 14. Block diagram of the frequency response
measurement.

43
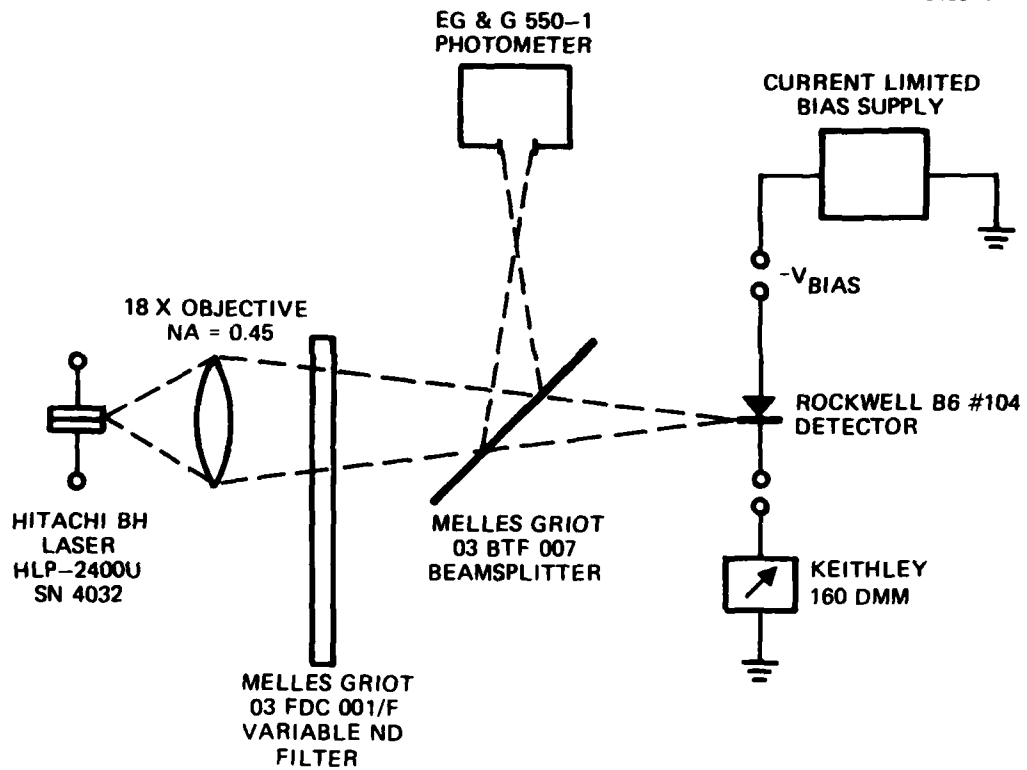
Figure 15. Laser-photodiode optical arrangement.
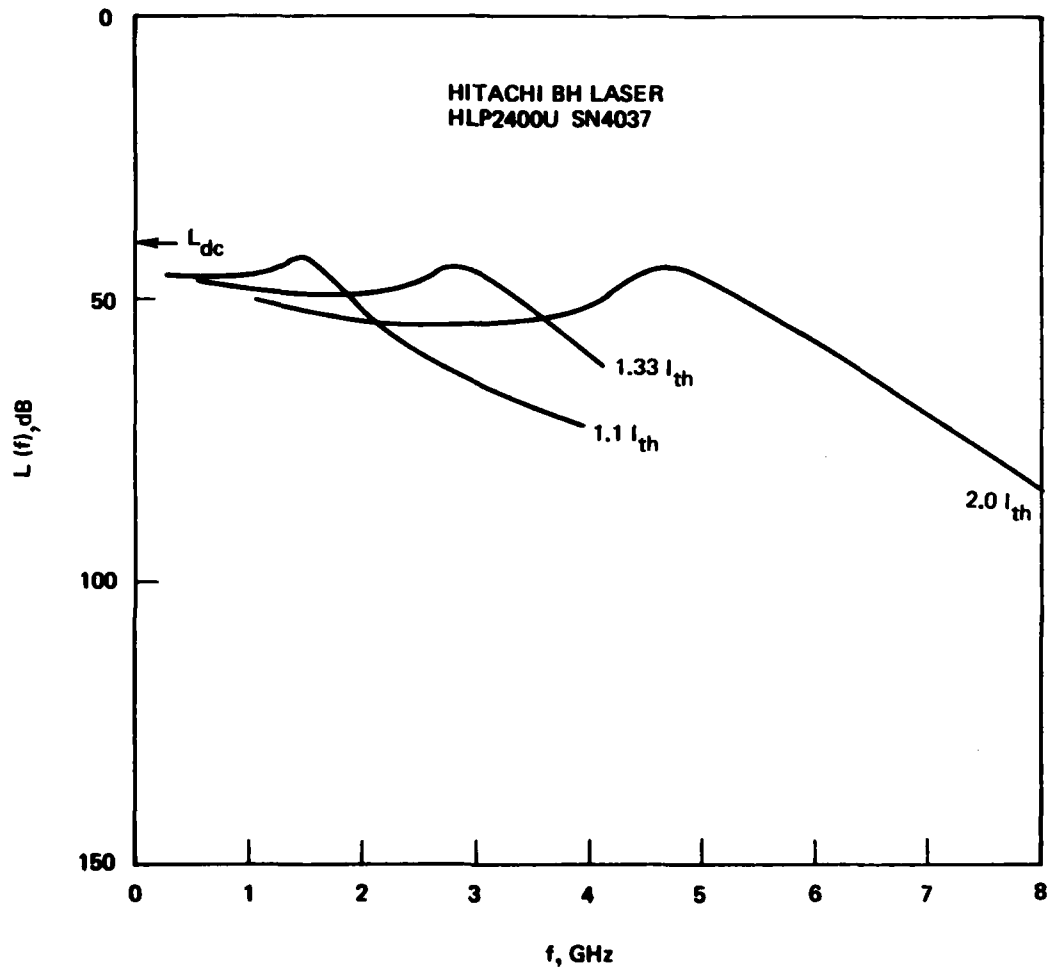
Figure 16. Response of the Hitachi BH laser.
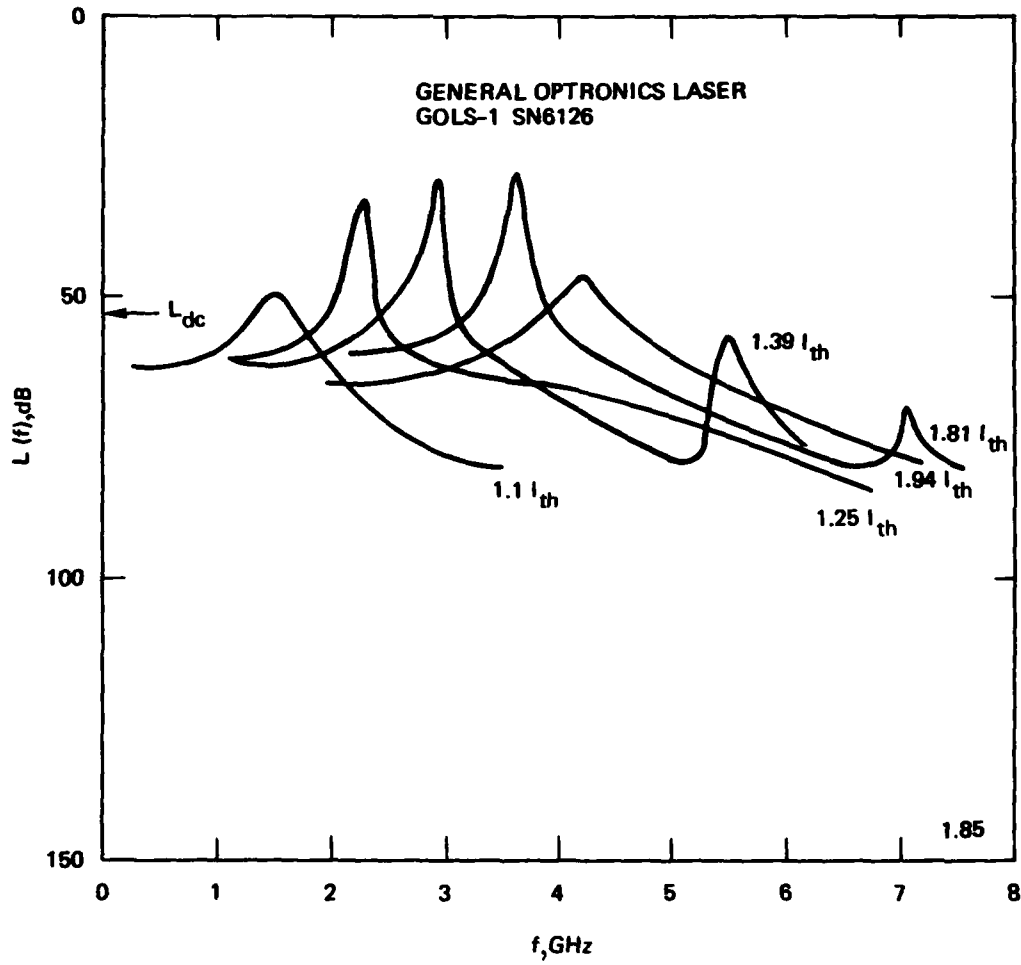
Figure 17. Response of the General Optronics laser.

Figures 16 and 17 confirms our speculation. Figure 18 shows a typical plot of the relaxation oscillation frequency ($f_o = \omega_o/2\pi$) as a function of laser drive (I/I_{th}) for the BH laser tested. As expected, f_o follows the behavior of Eq. (18) with $1/[2\pi(\tau_p\tau_s)^{1/2}]$ ranging from 3.7 GHz for the BH/LOC laser to 5.35 GHz for the CSP laser. In some of the lasers, the magnitude of the resonance decreases with increasing drive current. We believe circuit parasitics cause this effect. Furthermore, all the lasers tested showed a dip in the modulation response at a frequency lower than the resonance frequency. We believe that this effect is a result of the out-diffusion of injected carriers. Our results indicate that efficient analog modulation of existing commercial (GaAl)As injection lasers is limited to ∿5 GHz. Frequencies beyond 5 GHz will require excessive drive currents ($I > 2I_{th}$), leading to a relatively large output power density. Operating injection lasers at high power densities could reduce their reliability and significantly shorten their life.

D. CONCLUSIONS

The results obtained in this section provide some guidelines and techniques that can be used to improve the high-frequency modulation characteristics of (GaAl)As injection lasers. First, a reduction of the laser cavity length will decrease the photon lifetime τ_p of the laser and thus increase the maximum frequency f_o. For example, a reduction of the laser cavity length from a typical 300 μm to 75 μm can increase f_o to beyond 10 GHz. Second, the effect of circuit parasitics has been examined in detail for the first time. It is of utmost importance to design new laser structures and microstrip circuits that can minimize circuit parasitics. The laser structures and microstrip circuits can be characterized using existing microwave test equipment.
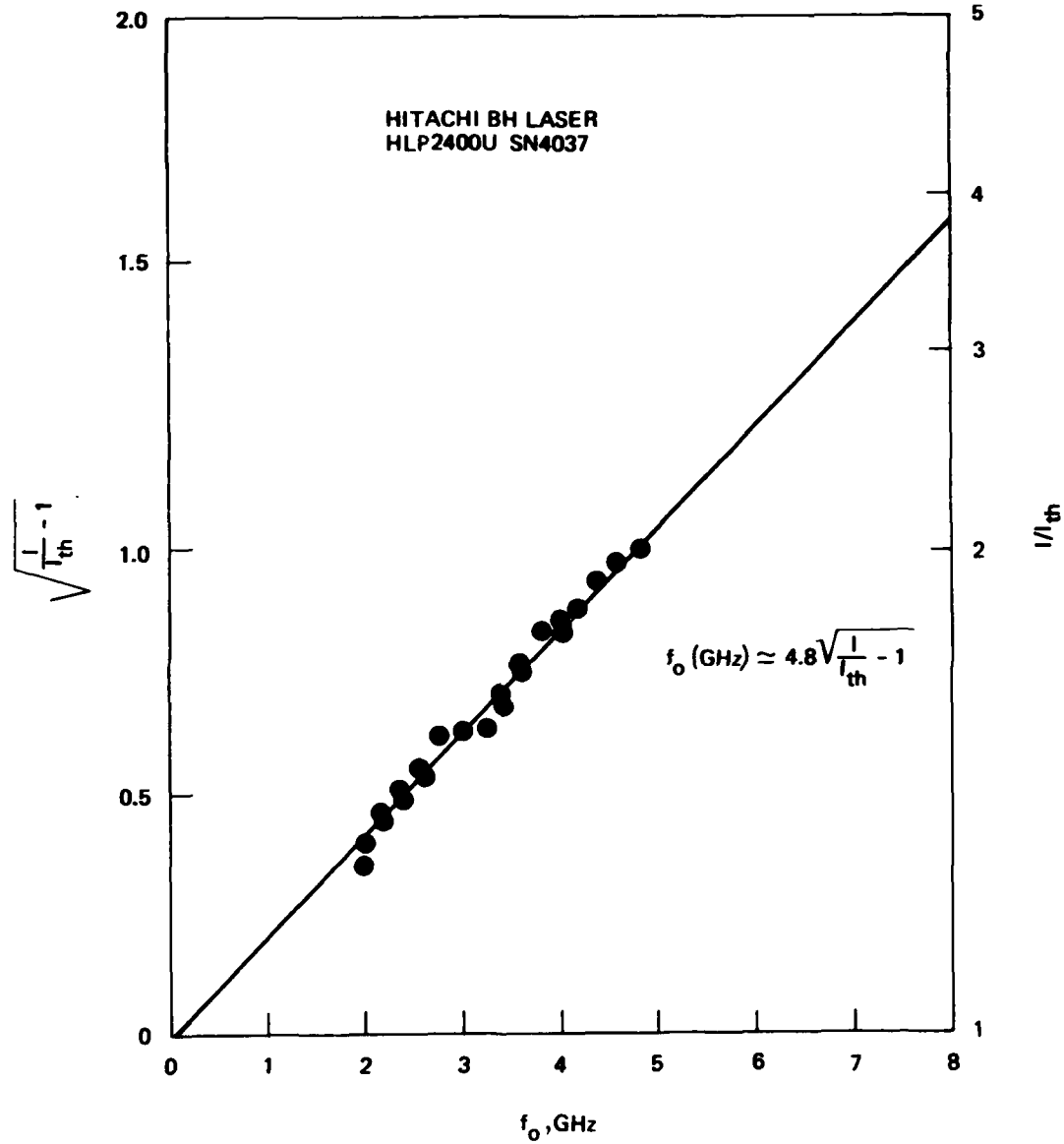
Figure 18. Relaxation oscillation frequency as a function of bias for the Hitachi BH laser.

SECTION 4

STUDY OF MODE-LOCKING IN (GaAl)As INJECTION LASERS

This section describes the important parameters affecting the mode-locking of (GaAl)As injection lasers operating in an external optical cavity. In particular, we describe the characteristics of both single- and multilongitudinal-mode lasers from a variety of commercial manufacturers. We have characterized both self-pulsing and nonpulsing injection lasers, and our results indicate that "good" mode locking (pulses with 100% modulation depth and less than 60 psec pulse width) can only be obtained in lasers having either a narrow-band noise resonance or self-pulsations and operating at current below that necessary to induce the sharp resonances in the isolated laser. Furthermore, the amplitude, pulse width, and frequency of the mode-locked pulses are a strong function of the external cavity length and laser current. We have successfully mode-locked an injection laser and time multiplexed the light output to produce pulses with $\sim$2-GHz repetition rate.

A. EXPERIMENTAL SETUPS AND DC CHARACTERISTICS

Figure 19 shows the various experimental arrangements for the external cavity geometry. Initially, we used the spherical mirror (Figure 19a) external cavity. However, because of its limited flexibility (i.e., the cavity length cannot change) and the difficulty in alignment, we discontinued it and used the other arrangement (Figure 19b) for the remaining experiments. We have used several different types of commercial (GaAl)As stripe geometry lasers; their important characteristics are summarized in Table 2. All of the lasers operate cw at all times.

The external resonator consisted of a 40x microscope objective and a flat mirror. In the experimental arrangement, the laser is mounted at the end of a microstrip bias tee with a 47 Ω resistor placed in series with the rf input to provide impedance matching. The external cavity was aligned by collimating the output beam from one facet of the laser and adjusting the return beam to increase the laser output from the other facet. The final alignment was accomplished using PZT-controlled micrometers. The light output from the

DC o—⎓⎓⎓—⊣⊢—⎓⎓⎓—o RF

SPHERICAL
MIRROR

LASER

HEAT SINK

DETECTOR

L

(a)

9039-7RI

MIRROR   DC o—⎓⎓⎓—⊣⊢—o RF

LASER

HEAT
SINK

DETECTOR
AND
AMPLIFIER

SPECTRUM
ANALYZER

L

(b)
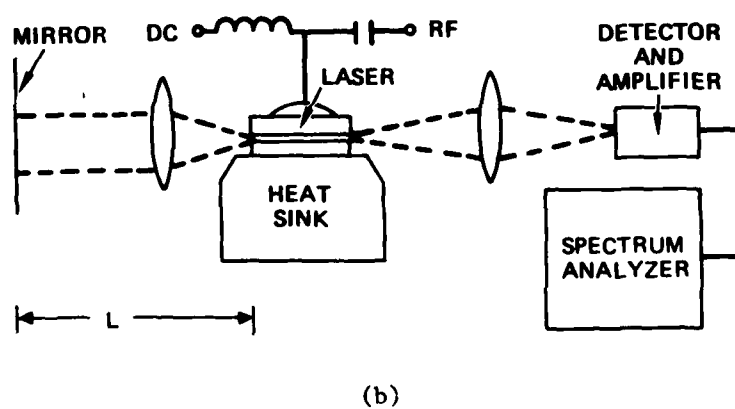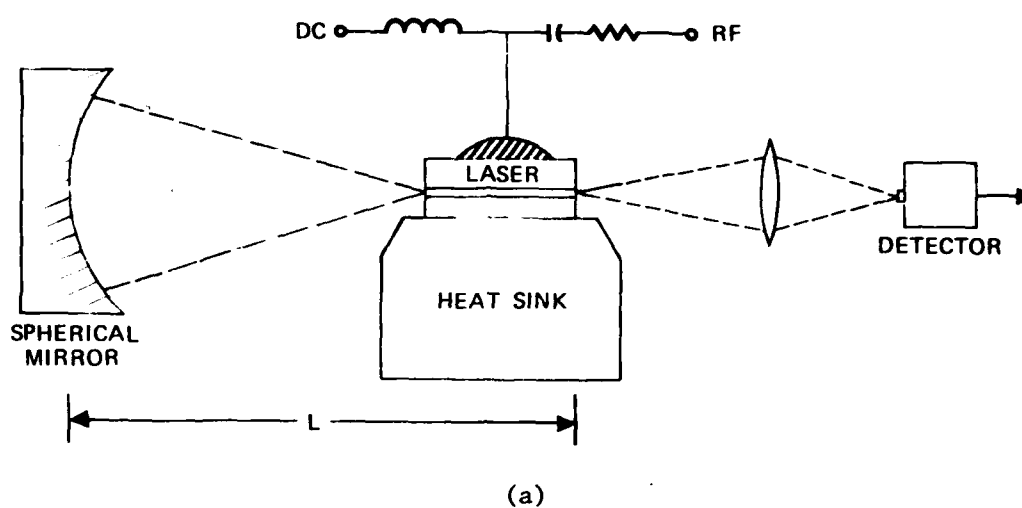
Figure 19.   Experimental set-ups graphically displaying the
external cavity arrangements used.

50

Table 2. Summary of Laser Structures Used in the Experiments[a]

Laser Type	Longitudinal Modes (spectral width)	Threshold Current, mA	Dynamic Characteristics	Symbol	Number of Lasers Tested
Buried heterostructure (BH) Hitachi	Single ($\Delta\lambda_{1/2} \lesssim 3$ Å)	20	Nonpulsing	BH-NP	1
Buried heterostructure (BH) Hitachi	Multimode ($\Delta\lambda_{1/2} > 40$ Å)	29, 30	Narrow band noise resonance (NR)	BH-SP	2
Channel substrate planar (CSP) Hitachi	Single ($\Delta\lambda_{1/2} \lesssim 3$ Å)	60, 75	Nonpulsing	CSP-NP	1
Channel substrate planar (CSP) Hitachi	Multimode ($\Delta\lambda_{1/2} < 10$ Å)	90	NR	CSP-SP	2
Constricted double heterostructure (CDH) RCA	Multimode ($\Delta\lambda_{1/2} < 15$ Å)	75 to 80	Nonpulsing	M-CDH-NP	3
Constricted double heterostructure (CDH) RCA	Single ($\Delta\lambda_{1/2} \lesssim 3$ Å)	80 to 85	Nonpulsing	S-CDH-NP	5
General Optronics stripe (G.O.)	Multimode ($\Delta\lambda_{1/2} < 10$ Å)	60 to 100	NR	G.O-SP	4
General Optronics stripe (G.O.)	Multimode ($\Delta\lambda_{1/2} > 50$ Å)	60 to 100	NR and self-pulsing	G.O-SP	5

[a]All of the lasers, either with a narrow-band noise resonance or self-pulsations (except the BH), tested were specially selected by the respective manufacturers to provide the observed characteristics. The pulsing BH lasers started pulsing after operation at high power levels. We would like to emphasize that the characteristics of these specially selected lasers are not representative of the commercially available lasers provided by the above manufacturers.

T7429

second facet of the laser was collected and focused onto a Si avalanche diode
(Telefunken model S171P, or Spectra Physics 403B) using a microscope objective.
The rise and fall times of the detector were ∿200 and 60 psec, respectively.
In some experiments, we followed the detector with a B&H amplifier having
a 3.1 GHz bandwidth and 30 dB gain. The rf input to the laser was provided
by an HP sweep oscillator (8690B). The maximum rf power going into the laser
was estimated to be less than a few milliwatts for the cases considered.
The output from the avalanche diode was fed to either an HP spectrum
analyzer (8565A) or a Tektronix sampling oscilloscope (S4).

Figure 20 shows typical light output versus current characteristics for
different types of laser structures operating with an external resonator (ER).
The lasers used are described in Table 2. For comparison, the light output
characteristics with no external resonator (NER) present are also shown. An
important figure of merit for a laser-external resonator combination is the
threshold reduction factor[12] K, which is given by

$$K = \frac{I_{th}\ (ER)}{I_{th}\ (NER)} \quad , \tag{21}$$

where I_{th} (ER) and I_{th} (NER) are the threshold current with and without the
external resonators, respectively. In a previous paper,[13] we have shown that
the value of K under cw operation can be written as

$$K = \frac{\alpha_o d + (d/\Gamma)\ [\alpha_{fc} + (1/2\ell)\ \ln(1/RR_{eff})]}{\alpha_o d + (d/\Gamma)\ [\alpha_{fc} + (1/\ell)\ \ln(1/R)]} \quad , \tag{22}$$

where α_o is a loss constant, α_{fc} is the distributed loss, Γ is the tranverse
optical confinement factor, d is the active region thickness, ℓ is the diode
length, R is the mirror reflectivity, and R_{eff} is the total fraction of light
reflected back into the laser from the external and diode mirror combination.
By using an R_{eff}, we are assuming a uniform photon density in the external

52

1.0

0.8

WITHOUT
EXTERNAL
CAVITY

WITH THE
EXTERNAL
CAVITY

0.6

I_{th} (NER) $\cong$ 24 mA

I_{out} (REL UNITS)

0.4

I_{th} (ER) =21.5 mA

$\Delta I_{th} = \dfrac{I_{th} (NER) - I_{th} (ER)}{I_{th} (NER)} = 0.104$

0.2

$K = \dfrac{I_{th} (ER)}{I_{th} (NER)} = 0.895$

0   10   20   30   40   50

I, mA

(a)

1.2

I_{th} (NER) $\cong$ 65 mA

WITH EXTERNAL
CAVITY (ER)

1.0

I_{th} (ER) $\cong$ 57.5

$\Delta I_{th} = \dfrac{I_{th} (NER) - I_{th} (ER)}{I_{th} (NER)} = 0.115$

0.8

$K = \dfrac{I_{th} (NER)}{I_{th} (NER)} = 0.884$

I_{out} (REL UNITS)

0.6

WITHOUT
EXTERNAL
CAVITY (NER)

0.4

0.2

0   20   40   60   80   100

I, mA

(b)
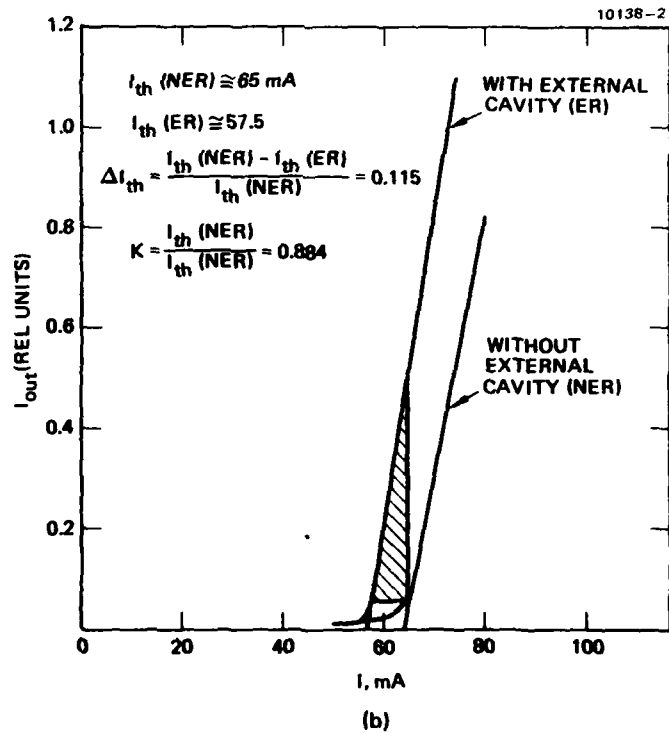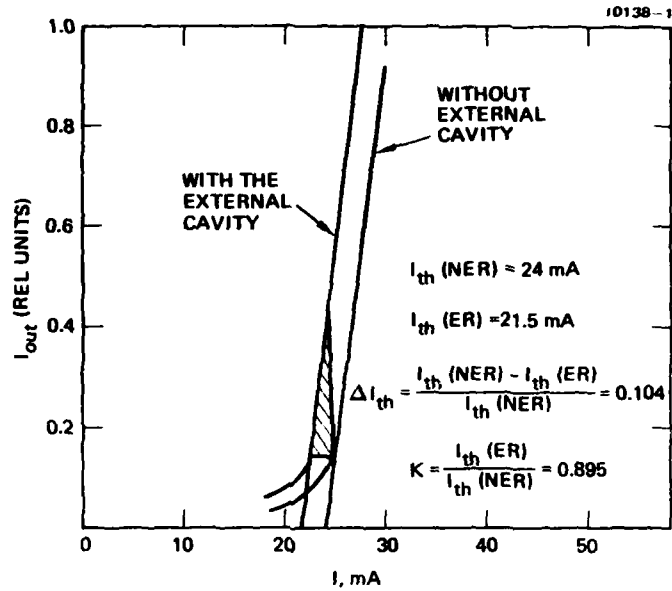
Figure 20.   Experimental light output versus
current characteristics, showing
relatively low threshold lasers
($I_{th} \sim$20-30 mA) and lasers with
higher threshold (I $\sim$60-100 mA).

53

cavity. This assumption, although adequate for cw operation, breaks down in the description of short optical pulses. The effective reflectivity R_{eff} can be written as[13]

$$R_{eff} = \frac{(\sqrt{R} + \sqrt{R_f})^2}{(1 + \sqrt{R_f \cdot R})^2} \quad , \tag{23}$$

where R_f is the light reflected from the external mirror that reaches the diode. Figure 20 shows K to be ~ 0.1. Substituting typical values for the diode parameters ($\ell = 1.5 \times 10^{-2}$ cm, $d = 0.3$ μm, $\Gamma = 0.8$, $R = 0.3$, and $\alpha_{fc} = 20$ cm^{-1}) into Eqs. (21) and (22) gives a range for R_f of from 0.1 to 0.2 when we assume that α_o lies between 100 and 200 cm^{-1} (a typical range).[13] This shows that only a small fraction of the light is returned to the laser. However, as shown below, the amount of optical feedback is more than sufficient to mode-lock the injection laser.

B. DYNAMIC CHARACTERISTICS OF INJECTION LASERS OPERATING IN AN EXTERNAL OPTICAL CAVITY

The dynamic characteristics of injection lasers operating in an external optical cavity have been discussed by many authors.[14] Broom et al.[15] obtained self-induced sinusoidal resonances at a frequency corresponding to either the inverse transit time or a harmonic of the relaxation oscillation frequency. The experimental results were explained by assuming an interaction between photons, injected carriers, and longitudinal mode effects. No account of the delayed photon feedback from the external cavity was considered. Paoli[16,17] and Ripper have characterized the operation of self-pulsing lasers operating in an external cavity. They concluded that sharp pulsations could be obtained by using either electrical or optical feedback. Pulses as short as 180 psec were obtained. Furthermore, they obtained frequency locking and jumping effects.

Several workers ahve recently observed a sharp pulsation of the light output when the laser was driven at the inverse transit time f_c of the external cavity.[18-24] The initial demonstrations have attributed the effect to active

54

mode-locking and have been able to generate 20-psec-wide pulses at a 3-GHz repetition rate.[18] Recently, Ippen et al. have demonstrated that 5-psec-wide pulses can be generated from degraded (GaAl)As injection lasers.[21] These results raise two questions: (1) what mechanism is responsible for self-pulsations in semiconductor lasers, and (2) are there any relationships among self-pulsations, induced resonances, and the recent mode-locking experiments. This section comments briefly on the first question and concentrates on the latter.

Several models have been proposed to explain the origins of self-pulsations.[25-31] Most assume that self-pulsations are produced by either a saturable absorber[25-28,29] or a superlinear gain which increases with photon density. The saturable absorption can arise from nonuniform current flow[25,26] and absorption centers distributed throughout the active region[27,29] or localized near the laser facets.[29] The superlinear gain can result from electron traps distributed throughout the active region,[28] lateral mode instability,[30] or excess laser noise.[31] Other models, such as second-order mode-locking[32] and a recent model proposed by Casperson[33] appear less likely. Increasing evidence suggests that self-pulsations might be related to dark line defects[34] and mirror degradation.[35,36] In some recent experiments, Nash et al.[35] and Mizuishi et al.[36] have been able to either reduce or eliminate the effects of pulsations by using facet coatings.

These comments on the mechanism responsible for self-pulsations permit us to proceed to the second question. In a series of recent publications, we have shown that an external cavity can significantly alter the characteristics of an injection laser that contains either electron traps[13,37] or saturable absorbers.[38] Our results predict either enhancement or suppression of self-pulsations depending on the density of electron traps or saturable absorbers and the length of the external cavity. We have further speculated that our calculations can explain many of the previous results on induced resonances and mode-locking. In this and the following sections, we provide calculations and further experimental evidence to support our speculations.[39]

To correlate our experimental results (given in Sections 4-C and 4-D) with theory, we have used a model consisting of the conventional rate equations modified by two important parameters. First, as proposed by Copeland,[28] we

assume that the injection laser contains electron traps. Second, we take the external cavity into account by using a delayed photon feedback term. Even though we use the electron trap model, we would like to emphasize that our calculations are quite general and not model dependent. This assertion was recently verified by using a saturable absorber model and obtaining results similar to the electron model.[38] The equations describing the process are

$$\frac{dN_e(t)}{dt} = \frac{J}{ed} - \frac{N_e(t)}{\tau_s} - AN_{ph}(t)\left[N_e(t) - N_o\right] + \frac{dT(t)}{dt} \, , \qquad (24)$$

$$\frac{dN_{ph}(t)}{dt} = \frac{-N_{ph}(t)}{\tau_{ph}} + AN_{ph}(t)\left[N_e(t) - N_o\right] + \beta N_e(t)/\tau_s$$

$$- \sigma_o c_o N_{ph}(t)\,(T_o - T) + \frac{R_f N_{ph}(t-\tau)}{\tau'_{ph}} \qquad (25)$$

and

$$\frac{dT(t)}{dt} = \sigma_o c_o N_{ph}(t)\left[T_o - T(t)\right] - \sigma_e v N_e(t)T(t) \quad , \qquad (26)$$

where N_e is the electron density (in cm^{-3}), N_{ph} is the photon density (in cm^{-3}), J is the current density (in A/cm^2), e is the electronic charge (in C), and d is the thickness of the active region (in cm). The first two equations with the exception of the last terms (those involving T and R_f) are the conventional rate equations. The effects of transverse optical confinement and current spreading are neglected. The term $(R_f N_{ph}(t-\tau)/\tau'_{ph})$ represents the delayed feedback from the external mirror where τ, the round-trip time in the external cavity, is given by $1/f_c = \tau = 2L/c$, where L is the external cavity length, and c is the speed of light in vacuum; τ'_{ph} is the photon lifetime related to the mirror loss only and is given by $\tau'_{ph} = (c/nL)\ln(1/R)$, where n is the index of GaAs; R_f is the amount of light fed back into the laser.

Equation 26 represents the equation of motion for the electron traps, T is
the density of empty traps, T_o is the total density of traps, σ_e is the
electron capture cross section, v is the thermal velocity, and σ_o is the
photon capture cross section by a trap occupied by an electron. For the cal-
culations, we use

$$A = 1.5 \times 10^{-6} \ cm^3/sec$$

$$\tau_s = 3 \times 10^{-9} \ sec$$

$$\tau_{ph} = 2.9 \times 10^{-12} \ sec$$

$$d = 1 \times 10^{-4} \ cm$$

$$N_o = 5 \times 10^{17} \ cm^{-3}$$

$$\beta = 10^{-4}$$

$$c_o = 8 \times 10^9 \ cm/sec$$

$$\sigma_e = 1.5 \times 10^{17} \ cm^2$$

$$v = 4.42 \times 10^7 \ cm/sec$$

$$\sigma_o = 3 \times 10^{-6} \ cm^2.$$

All the calculations were performed by integrating Eqs. 24 to 26 using the
Runge-Kutta fourth-order algorithm. The system is excited with a step change
in current and run until steady-state oscillation or its absence is confirmed.
The important parameters affecting the pulsations are $\sigma_o T_o$, β, and τ.
Increasing $\sigma_o T_o$ increases the amplitude and decreases the pulse width of the
pulsations. This parameter is similar to the density of saturable absorbers
in other models. Increasing β (i.e., the spontaneous emission factor) quenches
the pulsations. Relatively large values of β are necessary (10^{-2} to 10^{-3}) to

57

quench pulsations. The effect of τ is to produce a series of resonant suppression and enhancement bands depending on whether τ is small or large. Also, the rate equations assume a single longitudinal mode and do not take into account the optical phase. However, the model adequately describes the process and is able to explain many of the experimental results.

Figure 21 shows the effect of an external cavity on the light output of an injection laser which does not pulse but still contains a high density of electron traps. Note that it is possible to induce pulsations, and that the amplitude and pulse width are strong functions of the actual trap density. This calculation can help explain the sharp contrast between the recent mode-locking experimental results[21] and the older results on induced sinusoidal oscillations.[15] Figure 22 shows the effect of varying the external cavity length on the amplitude of the induced pulsations. Note that there is a resonant enhancement of the pulse amplitude for a cavity length of ∿19 cm, and that it is possible for the pulsation to occur at $2f_c$ when the external cavity is lengthened beyond 25 cm. Figure 23 shows the variation of the induced pulse amplitude with injection current. Note that an efficient pulse output is only obtained for a small range of currents. Also, varying the external cavity length will shift the current where the maximum pulse amplitude occurs. A shift to lower current occurs when the external cavity is lengthened.

The above results can be understood qualitatively by considering two descriptions of the induced pulsation process. The first description is based on the recognition that the calculated induced pulsation is very similar to the results obtained using a passive mode-locked dye laser. Thus, some of the results applicable to the latter system should be applicable to the semiconductor laser systems. Passive mode locking using a saturable absorber with a slow recovery time has been described by New[40] and Haus.[41] In this type of mode locking, the saturable absorber and the laser gain act together to compress the leading and trailing edges of the circulating pulse. Several requirements must be met before such a process can produce short pulses that are much shorter than the recovery time of the saturable absorber. First, the optical cross section of the saturable absorber must be larger than the cross section for stimulated emission. This means that the absorber must be
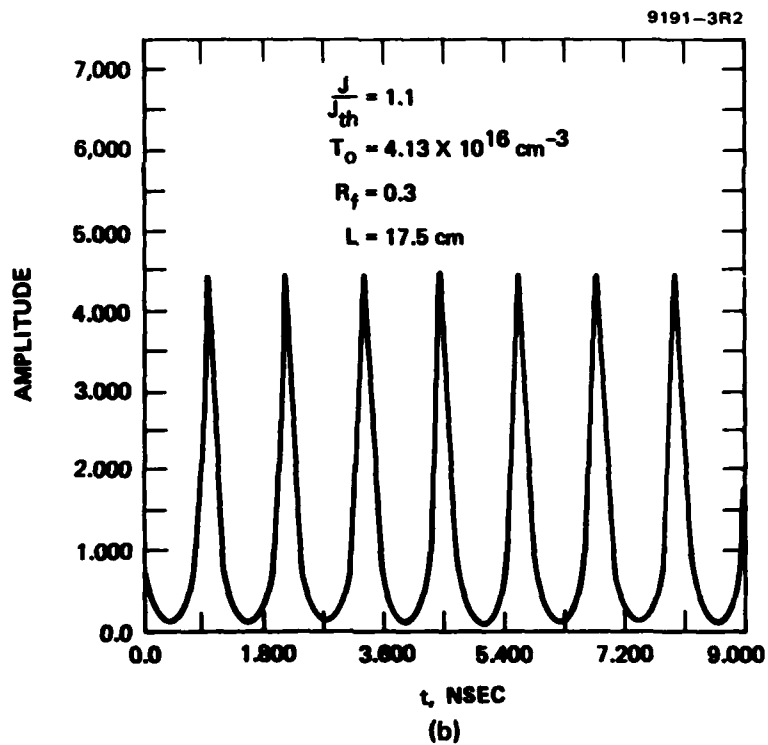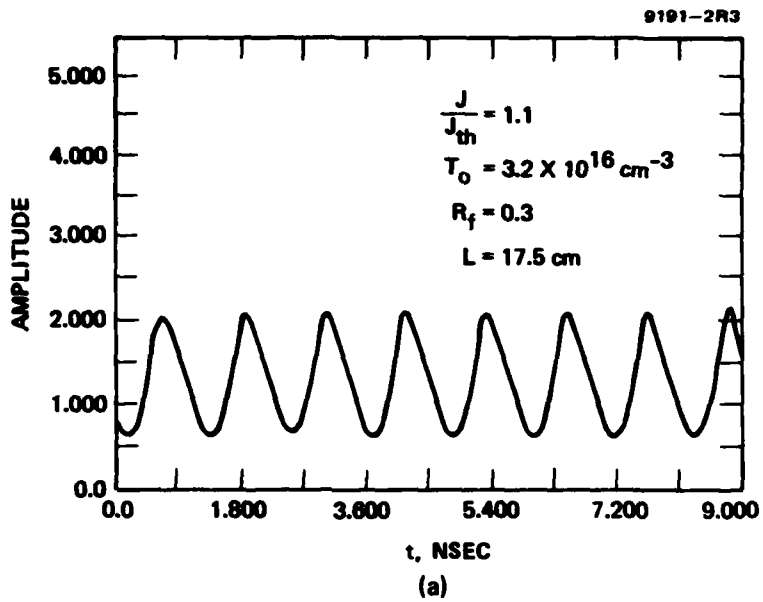
Figure 21.   Calculated plot showing induced
pulsations when an external cavity
is aligned with a laser having a
high density of electron traps.

59

$$\frac{J}{J_{th}} = 1.1$$

$$T_0 = 4.13 \times 10^{16}/cm^3$$

$$R_f = 0.3$$

9191—4R2
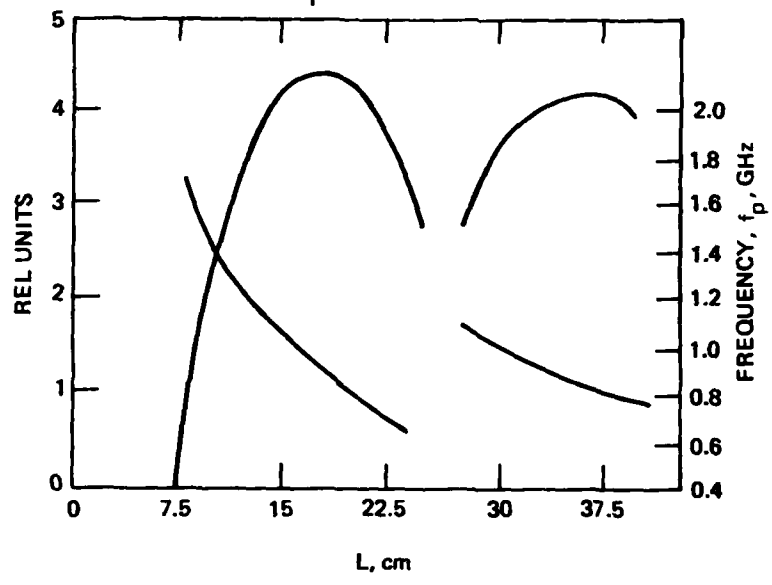
Figure 22. Calculated plot showing the variation of induced pulse amplitude versus external cavity length.
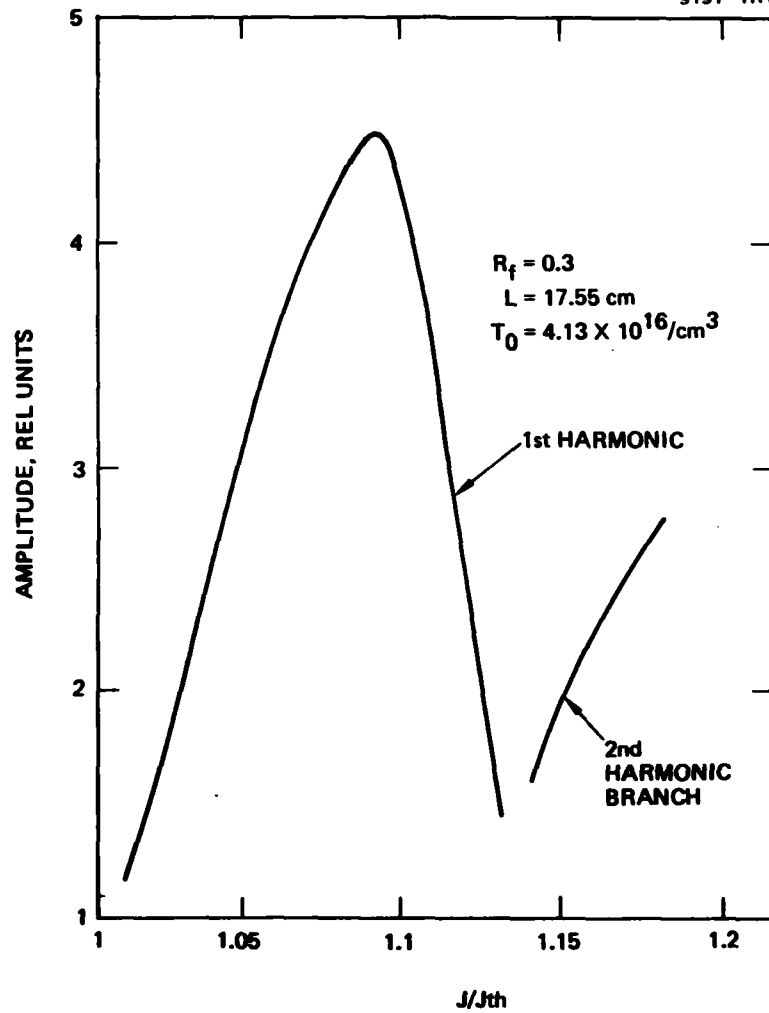
Figure 23. Calculated plot showing the
variation of induced pulse
amplitude versus current.

easier to saturate than the laser gain. For a semiconductor laser with electron traps, the absorber cross section is σ_0, and the stimulated emission cross section is $\sigma_L = A/c_0$. Using the numbers in Section 4-B, we find $\sigma_0/\sigma_L \simeq 6$, and this requirement is easily met. The second requirement is that the relaxation time of the gain must be comparable to the pulse repetition rate. This requirement arises from the stability conditions derived by Haus, which require that the net gain of the laser system be negative after passage of the pulse. Thus, for short pulses, the gain must be shut off after the passage of the pulse. This second requirement forces us to use an external optical cavity with reasonable length in the mode-locking of the semiconductor laser systems. A typical value for the gain relaxation time τ_G is ~ 1 nsec (i.e., we expect $\tau_G \simeq \tau_s$), and we expect stable pulses with gigahertz repetition rates. The latter value is typical for all the reported mode-locking results. We expect that the maximum pulse-repetition frequency depends on the actual laser used, since we expect variations in the spontaneous lifetime. Finally, the approximate analytical results derived by Haus can provide a qualitative measure of the minimum pulse width and how it varies with laser parameters. From his results, the minimum pulse width $\tau_{p_{min}}$ can be derived as

$$\tau_{p_{min}} \propto \left(\frac{Q_R}{Q_A}\right)^{-1/2} \cdot \frac{1}{\omega_c} \quad , \tag{27}$$

where $Q_{R,A}$ represents the Q of the cavity resonator and the saturable absorber. Simplifying Eq. (27) to show the effects of the cavity and absorber losses yields

$$\tau_{p_{min}} \propto \left(\frac{\alpha_L}{\alpha_A}\right)^{1/2} \frac{1}{\omega_c} \quad , \tag{28}$$

where ω_c is the radian round-trip frequency, α_L is the laser threshold loss, and α_A is the absorber loss given by $\alpha_A \simeq \sigma_0 T_0$ in the case of electron traps. Equation (28) can help explain some of our calculations qualitatively (e.g., the difference between Figures 21(a) and 21(b)) and can be used to predict the

parameters affecting τ_{pmin}. We conclude that to minimize the pulse width, we must increase the density of saturable absorbers and decrease the laser threshold losses.

Also note tha Haus neglected the effect of spontaneous emission in his discussion. However, from our numerical calculations we know that a large spontaneous emission factor tends to suppress induced pulsations. This arises from the higher damping arising from the spontaneous emission. The effect of spontaneous emission can help explain why Ippen et al.[21] observed a narrowing of the pulse output when they narrowed the bandwidth of their system. Narrowing the bandwidth limits the number of longitudinal modes present and thus tends to reduce the total spontaneous emission in comparison to a laser with no bandwidth control.

A second qualitative description of the induced pulsations has been given by Lau et al.,[38] who introduced the concept of a microwave gain transfer function, $g_p(\omega)$. The function $g_p(\omega)$ describes the conditions necessary for microwave oscillations. For microwave oscillations to occur, $g_p(\omega)$ must be greater than zero over a certain frequency band. The amplitude of $g_p(\omega)$ increases with saturable absorber density and with increased optical coupling from the external cavity. In addition, the frequency at which $g_p(\omega)$ is a maximum increases as current increases and decreases as the density of saturable absorbers increases. These observations tend to explain qualitatively the operation of an injection laser with either saturable absorbers or electron traps operating in an external cavity. If the frequency corresponding to the inverse transit time f_c or a harmonic lies within the gain line, and if the external cavity coupling is high enough so that $g_p(\omega)$ becomes positive, induced pulsations will occur. Varying either the current or the external cavity length will produce frequency shifts in either $g_p(\omega)$ or f_c and lead to changes in the amplitude of the induced pulsation.

C. EXPERIMENTAL RESULTS WITH NONPULSING SEMICONDUCTOR LASERS
    OPERATING IN AN EXTERNAL OPTICAL CAVITY

This section describes the characteristics of nonpulsing injection lasers operating in an external cavity. Figures 24 and 25 display typical light

63

10138 3R1

$I - 1.35 I_{th}$

0.01 GHz   1.8 GHz

RELATIVE POWER 5 dB/DIV

$I = 1.45 I_{th}$

1.7 GHz   4.1 GHz

$I = 1.6 I_{th}$

1.7 GHz   4.1 GHz
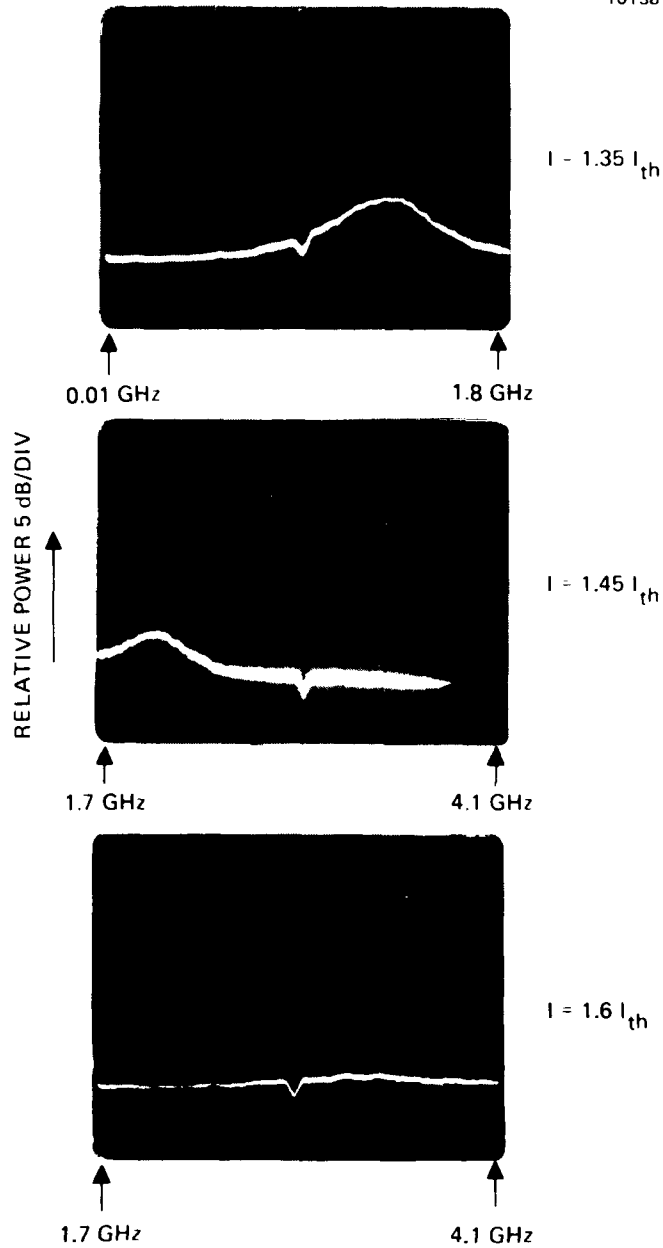
Figure 24.
Experimental light output versus frequency plots
for the BH-NP. The plot gives the noise frequency
response versus current. No external cavity is present.
Similar plots are obtained for the CSP-NP. The reader
should note the relatively broad noise resonance.

64

10138-5R1

I = 1.05 I_th

RELATIVE UNITS 10 dB/DIV

I = 1.11 I_th

I = 1.25 I_th

0.01 GHz   1.8 GHz
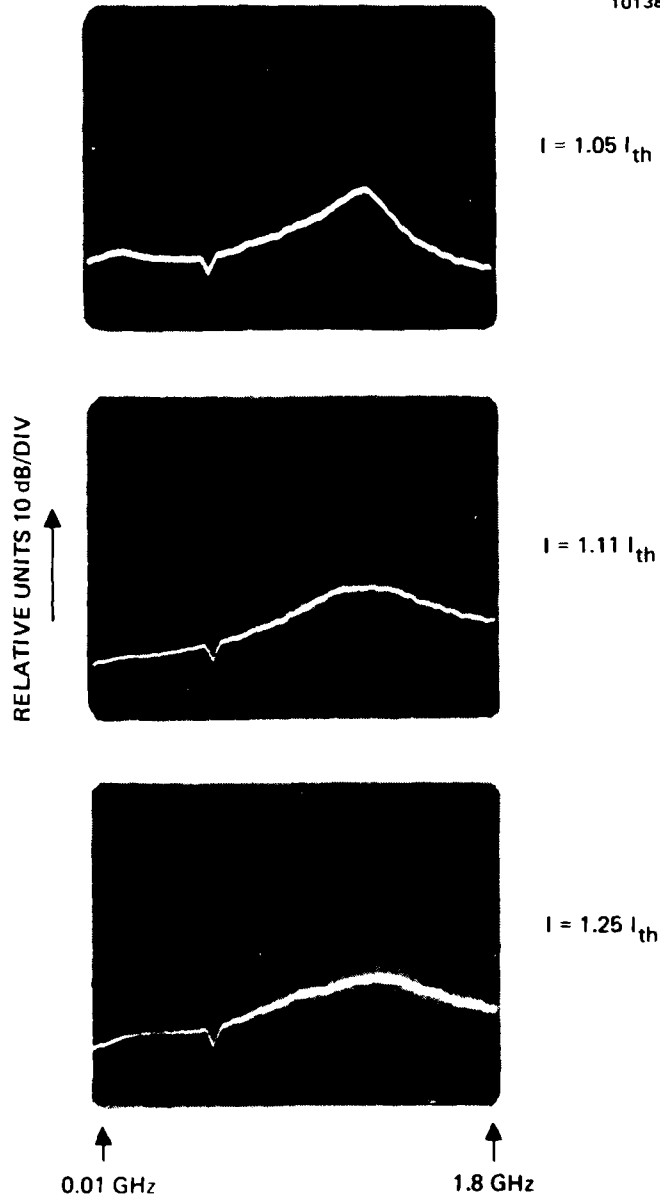
Figure 25.   Experimental light output versus
frequency plots for the S-CDH-NP.
No external cavity is present.

65

output versus frequency plots for various nonpulsing lasers. Several observations can be made. Every laser exhibits a relatively broad noise resonance that occurs above 500 MHz and varies with current. In the BH-NP and the CSP-NP (not shown), the amplitude of the noise resonance decreases as current increases above threshold. This is the expected response for a well-behaved laser. For the CDH lasers, the noise resonance does not decrease as current increases and may actually increase somewhat. This last behavior is similar to that reported by Hakki[31,42] and could be related to an unsaturated mode gain. Figure 26 displays light output versus frequency plots when an external cavity is aligned with the lasers previously discussed. These photographs show that resonances corresponding to harmonics of f_c can be induced. The resonance bandwidth is typically 50 MHz. The significant low-frequency noise in single-mode lasers (S-CDH-NP, CSP-NP) broadens and destabilizes the induced resonance. The low-frequency noise is detrimental to the stabilization of the light output and to the locking action of an external rf input. We believe that the low-frequency noise is related to the longer coherence length of the single-mode laser. If we operate the lasers above the shaded region of Figure 20, the induced resonances broaden significantly (≥ 100 MHz). To attempt to mode lock the injection laser, an external rf signal was introduced into the laser. The frequency of the rf signal was adjusted to correspond to the inverse transit time f_c. Photographs displaying the light output are shown in Figure 27. It is clear from the figure that the pulse widths attained are relatively broad ($\tau_{p_{1/2}} \simeq 300$ to 400 psec) except for the M-CDH-NP. The modulation depth is typically 50 to 100%. It is always possible to obtain pulsations by applying a large rf signal and operating the laser near threshold. However, this phenomenon is predicted by the conventional rate equations[43] and is produced by harmonic distortion. In this mode of operation, the pulse amplitude and pulse width are relatively insensitive to frequency (over a 100-MHz bandwidth). The short pulse widths ($\tau_{p_{1/2}} = 200$ psec) obtained with the M-CDH-NP lead us to believe that this laser may have a higher density of either saturable absorbers or electron traps. However, the density is not high enough to produce pulsations in the isolated laser. The same laser without an external cavity produces pulses having widths of ∿300 psec, which is lower than

(a)   I = 73 mA
       L = 22.2 cm

(b)   I = 81 mA
       L = 20.95

       1.7 GHz   4.1 GHz

(c)   I = 57 mA
       L = 21.9 cm

0.01 GHz   1.8 GHz
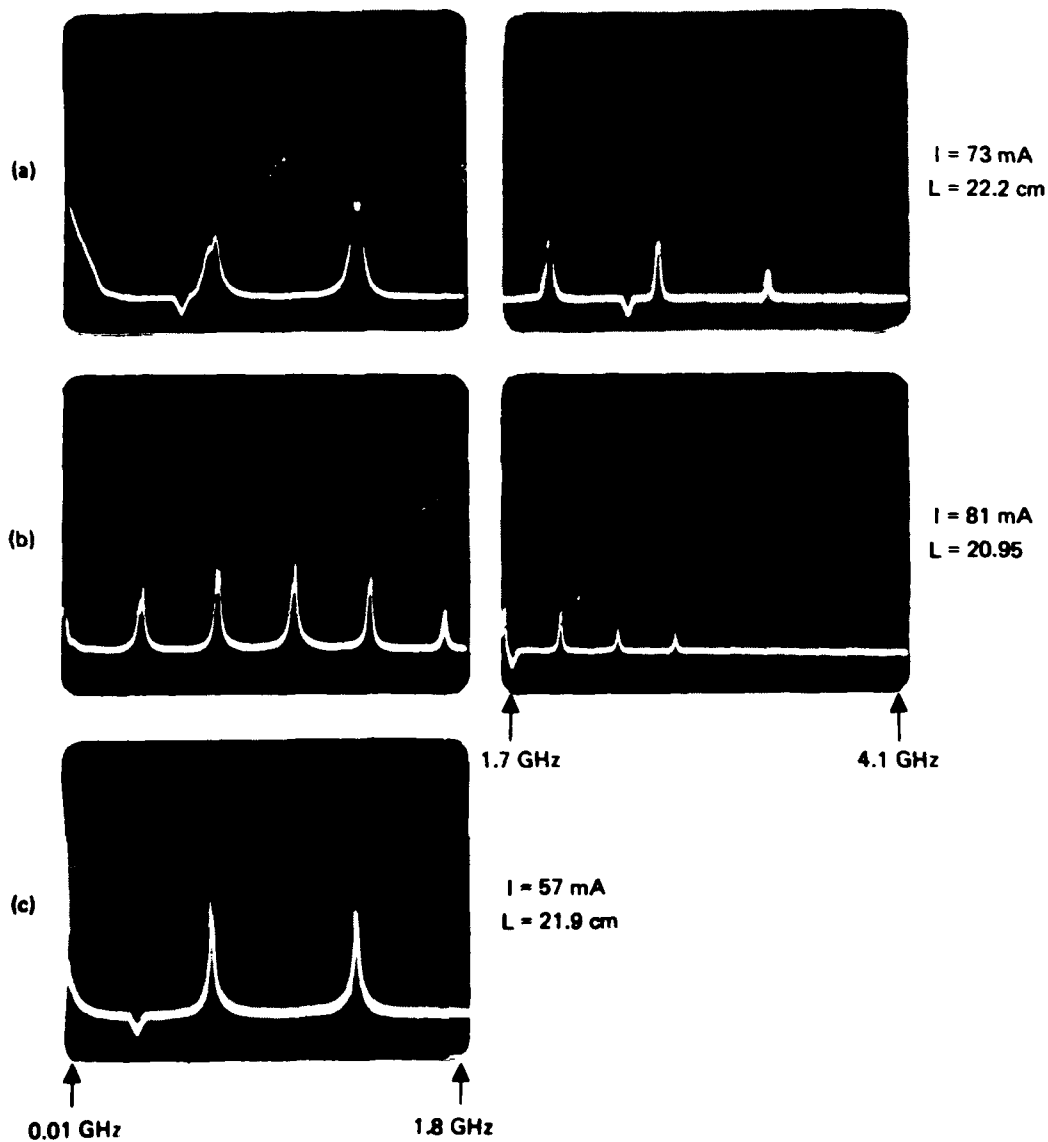
Figure 26. Experimental light output versus frequency plots when an
            external cavity is aligned with the lasers described in
            Figures 29 and 30. (a) S-CDH-NP, (b) M-CDH-NP, (c) CSP-NP.

67
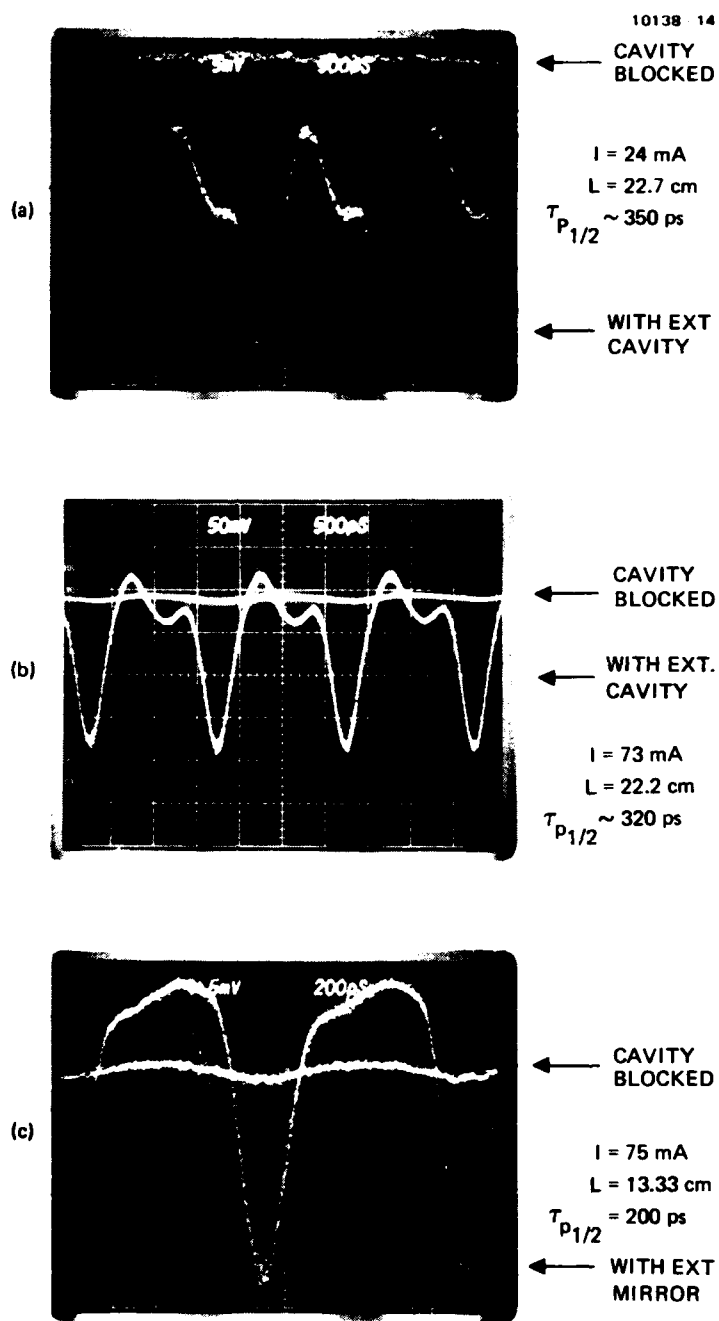
Figure 27. Experimental temporal display showing the light output when the lasers described in Figures 29 and 30 are operated in an external cavity and modulated at f_c. (a) BH-NP (similar results are obtained for the CSP-NP), (b) S-CDH-NP, (c) M-CDH-NP. (No B&H amplifier was used.)

68

for any of the other nonpulsing lasers tested. It appears plausible that lasers with a high density of electron traps or saturable absorbers are more apt to emit short pulses when driven with an rf source. This should occur whether the laser actually self-pulses or not. In contrast, there appears to be some correlation between lasers with a regular frequency response (BH-NP, CSP-NP) and the inability of those lasers to emit short pulses.

D. EXPERIMENTAL RESULTS USING SEMICONDUCTOR LASERS HAVING EITHER A NARROW-BAND NOISE RESONANCE OR SELF-PULSATIONS OPERATING IN AN EXTERNAL OPTICAL CAVITY

This section describes the dynamic characteristics of lasers having either a narrow-band noise resonance or self-pulsations operating in an external optical cavity. Figures 28 through 30 show typical photographs of light output versus frequency as a function of current for various types of lasers displaying sharp narrow-band resonances. The measurements were taken without an external cavity. Note the sharp resonance compared to the lasers described in Figures 24 and 25. The sharp resonance develops at a current slightly above threshold, and, in some of the lasers, the output breaks into a self-oscillation similar to that reported by previous workers.[44,45] The bandwidth of the resonance is typically less than 10 MHz, except for the CSP-SP, which has a $\sim$25 MHz bandwidth. When these lasers are operated in an external cavity and the current lies within the shaded region of Figure 20, we are able to induce sharp resonances at the inverse transit time f_c or a harmonic. This is shown in Figure 31. The bandwidth of the induced resonance can be less than 1 MHz, and blocking the external cavity quenches the resonance.

For the lasers described in Figure 31, we can induce a sharp pulsation of the light output when the current is modulated at the inverse transit time f_c. In some cases, a modulation of the light output occurred at $2f_c$. The frequency bandwidth for the interaction was typically a few megahertz. The pulse outputs for several lasers are shown in Figures 32 and 33. Note that the pulse width is detector limited and the modulation depth is close to 100% for those lasers having a sharp narrow-band noise resonance (Figures 28 and 29). We have obtained efficient mode-locked pulses with frequencies ranging from 400 MHz to 1.2 GHz, by using the experimental setup described in Figure 19(b)
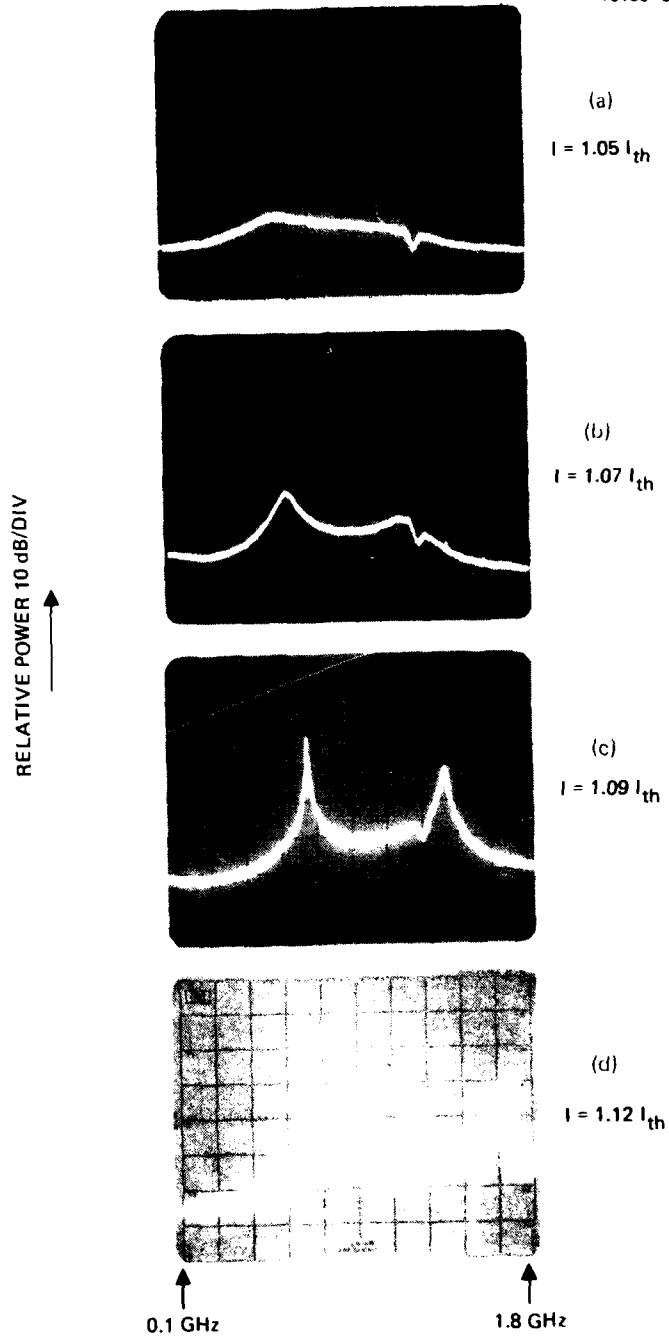
Figure 28. Experimental light output versus frequency plots for the BH-SP laser. No external cavity is present. The reader should note the relatively narrow band noise resonances.

(a)

$I = 1.16 I_{th}$

(b)

$I = 1.18 I_{th}$

RELATIVE UNITS 10 dB/DIV

(c)

$I = 1.20 I_{th}$

0.01 GHz   1.8 GHz

(d)

(e)

0.01 GHz $I = 1.23 I_{th}$ 1.8   0.01 GHz $I = 1.25 I_{th}$ 1.8 GHz
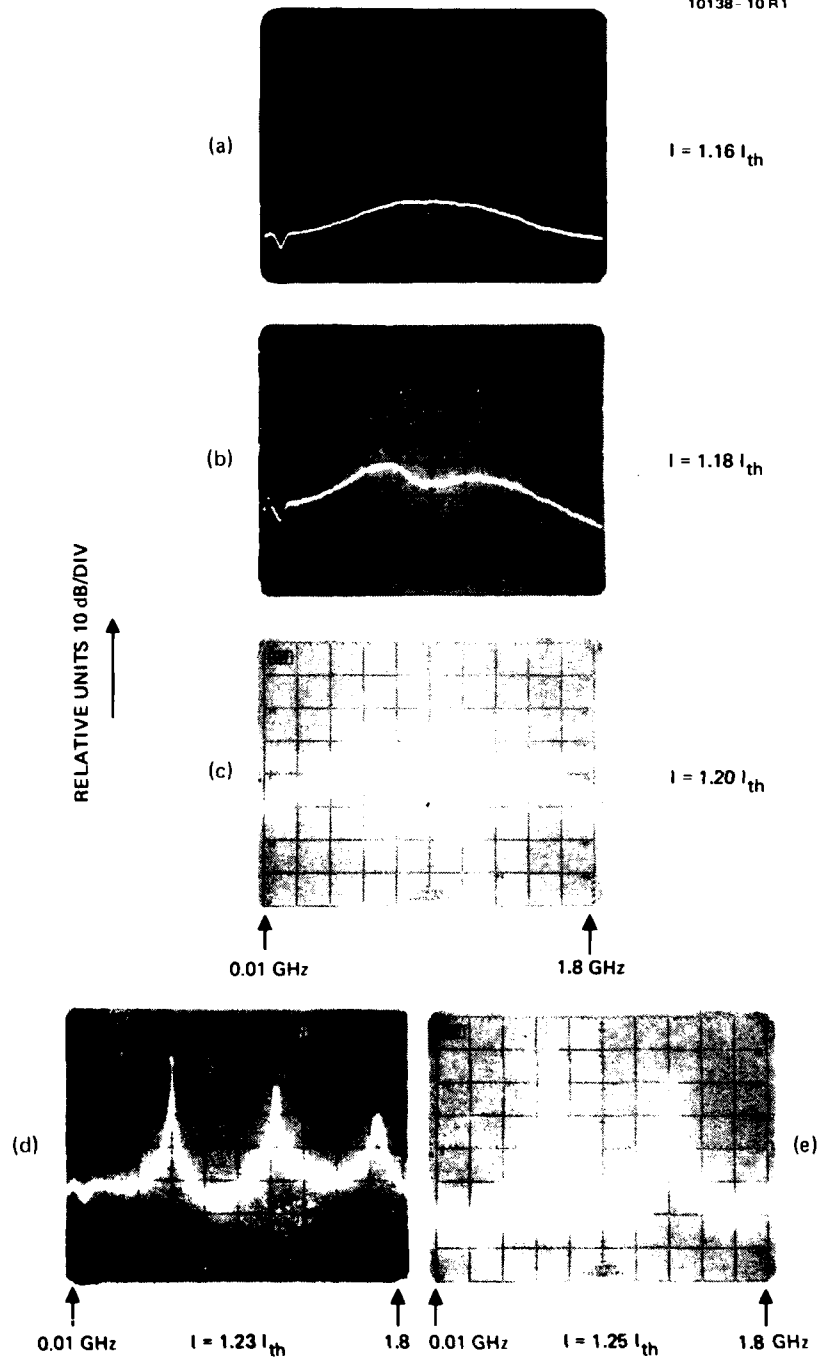
Figure 29.   Experimental light output versus frequency plots for the G.O.-SP laser. No external cavity is present.

71
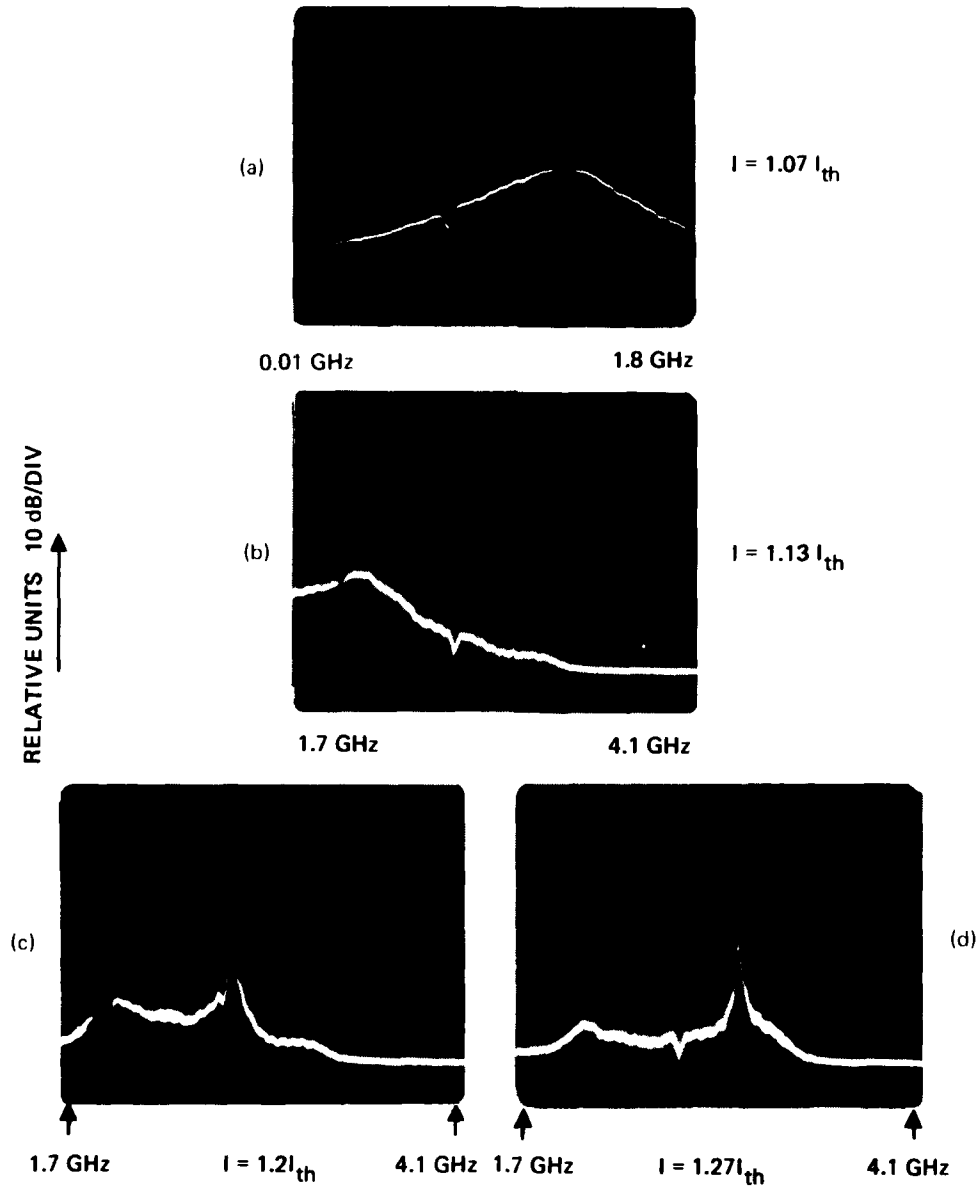
Figure 30. Experimental light output versus frequency for the CSP-SP laser. No external cavity is present.
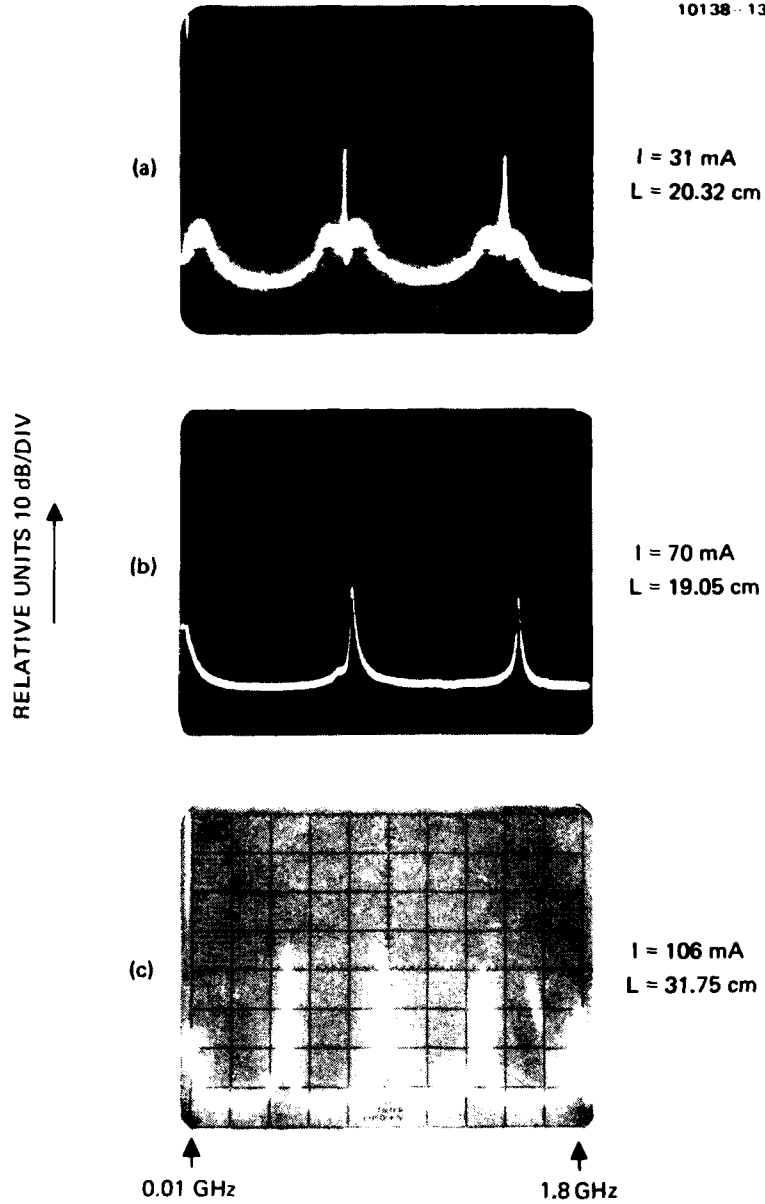
Figure 31. Experimental light output versus frequency
plots when an external cavity is aligned
with the lasers described in Figures 33
through 35. (a) BH-SP, (b) CSP-SP,
(c) G.O.-SP.

73

(a)

I = 72 mA

L = 23.5 cm

$\tau_{P_{1/2}}$ = 300 ps

(b)

I = 31 mA

L = 22.9 cm

$\tau_{P_{1/2}} \leq$ 200 ps

(c)

I = 107 mA

L = 17.15 cm

$\tau_{P_{1/2}} \leq$ 200 ps
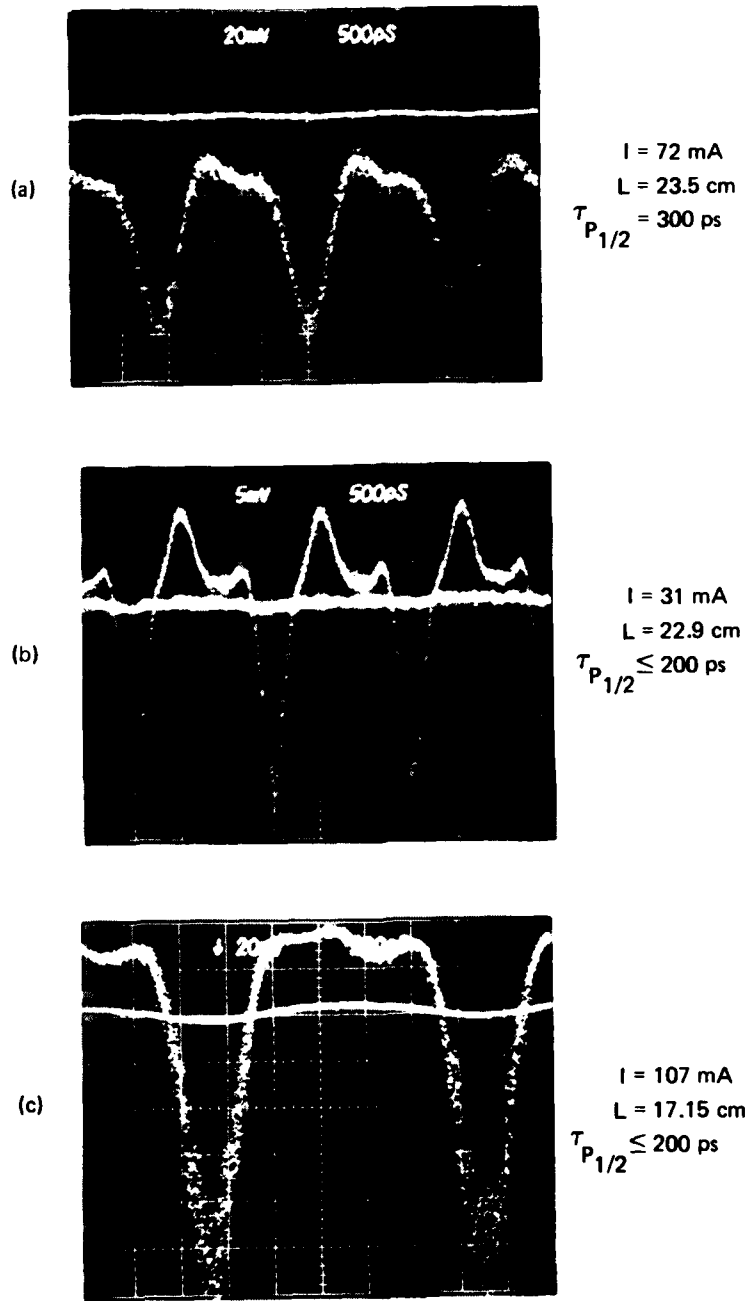
Figure 32. Experimental temporal display showing
the light output when the lasers
described in Figures 33 through 35 are
operated in an external cavity and
modulated at f_c. (a) CSP-SP, (b) BH-SP,
(c) G.O.-SP. (No B&H amplifier was used.)

74

(a)

I = 105 mA
L = 30.48 cm
$\tau_{P_{1/2}} \leq 200$ ps

(b)

I = 97 mA
L = 30.48 cm
$\tau_{P_{1/2}} \leq 200$ ps
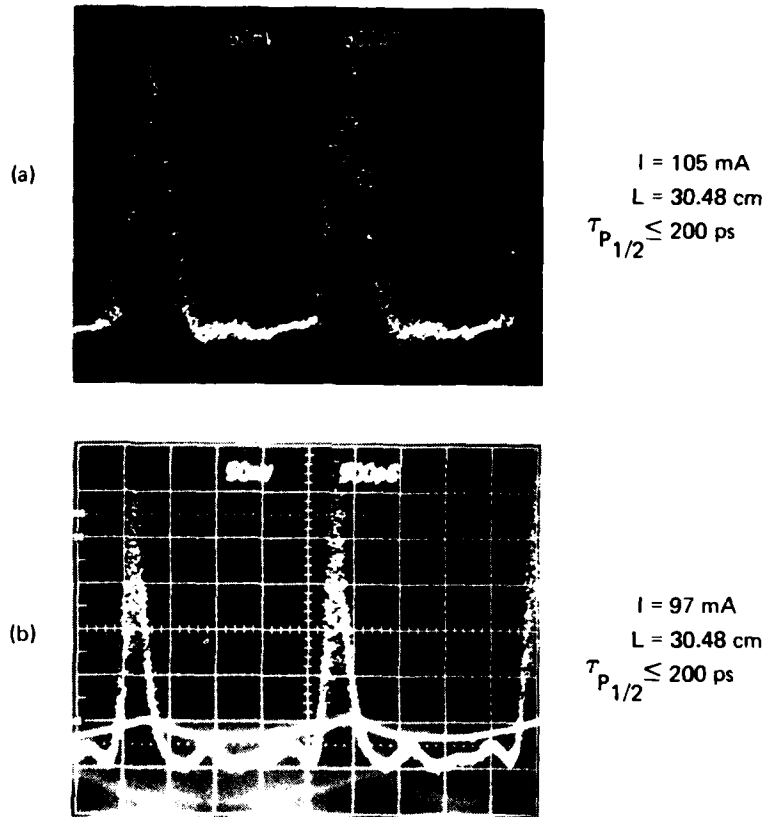
Figure 33. Experimental temporal display showing
the light output in a laser with a high
density of saturable absorbing defects,
and operating in an external cavity.
(G.O.-SP). (a) No modulation current
applied, (b) with modulation current
at f_c.

75

and the lasers described in Table 2. In earlier experiments using the spherical cavity geometry and different laser diodes than those in Table 2, we were able to obtain mode-locked pulses at frequencies of 1.5 GHz and 3 GHz. The optimum frequency depends on the actual laser structure used.

The amplitude, pulse width, and frequency of the mode-locked pulses depend on several factors. First, assuming that lasers displaying a sharp narrow band noise resonance have a high density of saturable absorbing defects,[31] then it follows from Section 4-B that the process can be described using either the small-signal microwave gain concept or the numerical calculations with saturable electron traps. In either case, pulsations can be induced when (1) the density of saturable absorbers is high, (2) the optical coupling from the external cavity is above a certain level ($R_f > 0.1$), and (3) one of the induced cavity harmonics falls within the positive gain line. We expect the amplitude, pulse width, and frequency of the induced pulsations to vary both with external cavity length and injection current. In lasers where the noise resonance bandwidth is comparatively wider (Figure 30) than the lasers described in Figures 28 and 29, we find broader mode-locked pulses ($\tau_{P_{1/2}} \sim 400$ psec), as shown in Figure 32(a). In strongly self-pulsing lasers with very well defined noise resonances, it is possible to induce pulsations without an external rf signal (shown in Figure 33). Blocking the external cavity quenches the mode-locked pulses, while applying an rf signal at f_c tends to stabilize and possibly narrow the pulses. This result implies a type of passive mode locking and is similar to the observations made by Ippen[21] et al. and Paoli et al.[46] Figure 34 shows the effect of varying the external cavity length and the injection current on the output characteristics of a GO-SP laser. Note the resonant behavior for the amplitude of the pulsations as we vary the injection current (Figure 34(a)). In regions far from the optimum current, the pulse width tends to broaden significantly ($\tau_{P_{1/2}} \simeq 400$ psec). Figure 34(b) shows the effect of varying the length of the external cavity. For lengths greater than 30 cm, the induced pulsation occurs at the second cavity harmonic (c/L). Comparison of the experimental results (Figure 34) with the numerical calculations (Figures 22 and 23) shows good agreement. The slight discrepancies for the length were the maximum pulse amplitude occurs can be corrected by assuming a slightly lower electron trap density.

76

Figure 34(a).
Experimental pulse
amplitude versus
current. Note the
broadening of the
pulsewidth from
J below 1.03 J_{th} and
above 1.1 J_{th}.

L $\cong$ 22.85 cm

f_o = 639 MHz

G.O. - SP

PULSE BROADENS
TO 400 ps

PULSE BROADENS TO 400 ps

RELATIVE AMPLITUDE

(J/J_{th})

I = 1.07 I_{th}

G.O. - SP

$f = \dfrac{c}{L}$ BRANCH

$f = \dfrac{c}{2L}$ BRANCH

RELATIVE AMPLITUDE

EXTERNAL CAVITY LENGTH (L), cm
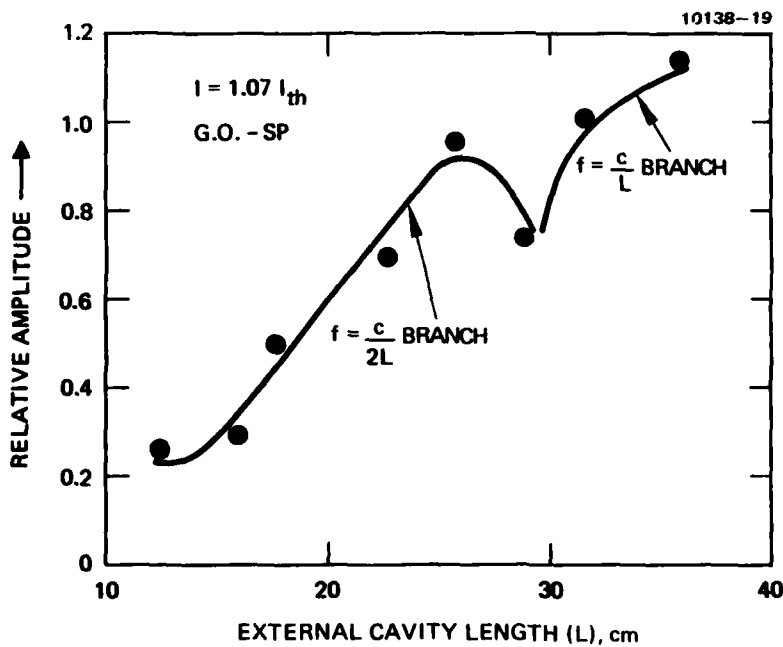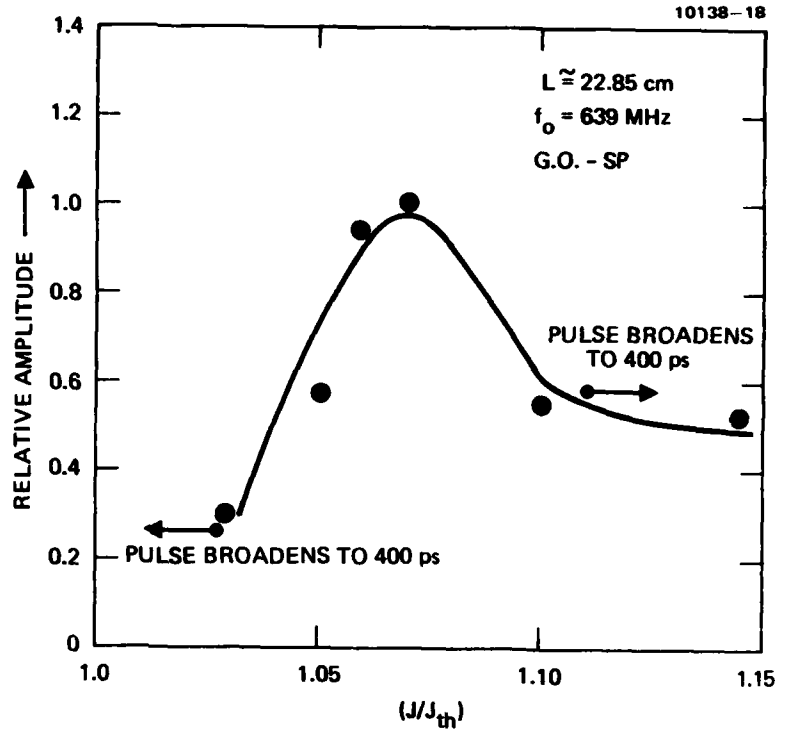
Figure 34(b).
Experimental pulse
amplitude versus
external cavity
length. Note that
the frequency of the
mode-locked pulses is
$c_o/2L$ for L < 30 cm,
while it is c_o/L for
L > 30 cm.

77
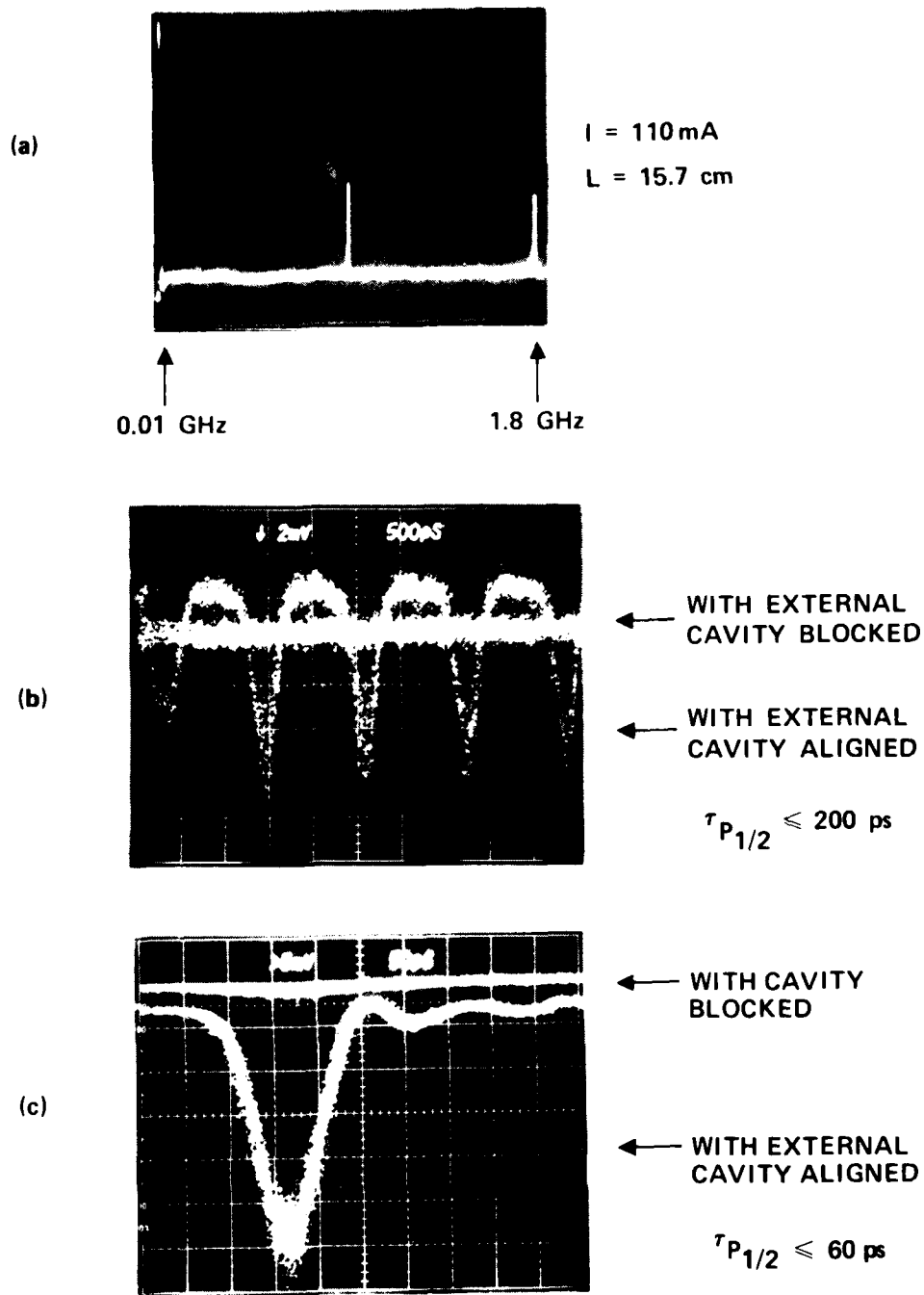
Figure 35. Experimental light output plots for an AR coated laser-external cavity combination. (a) Experimental light output versus frequency with the external cavity aligned. Note the sharp induced resonance. (b) Temporal display when an rf signal with a frequency corresponding to f_c is applied to the laser. The laser used was the same as that described in Figure 38. (No B&H amplifier was used). (c) High resolution temporal display taken with a spectra physics 403B detector.

Figure 35 describes the temporal output obtained after we AR-coated one facet (using a sputtered one-quarter wavelength Al_2O_3) of the injection laser described in Figure 33. We have been able to obtain detector-limited pulses with ~ 1 GHz repetition rate for the AR-coated laser-external mirror combination. The bandwidth for the mode-locking was less than 5 MHz. The threshold current of the AR-coated laser increases from 105 mA (no AR coating) to 122 mA (after the AR coating). Using Eqs. (3) through (5) from Ref. 13, we calculate reflectivity of the AR-coated facet to be 4 to 6%. The maximum repetition rate for the mode-locking is apparently limited by the injection laser and not by the external cavity length. Reducing the external cavity length to below 13 cm ($f_c = 1.15$ GHz) decreases the pulse amplitude at f_c and causes the mode-locking frequency to jump to a lower value ($f \simeq 1/2$ c/2L). We were also able to increase the external cavity length beyond 32 cm without observing a jump in frequency. However, the pulse amplitude is very unstable beyond this length.

In Section 4-B we discussed the model used to describe an injection laser with saturable absorbers operating in an external optical cavity. We stated that the model does not include the effects of multilongitudinal modes and the possible coupling between them. To access the possible correlation between the longitudinal modes of the laser and mode locking, we have measured the spectral width of the lasing emission for all the lasers used. These data are summarized in Table 2 (under the longitudinal mode heading). We have observed that only in those lasers having either a narrow-band noise resonance or self-pulsations and also having a relatively wide spectral width ($\Delta\lambda_{1/2} > 50$ Å) can we obtain pulses that are detector limited and have 100% modulation depth. We have also observed that "good" mode locking cannot be obtained in lasers having a narrow-band noise resonance and a narrow spectral width ($\Delta\lambda_{1/2} < 10$ Å). In the latter case, the temporal output resembles Figure 32(a), and a significant amount of low frequency noise is present. However, we have also observed that the narrow-band noise frequency f_p occurs in these lasers at a very high value ($f_p > 1$ GHz) and has a very rapid variation with current compared to lasers having a wide spectral width. Furthermore, the amplitude of the noise resonance begins to decrease after a certain

79

drive current. A plot showing the variation of narrow-band noise resonance frequency versus current for the various types of lasers is shown in Figure 36. Note that the variation of f_p with current is quite different for those lasers having a narrow spectral width than for those with a wider spectral width. Several characteristics are worth noting. First, the pulsation frequency is higher for lasers having a narrow spectral width. Second, there is a turning point in the curves where the pulsation frequency changes very rapidly with current. If we assume that all the lasers are identical except for the density of saturable absorbers, then the lasers with the lower pulsation frequency will have a higher density of saturable absorbers.[13,28] This observation suggests that effective mode locking occurs only in lasers having a minimum saturable absorber density. Of course, this minimum depends on the amount of optical coupling from the external cavity, as has been previously calculated.[37,38] Furthermore, the effect of the longitudinal mode coupling in the external cavity is to significantly reduce the pulse width as compared to what would be calculated using the model described in Section 4-B. Ippen et al.[21] recently observed pulses with 5 psec width using an external cavity geometry. However, they observed that the lasers used did not show any self-pulsations. Our observations are not consistent with these results.

Thus far in our discussion, we have not mentioned the temporal stability of the mode-locked pulses. In some of the lasers tested, the mode-locked pulses degrade little over a 24-hr period, and the alignment of the external cavity can be maintained with minor mirror adjustments. But in other lasers, the degradation is significant. Increases of 10 to 20% in the threshold current have been observed after operation of a few tens of hours. Increases in the low-frequency noise, which makes it increasingly difficult to achieve good rf locking action have also been observed. In one laser, with detector-limited pulses and 100% modulation depth, the light output degraded rapidly after 1 hr of operation in an external cavity. An examination of the laser facets revealed a blackening of the facet and well-defined cracks, features indicative of catastrophic facet damage. We do not yet understand the cause of this degradation. However, it is worthwhile to point out that the peak powers obtained during mode locking can be very high (0.5 to 1.0 W) and could possiblly exceed the power desnity required for catastrophic facet damage. More work is needed to clarify this point.
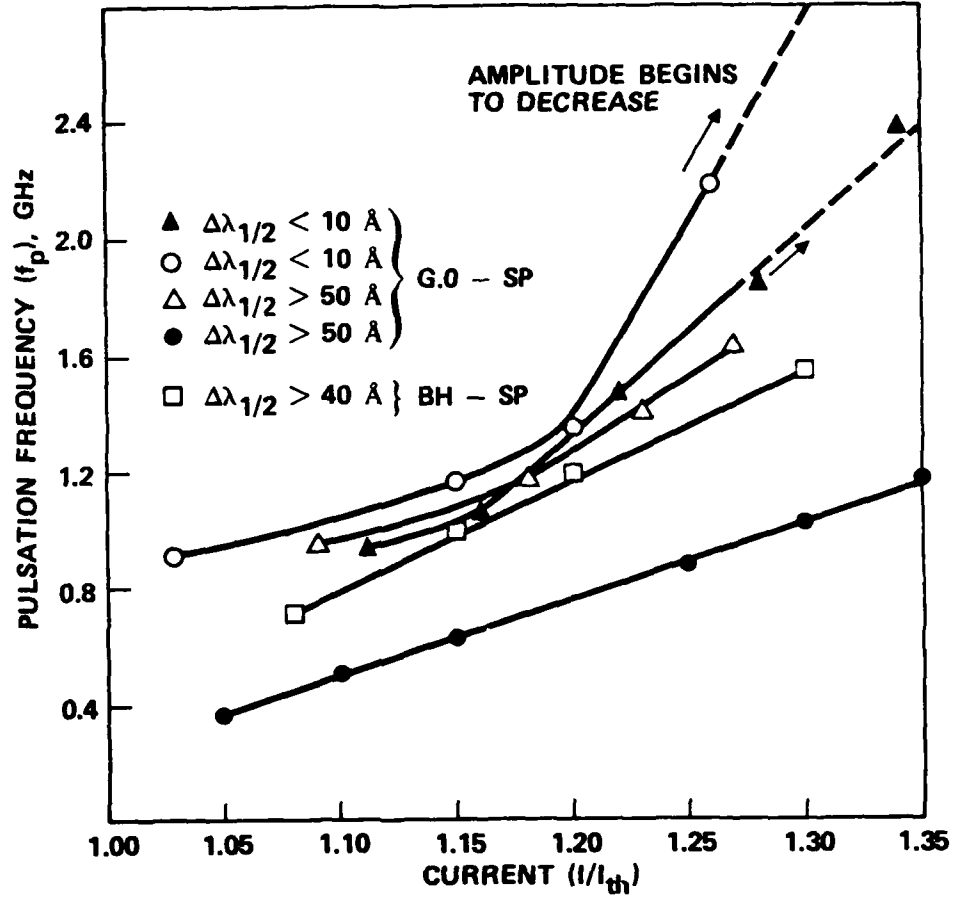
Figure 36.   Experimental plot showing the frequency corresponding to the fundamental component of the narrow band noise resonance as a function of dc drive.

81

E.   TIME MULTIPLEXING OF THE LIGHT OUTPUT

Figure 37 shows the experimental arrangement for the multiplexing of the light output. (The laser-external geometry is described in Section 4-A.) The multiplexer consists of a pair of prisms and a beam splitter. The light output from the laser is split using the beam splitter and recombined after a suitable time delay Δt. To double the frequency of the light output requires a Δt of $1/2f_c$. Figure 38 shows the temporal light output before and after the multiplexing. The highest frequency we have obtained after the multiplexing is >2.0 GHz. We have also examined the light output using a spectrum analyzer and have found that the fundamental frequency at f_c can be suppressed by 40 dB by properly controlling the time delay.

F.   DELIVERABLE MODE-LOCKED LASER UNIT

In Figure 39 we show the mode-locked laser unit that was recently delivered to the Naval Research Laboratories in Washington, D.C. A schematic of the unit is shown in Figure 40. The various sub-elements are schematically shown in Figure 40. The rail was purchased from the Burleigh Co. The special attachments for the various microscope objectives and the laser assembly were machined using Ni. The outer surface was anodized.

G.   OPTICAL FIBER RESONATOR

In the previous subsections we have described the operation of injection lasers with conventional external cavities. In this subsection we briefly discuss the use of an optical fiber external resonator. A schematic of the experimental setup is shown in Figure 41. The fiber resonator consists of a piece of multimode graded index optical fiber with numerical aperture equal to 0.14. Both ends are cleared and one end of the fiber is coated with 2,500 Å of Au to form a reflector. A sperical lens is formed on the other end of the fiber using thermal melting. A typical radius of curvature for the lens is 80 to 120 μm. Using the fiber resonator we have been able to reduce the laser threshold by 6 to 10%. Furthermore, we have been able to obtain mode locking.

10298-6

MOVABLE PRISM

FIXED PRISM

MULTIPLEXER

L_1

L_2

BEAM SPLITTER

OUTPUT

MODE-LOCKED LASER

THE TIME DELAY, Δt, IS

IS GIVEN BY $\Delta t = \dfrac{2(|L_2 - L_1|)}{c_0}$
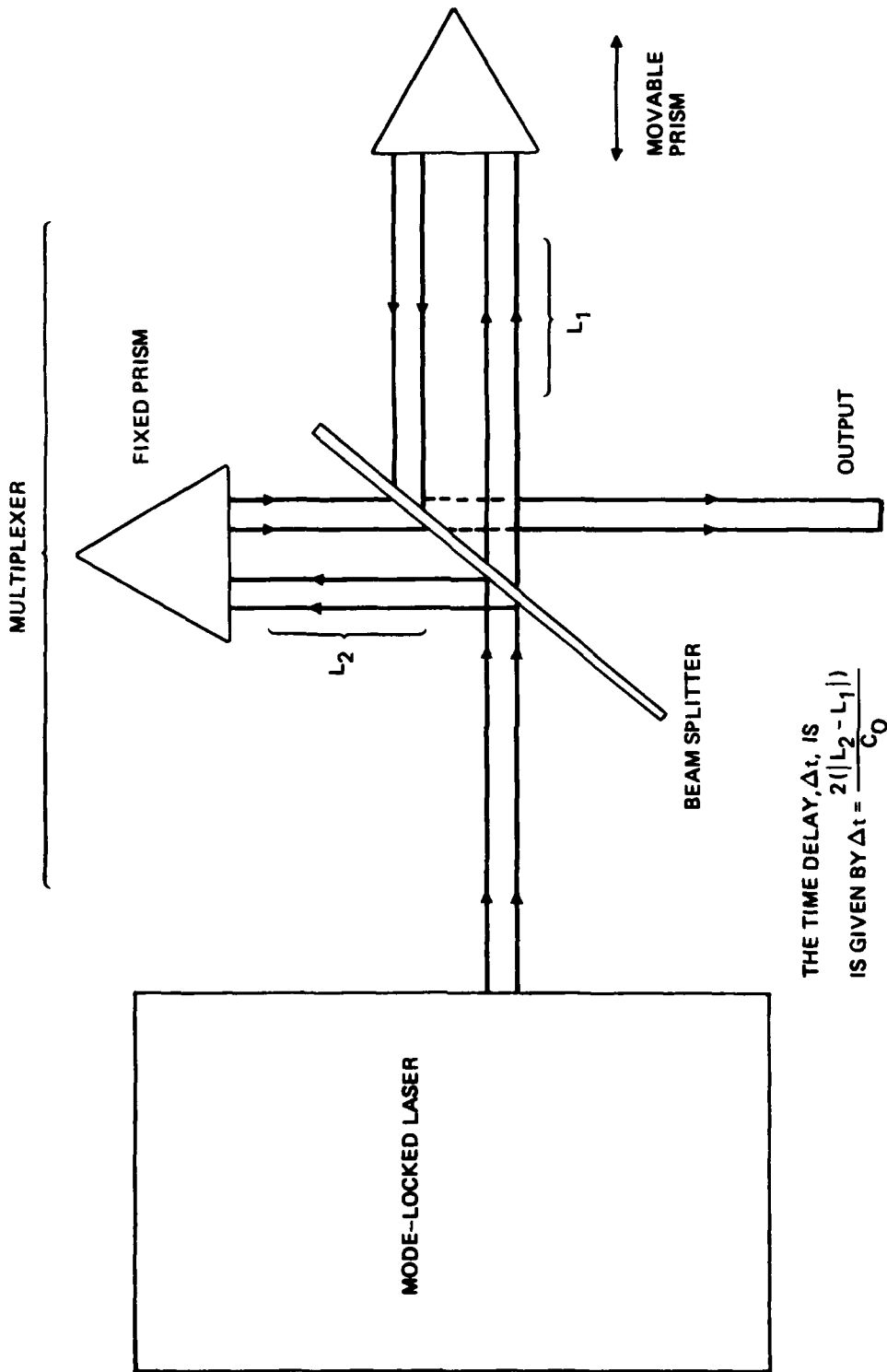
Figure 37. Schematic of the experimental set-up showing a mode-locked laser unit and time multiplexer.

83
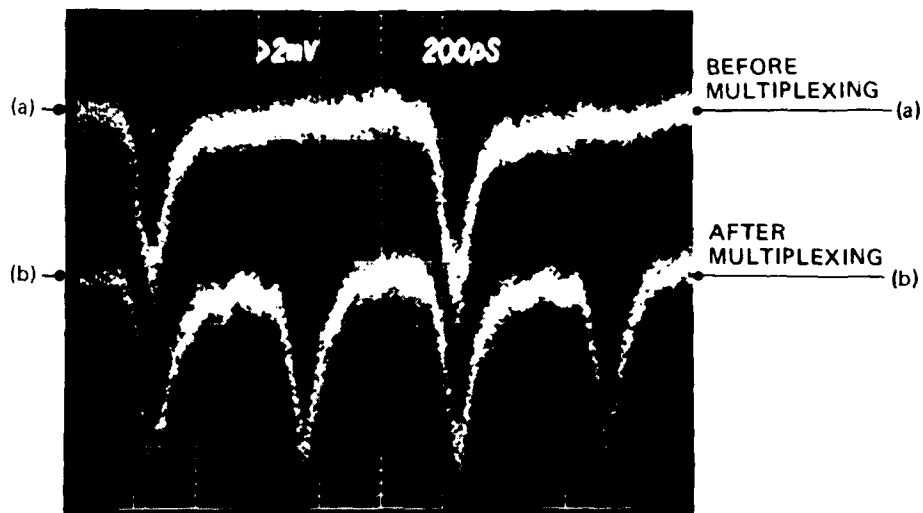
Figure 38.   The photographs above display the output versus time
from a mode-locked GaAs injection laser.   (a) shows
the initial light output from the mode-locked laser,
(b) shows the light output after frequency doubling
has been accomplished.   The frequency doubling is
performed using a combination of prisms and a beam
splitter.   The measurements were taken using a new
detector (IDPC) recently developed at HRL.   The
repetition rate is 2 GHz.

84

10668-8

MODE-LOCKED LASER UNIT
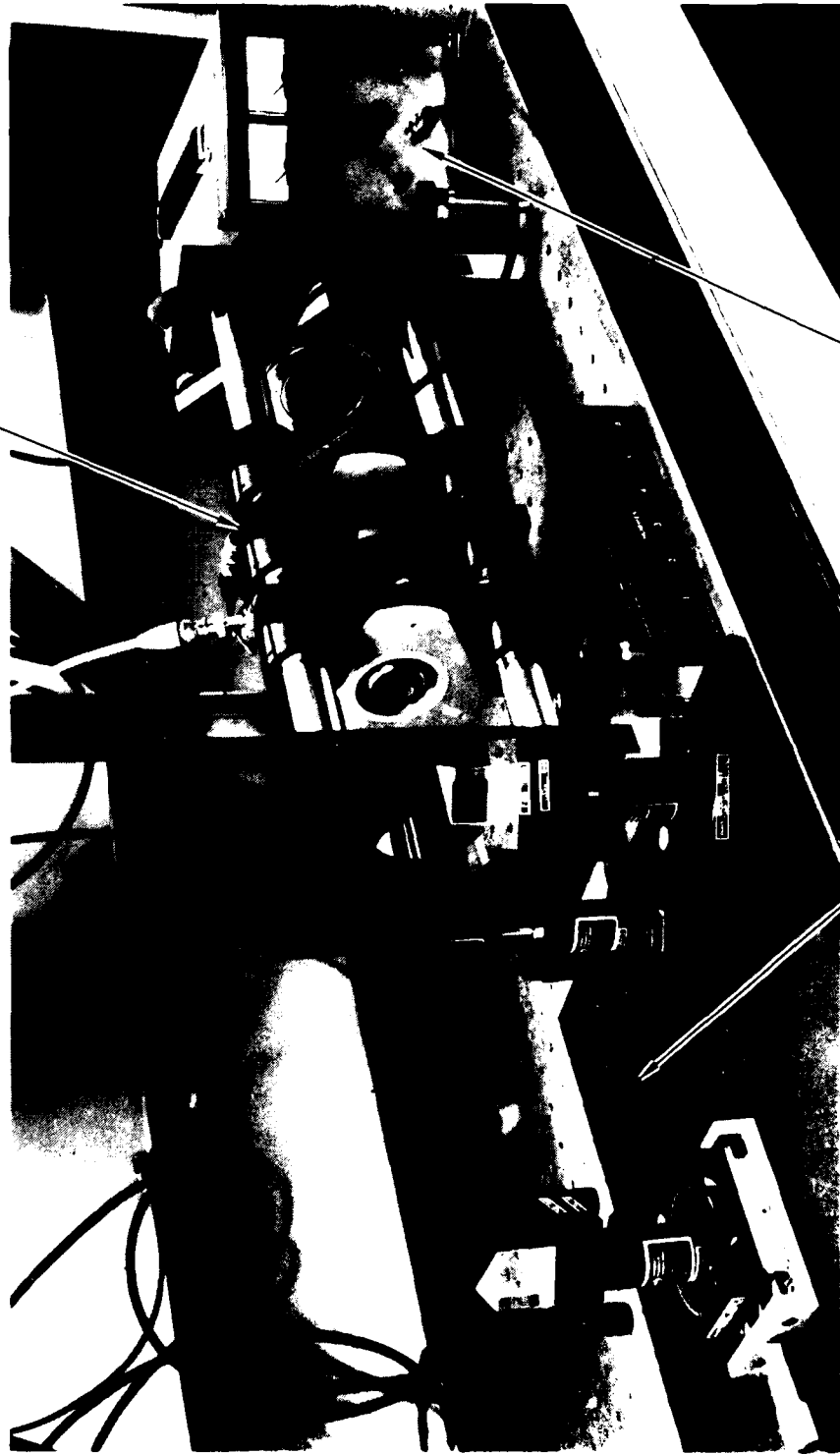
DC POWER SUPPLY

MULTIPLEXER

ML3784

Figure 39. Photograph of the complete mode-locked laser unit, multiplexer and dc power supply.

EXTERNAL CAVITY MIRROR

EXTERNAL CAVITY LENS ASSEMBLY

LASER ASSEMBLY

OUTPUT LENS ASSEMBLY
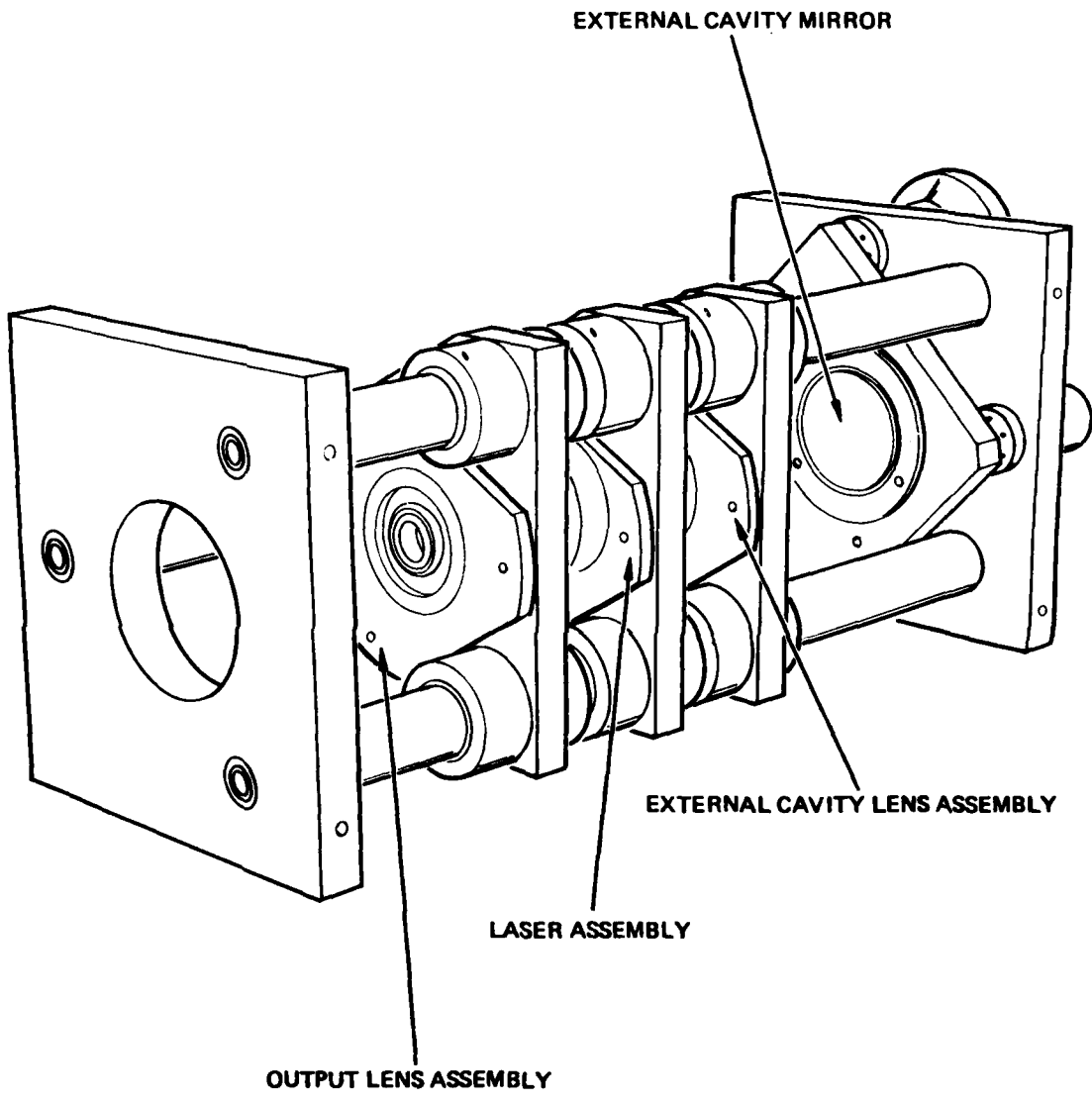
Figure 40.   Schematic of the mode-locked laser unit

8800-1
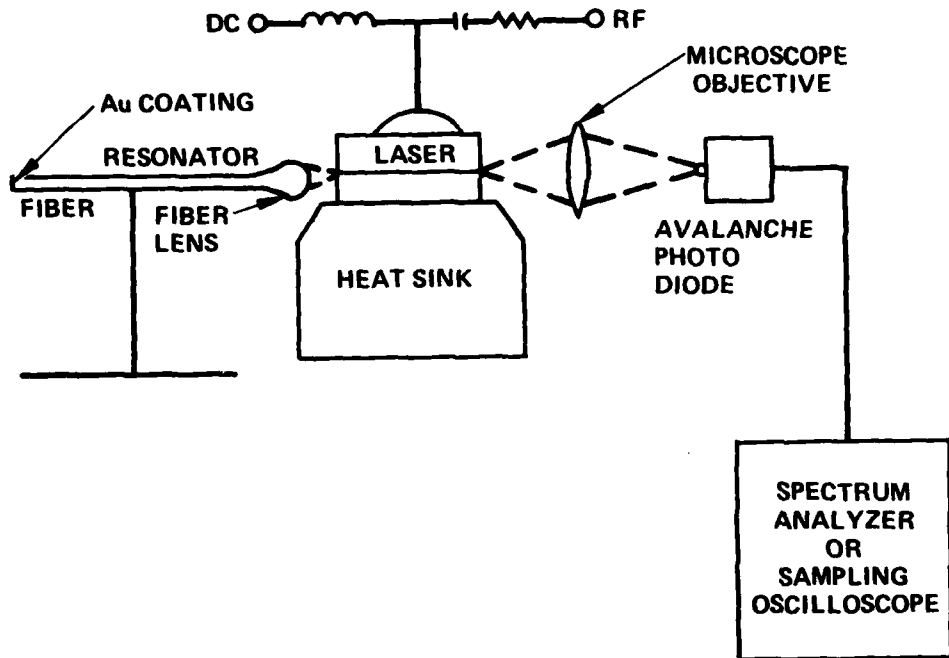
Figure 41. Experimental arrangement showing an optical fiber external resonator.

A typical result is shown in Figure 42. The photograph shows the effect of the fiber on the light output. Alignment of the fiber resonator produces a sharpened output. Depending on the laser structure used (as described in the previous subsections) we can obtain sharp pulsations of the light output. The modulation depth is $\sim$50%. One of the major problems we encountered is the high noise level in the light output, which produces significant jitter. We believe the source of the noise is modal interference effects. Furthermore, the noise level can be reduced by using a polarization preserving single-mode fiber.

H.   CONCLUSION

We have described the operation of injection lasers operating in an external cavity. We found that mode-locking of injection lasers operating in an external cavity is directly related to either an anomalous narrow-band noise resonance or self-pulsations. We have been able to obtain detector-limited pulses (less than 60 psec) with 100% modulation depth and frequencies varying from 400 MHz to 1.2 GHz by operating an injection laser in an external cavity. We have found that the amplitude, pulse width, and frequency of the mode-locked pulses is a strong function of the external cavity length, the self-pulsation frequency (which is related to electron-trap or saturable absorber density), and the injection current. We find little or no mode locking in nonpulsing lasers with a regular noise resonance. Furthermore, it appears that mode locking may be hindered in single-mode lasers as a result of low-frequency noise.

The mode locking in (GaAl)As injection lasers can be qualitatively explained by using the conventional rate equations modified by either electron traps or saturable absorbers and the delayed feedback from the external cavity. The effect of the saturable absorbers on the mode-locking process is similar to the slow saturable absorber present in the passively mode-locked dye laser. The mode-locking frequency can be increased by decreasing the cavity lifetime.

It is worth noting that in some laser systems (like the YAG laser), a combination of active and passive mode-locking techniques leads to stable picosecond pulse generation, while either active or passive mode locking

88

8541-16
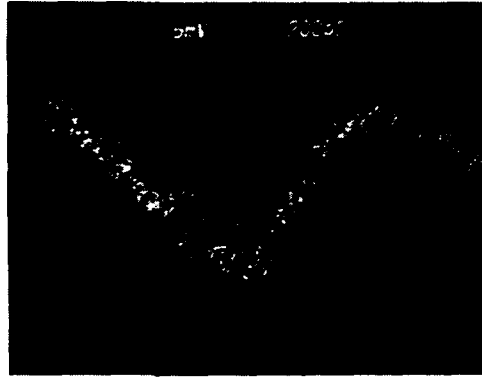
a) NO ALIGNMENT

b) ALIGNMENT

Figure 42.
Output pulse shape of a laser in
fiber resonator (negative going).
The fiber length is 9.3 cm.

89

applied independently of each other does not produce stable ultrashort pulses. We believe the semiconductor laser system may behave in such a manner.

Thus, it appears that the previously reported observations of mode locking in injection lasers were really manifestations of self-pulsations, and therefore related to laser defects. Finally, we believe that mode locking in injection lasers should be relatively easy to accomplish because of the large variety of self-pulsing lasers available. However, it may be possible to deliberately introduce regions of saturable absorption by leaving a portion of the current stripe near the facets unpumped, and selectively diffusing a dopant, such as zinc, in order to control the bandgap. Thus, it may be possible to control the mode-locking frequency and pulse width of the light output by using standard photolithographic techniques.

SECTION 5

HIGH-SPEED OPTICAL DETECTORS AND GUNN DIODES

This section describes our work on the fabrication and characterization of high-speed optical detectors, GaAs conventional and waveguide MESFETs, novel interdigitized photoconductive detectors, and GaAs waveguide Gunn diodes. This section provides a comprehensive evaluation of the important device properties. The realization of microwave-optical systems will require optical detectors that can respond to frequencies beyond 10 GHz. Thus, a thorough characterization of existing commerical and novel optical detectors is essential. This effort can lead to the optimization of detector parameters which will enable operation at frequencies beyond 10 GHz. Optimization of the high-speed detector performance is an important step in improving the optical-microwave interaction of microwave devices, such as MESFETs and IMPATTs, which will be used in optical-microwave applications.

A. COMMERICIAL HIGH-SPEED P-N JUNCTION DETECTORS

Table 3 lists the various commerical p-n junction detectors characterized. The rise and fall times of the detector are basically determined by the $R_L C_j$ time and the carrier transit time. Figure 43 is an idealized equivalent circuit of the detector and the load resistance R_L presented to it. R_j is the reverse-biased junction resistance (typically in excess of 1 MΩ), C_j is the depletion capacitance, R_S is the series or spreading resistance of the junction, L_S is the inductance of the bond wire, and i_{ph} is the photocurrent. Stray capacitance of the amplifier and load have been neglected. If i_{ph} were an impulse (i.e., $i_{ph} = Q_o \delta(t)$, where $\delta(t)$ is the Dirac delta function), the current through the load (neglecting transit-time effects and assuming R_S and L_S to be small) would be

$$i_L(t) = \frac{Q_o}{R_L C_j} S(t) \exp\left(-\left(\frac{t}{R_L C_j}\right)\right) \tag{29}$$

91

Table 3. HRL Response Time Measurements[a] of Various Commerical Picosecond Photodetectors

Manufacturer and Model Number	Type	Material	Spectral Sensivity[b], nm	Quantum Efficiency[b]	Active Area cm2	t_r[a], psec	t_f[b], psec	Comments on Response Time
1. Mitsubish PD1202B	APD	Si	500 to 900	~20% 800 nm	3×10^{-4}	~130	~700	Independent of focusing
2. NEC NDL2102	PIN	Si	500 to 110	~60% 830 nm	3×10^{-4}	~140	~800	tf depends on focusing
3. Opto-Electronics PD 10-01	PIN	Si	300 to 1100	~23% 820 nm	2.5×10^{-5}	~130	~130	Insensitive to focusing, ringing in "back porch"
4. Opto-Electronics PD 10-02 (with Optical Fiber)	PIN	Si	300 to 1100	~23% 820 nm	2.5×10^{-3}	~100	~160	~100 psec flat top observed; detector essentially identical to PD 10-01
5. Spectra-Phys. 403B	Micro-wave PN junction	Si	250 to 1060	Not Specified	Annular region, ~90 µm metallization	~50	~80	Very sensitive to focusing, ringing in "back porch"
6. Telefunken BPW28	APD	Si	450 to 950	~80% 600 nm	3×10^{-4}	~100	~140	Independent of focusing
7. Telefunken S171P	APD	Si	450 to 950	~80% 600 nm	3×10^{-4}	~80	~140	Identical to BPW28, except for mounting
8. Texas Intruments TIED 55	APD	Si	500 to 1000	~50% 800 nm	5×10^{-4}	~100	~400	Independent of focusing
9. Rockwell	APD	GaAs/GaAl/As	600 to 900	≥50% 820 nm	1.6×10^{-5}	60	<100	Very sensitive to focusing

[a] Rise and fall times measured with ~5 psec coherent dye laser pulses at 570 nm, including the response of the Tektronix S4 sampling head (t_r < 25 psec).

[b] Data specified by manufacturer; quantum efficiency specified without avalanche gain.

7429

92
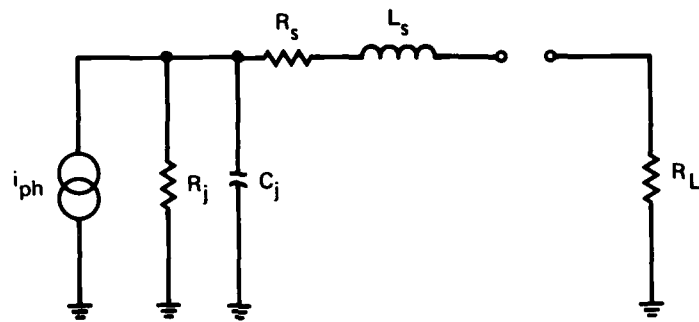
Figure 43.   Equivalent circuit for the detector.

where S(t) is a step function (=0 for t < 0, =1 for t > 0), and Q_o is the total charge of photocarriers collected in the pulse. The decay time (90% to 10%) resulting from RC effects is then

$$t_{f,RC}(90\% \text{ to } 10\%) = 2.2 \, R_L C_j \simeq 100 \text{ psec}$$

for $R_L \simeq 50 \, \Omega$ and $C_j \simeq 1$ pF.

Transit time effects tend to smear the pulse width. If the incident light pulse is $P_o \delta(t)$, the current response (neglecting parasitics) will be

$$i_{ph}(t) = \begin{cases} \dfrac{q\eta}{h\nu} \dfrac{P_o}{\tau} M & 0 < t < \tau \\[2ex] 0 & \text{otherwise} \end{cases} \qquad (30)$$

where η is the detector quantum efficiency (carriers collected per incident photon), $h\nu$ is the photon energy, τ is the carrier transit time, and M is the photocarrier multiplication (M = 1 for a PIN). The transit time is given by

$$\tau = \frac{W}{v} , \qquad (31)$$

where W is the width of the depletion region, and v is the carrier velocity. For high fields (i.e., $E > 10^5$ V/cm), v saturates at 10^7 cm/sec for holes and electrons in GaAs, Ge, and Si. For a depletion region of 10 μm, $\tau \simeq 100$ psec. Thus, the transit and RC times are approximately comparable for commercial high-speed detectors. Figure 44 shows the magnitude and phase response of the detector due to transit time effects.
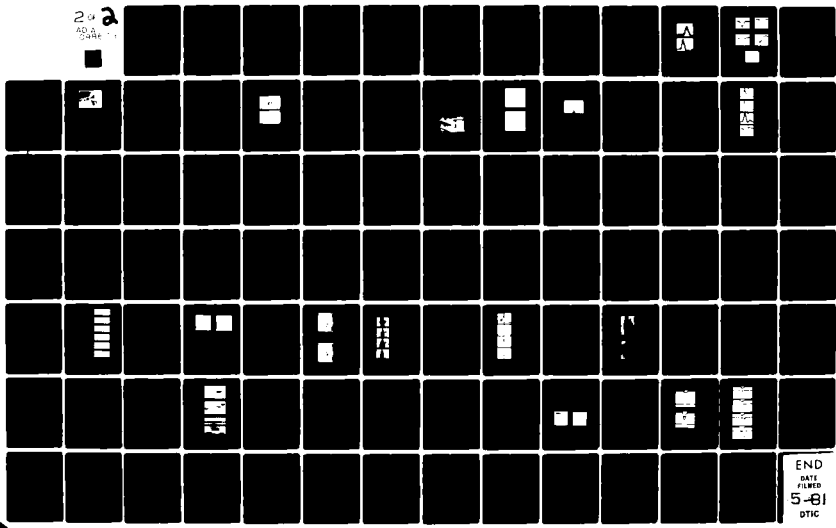
A
867
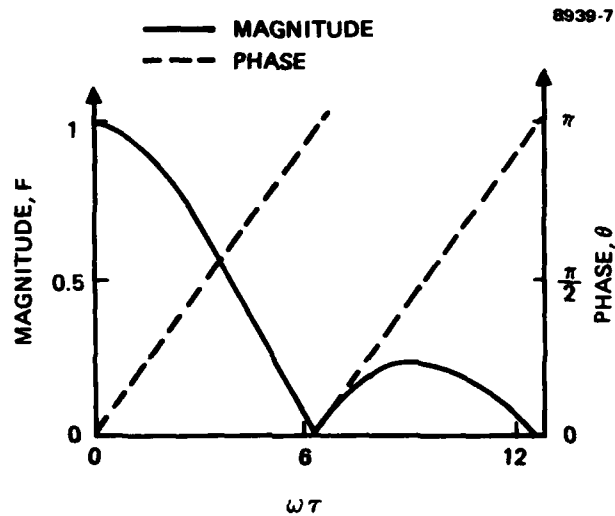
Figure 44. Phase and magnitude of the
transit-time response.

B. DETECTOR BANDWIDTH FOR ANALOG SYSTEM

The detector bandwidth is closely related to its response time. If the optical power is sinusoidally modulated as

$$P = P_o(1 + me^{j\omega t}) \quad , \tag{32}$$

the photodetector response will be

$$i_{ph}(t) = \frac{q\eta}{h\nu} P_o M \left[1 + me^{j\omega t} \left(\frac{1 - e^{-j\omega\tau}}{j\omega\tau} \right) \right] \quad , \tag{33}$$

and the current delivered to the load R_L (assuming only the shunt capacitance C_j) will be

$$i_L(t) = \frac{q\eta}{h\nu} P_o M \left[1 + me^{j\omega t} \left(\frac{1 + e^{-j\omega\tau}}{j\omega\tau(1 + j\omega R_L C_j)} \right) \right] \quad . \tag{34}$$

If the detector is RC limited, the power delivered to the load will have a 3-dB bandwidth of

$$f_{RC} = \frac{1}{2\pi R_L C_j} \quad . \tag{35}$$

For $R_L = 50\ \Omega$, C_j must be 0.5 pF or less to obtain a bandwidth in excess of 6 GHz. R_L can be decreased, but the effects of R_S become more significant as this is done. The -3 dB power point for a transit-time-limited detector is

$$f_\tau = \frac{0.45}{\tau} \tag{36}$$

For a 6-GHz bandwidth, the transit time must be 75 psec or less.

If the detector response can be modeled as $e^{-t/\tau}$ for $t > 0$, then the
-3 dB power point will be

$$f_{-3 \text{ dB}} \simeq \frac{0.35}{t_f} , \qquad (37)$$

where $t_f = 2.2 \, \tau$ is the 90 to 10% fall time. In this case, $t_f \leq 60$ psec for a
6-GHz bandwidth. If the detector is more accurately modeled by a Gaussian
pulse response (i.e., e^{-t^2/τ^2} for all t), the -3 dB power point will be

$$f_{-3 \text{ dB}} \simeq \frac{0.22}{t_r} , \qquad (38)$$

where t_r is the 10% to 90% rise or fall time and must be 35 psec or less for a
6-GHz bandwidth. The data in Table 3 show that the maximum $f_{-3 \text{ dB}}$ frequency
as given by Eq. (37) is ∿7 GHz for the Spectral Physics detector. The minimum
f_{-3dB} frequency is ∿2.5 GHz for the NEC PIN device. Our preliminary conclusion
is that commerical p-n junction detectors operating in the spectral range 0.5
to 0.9 μm can only provide efficient sensitivity for frequencies up to 7 GHz in
analog systems and can respond to pulses with 50 to 100 psec half-widths in
digital systems.

C. GaAs MESFET OPTICAL DETECTORS

This subsection describes our work on the high-frequency optical characteri-
zation of various GaAs MESFETs. This work was undertaken after our initial
results on the sensitivity of GaAs/(GaAl)As waveguide MESFET detectors (See
Section 5-D) suggested that using conventional shorter-gate GaAs MESFETs would
improve performance. Our measurements suggests that photoconductivity is
responsible for the optical response of a GaAs MESFET. This is in agreement

with the experimental results of Gammel and Ballantyne.[46] Thus, the analog response of the MESFET can be expressed as

$$\Delta I'_{DS} (f) = (C)(P_{in}) \left(\frac{\tau}{\tau_{tr}}\right)\left(\frac{1}{1 + (\omega\tau)^2}\right)^{1/2} , \qquad (39)$$

where

$\Delta I_{DS}(f)$ is the detected rf drain-source current

C is a constant which can be fit from experiment

P_{in} is the incident power

τ is the lifetime of the slower injected carrier (holes in this case)

τ_{tr} is the transit time of the faster carrier (electrons in this case)

$\omega = 2\pi f$, where f is the frequency of the modulated incident light.

In Eq. 39, all of the parameters except τ can either be calculated or determined from experiment. The only difficult problem is to calculate the hole lifetime. In our modeling, we assumed that the hole lifetime is primarily determined by surface recombination. This assumption should be valid in GaAs MESFETs without a passivating layer since the surface recombination of a free GaAs surface can be quite high.[47] Furthermore, the amount of surface recombination is a function of the electric field present within the recombination region[48] and thus is a function of the applied gate voltage. The following simple relationship between hole lifetime and surface recombination has been derived by Wang:[48]

$$\frac{1}{\tau} = \frac{1}{\tau_b} + \frac{V_s}{d'} \qquad (40)$$

where τ_b is the bulk lifetime, V_s is the surface recombination velocity, and d' is the effective thickness of the recombination region. The value of d' ranges from d to $1/\alpha$, where d is the thickness of the FET active region, and

98

α is the attenuation coefficient of the incident light. If we assume a very high surface recombination velocity, then Eq. (40) reduces to

$$\frac{1}{\tau} = \frac{V_s}{d'} \tag{41}$$

Since the value of d' is difficult to determine, we will assume it to be an adjustable parameter that can be obtained from the measurements. However, only those carriers generated within the high electric field active region can contribute to the high frequency response. This implies that the active region thickness is approximately equal to d'. Thus, the problem simplifies to the calculation of the surface recombination velocity. The simplest expression for the surface recombination velocity is given by

$$V_s = \frac{V_s'}{\cosh q \left[\dfrac{(V_t - \gamma \, (|V_g| + V_{bi}))}{kT}\right]} \quad |V_g| < V_p \tag{42}$$

$$= \frac{V_s'}{\cosh q \left[\dfrac{V_t - \gamma \, (|V_p| + V_{bi})}{kT}\right]} \quad |V_g| \geq V_p \quad ,$$

where V_p is the pinchoff voltage, and the surface potential is assumed to be altered by the applied gate voltage, which in turn affects the surface recombination velocity. The voltage V_t is a constant, characteristic of the type of surface, and V_{bi} is the built-in voltage. The factor γ is a geometrical factor that takes into account that the voltage at the position where the holes recombine is not equal to the applied gate voltage but is related to the fringing of the voltage around the gate electrode. To simplify the algebra, we assume $V_t \gg \gamma(V_g + V_{bi})$ since we expect γ to be small and V_t is assumed

99

to be the voltage caused by a midgap state ($V_t \approx 0.7$ eV). Eq. (42) reduces to

$$V_s = V_{so} \exp\left\{\frac{\gamma(|V_g| + V_{bi})}{kT}\right\} \quad |V_g| < V_p \qquad (43)$$

$$= V_{so} \exp\left\{\frac{\gamma(|V_p| + V_{bi})}{kT}\right\} \quad |V_G| \geq V_p$$

where kT is the thermal energy (0.026 eV for T = 300°K), and V_{so} is the surface recombination velocity for $|V_g| + V_{bi} = 0$. The value of V_{so} is assumed to be known.[47] The parameter γ can be determined from the experimental ΔI_{DS} versus V_{GS} data and is given by

$$\gamma = \frac{\left(\frac{KT}{q}\right)\ln\left(\frac{\Delta I_{DS_2}}{\Delta I_{DS_1}}\right)}{\left[V_{GS_1} - V_{GS_2}\right]} \qquad (44)$$

Figure 45 shows the variation of detected drain source current ΔI_{DS} versus gate-source voltage $|V_{gs}|$ under dc conditions. The dashed line represents a theoretical fit using Eqs. (39) and (43); the fit is excellent. Note the large detected currents (ΔI_{DS} as high as 20 mA) with only a maximum of 0.9 mW laser optical power. The input power to the GaAs MESFET is actually much less since we expect poor optical coupling to the active region. We believe the traps at the interfaces of the active region cause the large dc response. To better see how the theory predicts the optical response, the detected rf current $\Delta I'_{DS}$ (f = 2 GHz) is plotted versus $|V_{GS}|$ in Figure 46 for two different types of GaAs MESFETs. The dashed curve is a theoretical fit. The agreement between theory and experiment appears to be adequate over a certain range of frequencies.

10298-3
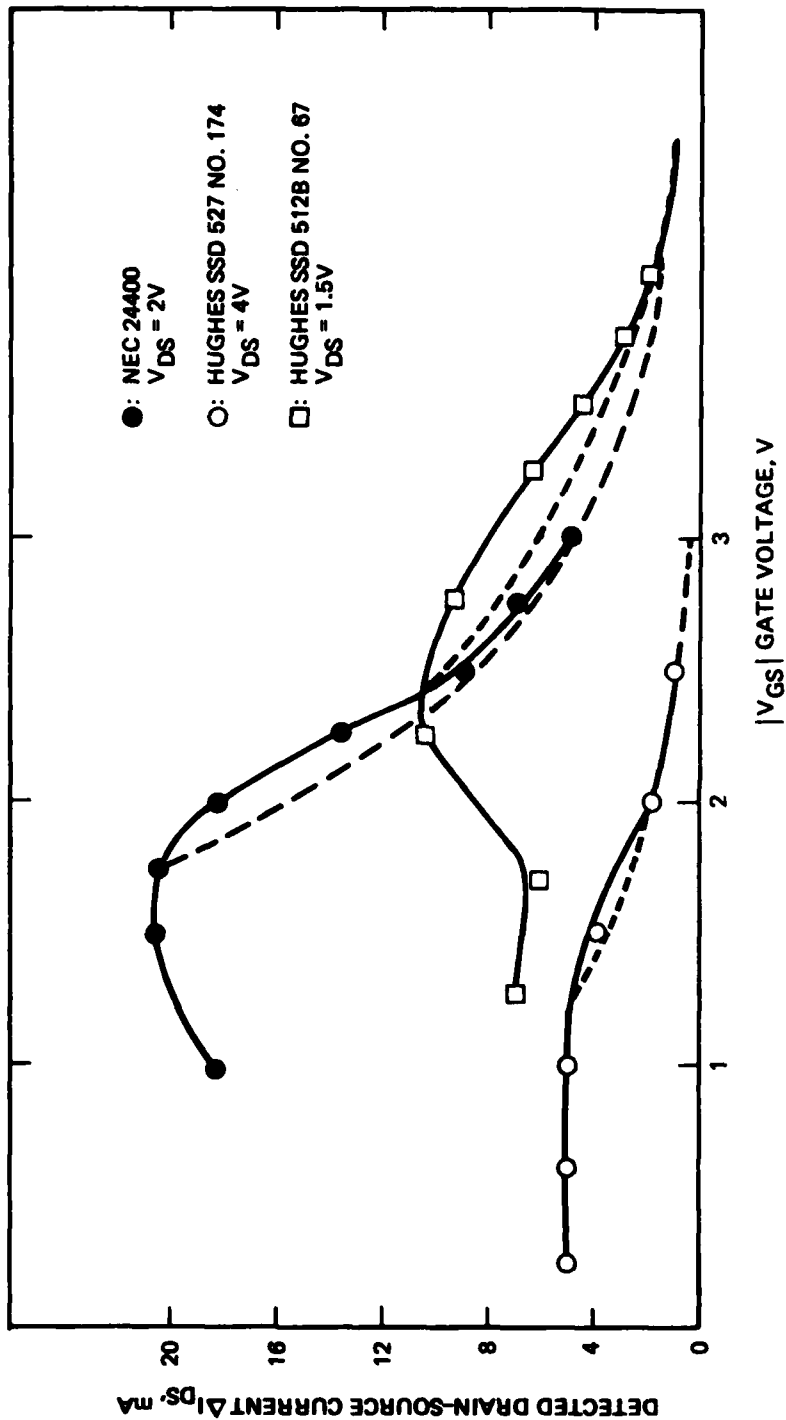
Figure 45. Detected dc drain-source current (ΔI_{DS}) versus gate voltage (V_{GS}). (The incident optical power is ∿0.9 mW).
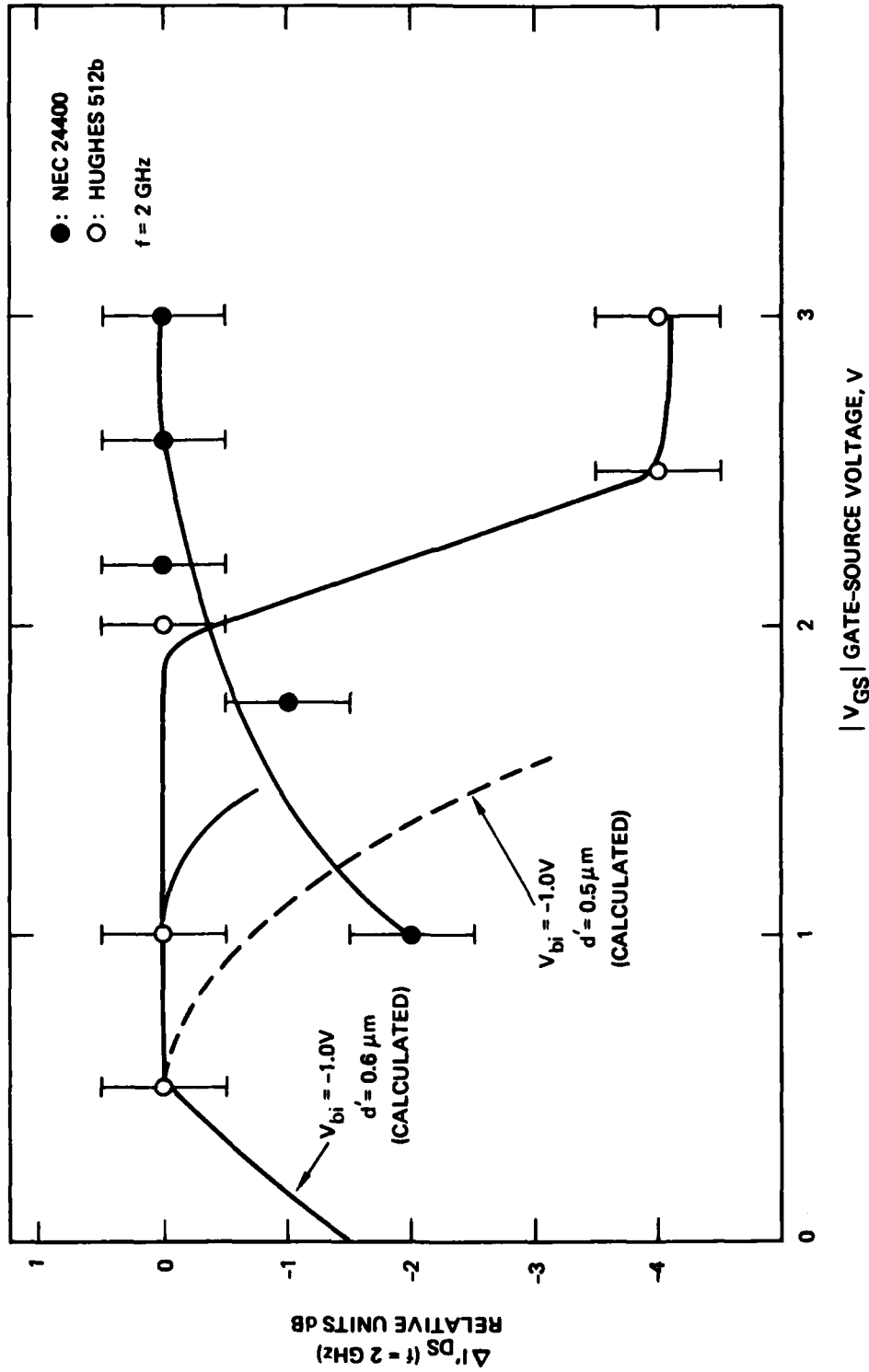
Figure 46. Detected rf drain-source current ($\Delta I'_{DS}$($f = 2 \times 10^9$/ sec) versus gate voltage (V_{GS}).

102

Table 4 summarizes the results for the parameters used in the theoretical fit. We have also measured the analog frequency response of GaAs MESFETs by shining a modulated (GaAl)As laser beam on the active region. We found that the frequency response is essentially flat for frequencies up to and probably beyond 4 GHz. Furthermore, the sensitivity is comparable to the Rockwell detector described in Table 3. Figures 47 and 48 show the optical pulse response of typical GaAs MESFETs; the pertinent data are summarized in Table 5.

Table 4. Summary of MESFET Detector Parameters

Device	γ	$d'(\mu)$, μm	$d(\mu)$, μm
Hughes FET SSD 512b	0.0271	0.5	0.2 to 0.3
Hughes FET SSD 527b	0.0321	0.5	0.2 to 0.3
NEC 24400	0.0290	0.6	0.2

$V_{so} = 1 \times 10^5$ cm/sec

$\tau_{tr} = 4 \times 10^{-12}$ sec (assuming $L_G = 1$ μm, and $V_e = 2 \times 10^7$ cm/sec)

$V_{bi} = -1.0V$

7429

The optical pulse response was measured using a mode-locked dye laser ($\lambda = 0.57$ μm) and a mode-locked (GaAl)As laser ($\lambda = 0.83$ μm). It appears that 0.5-μm-gate HAC MESFETs have a faster rise time than 1-μm-gate devices (100 versus 150 psec). Also, in some devices (0.5-μm-gate device) the fall time

103

10295-5
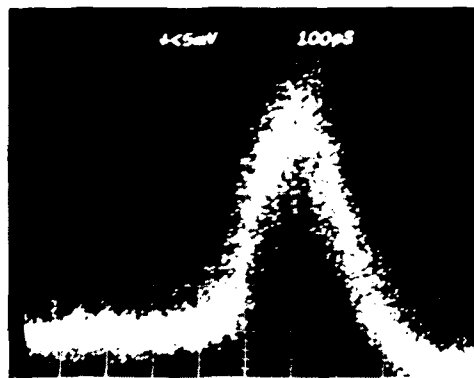
(a)

1 μm GATELENGTH

$\tau_{p_{1/2}} \simeq 100$ ps
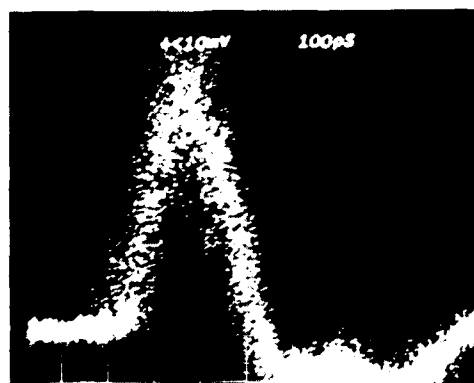
(b)

1/2 μm GATELENGTH

$\tau_{p_{1/2}} \simeq 80$ ps

Figure 47.   Optical pulse response for a HAC
GaAs MESFET.   (a) 1 μm gatelength,
(b) 1/2 μm gatelength (λ = 0.57 μm).

104
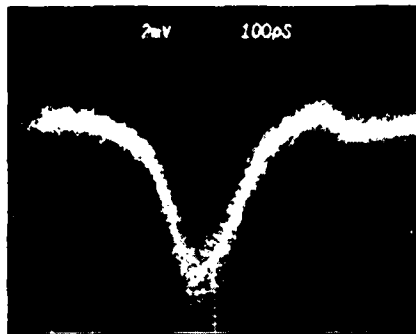
HAC (1 μ GATE LENGTH)
V_{DS} = 4.0 V, V_{GS} = −2.5 V
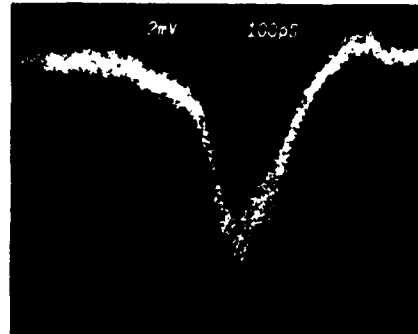
HAC (1/2 μ GATE LENGTH)
V_{DS} = 4.0 V, V_{GS} = −4.0 V
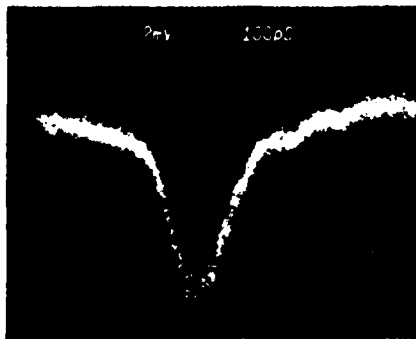
HP (1 μ GATE LENGTH)
V_{DS} = 3.8 V, V_{GS} = −1.5 V
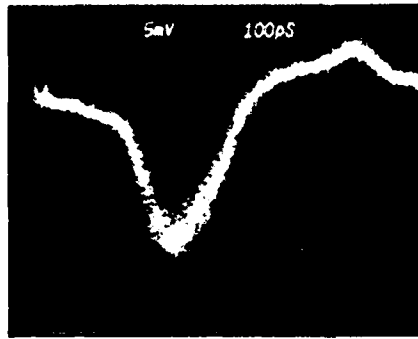
FUJITSU (POWER FET)
V_{DS} = 10 V, V_{GS} = −5 V
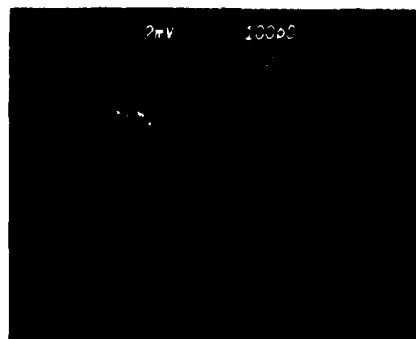
NEC
V_{DS} = 4.0 V, V_{GS} = −4.0 V

Figure 48.   Optical pulse response of GaAs MESFETs.
(λ = 0.8 3 μm).

105

Table 5. Summary of Important Detector Parameters for Various GaAs MESFETs

| Device Model Number	Type	Material	Spectral Sensitivity (λ), μm	Active Area, cm^2	t_r, psec	t_f, psec	$f_{-3 dB}$, GHz	Comments
HRL Fet SSD 512B	Power FET	GaAs	< 900	2 μm x 580 μm regions on either side of the 1 μm gate	150[c] 150[d]	150[c] 150[d]	>3.5[a]	Fall time difficult to measure because of ringing in the package
HRL FET L 157	Low-Noise FET	GaAs	< 900	2 μm x 580 μm regions on either side of the 1/2 μm gate	100[c] 100[d]	100[c] 150[d]	<3.5[b]	Fall time difficult to measure because of ringing in the package
HEC FET 2-400	Low-Noise FET	GaAs	900	Two 1.5 μm x 150 μm regions on either side of 1 μm gate	100[c] 100[d]	150[c] 150[d]	>3.5[a]	Fall time difficult to measure because of ringing in the package

[a] Measured using a modulated (GaAl)As laser.

[b] Calculated using Eq. (37) and assuming t_f = 100 psec.

[c] Measured using a mode-locked dye laser with λ = 0.57 μm.

[d] Measured using a mode-locked (GaAl)As laser with λ = 0.83 μm.

T7429

appears to increase at the longer wavelength (150 versus 100 psec). In addition, the measurements taken at 0.83 μm are relatively free of jitter and thus much easier to interpret. Finally, the fastest MESFETs we measured could detect a pulse with a ∿100 psec half-width (NEC 2400 and a HP 2001). Some of these observations can be explained. First, in the MESFET, the rise time of the device will be proportional to the electron transit time. Clearly, in the 0.5 μm gate device the electron transit time will be smaller than in the 1 μm gate device and thus we expect a shorter rise time. The device fall time is determined by the recombination of holes. Thus, any changes in the lifetime of the injected holes will change the device fall time. We believe this can explain the difference in the fall times at the two different wavelengths for the 0.5 μm gate MESFET. The shorter wavelength (λ = 0.57 μm) has a very small optical penetration depth ($1/\alpha$ ∿ 0.5 μm) and thus most of the carriers are generated near the surface. On the other hand, at the larger wavelengths the penetration depths are much larger ($1/\alpha$ ∿ 3 to 5 μm). Therefore, a significant portion of the carriers are generated in the semi-insulated substrate and thus alter the electric field distribution. Furthermore, the effect of surface recombination is significantly reduced in the latter case, thereby increasing the effective lifetime of the carrier.

The reduced jitter of the mode-locked (GaAl)As injection laser, in comparison to the mode-locked dye laser, is primarily a result of the relative stability of the external cavity arrangement in the semiconductor laser. Furthermore, pump variations are significantly reduced for the semiconductor laser system. This aspect of the mode-locked (GaAl)As injection laser should prove useful in laboratory situations.

D. GaAs/GaAlAs WAVEGUIDE MESFETS OPTICAL DETECTOR

In the previous subsections we discussed commercial high-speed detectors and GaAs MESFET detectors. In this subsection we discuss a novel heterostructure Waveguide detector. The detector consists of a GaAs MESFET integrated with an optical waveguide. Light is coupled into the waveguide and underneath the gate of the MESFET where it generates electron and hole pairs. A photograph and schematic are shown in Figure 49, and a schematic cross section is shown in Figure 50. The most important advantages resulting from

107

9253-2

55 μm

EDGE OF CHIP

STRIP-LOADED
WAVEGUIDE

SOURCE
ELECTRODE

DRAIN
ELECTRODE
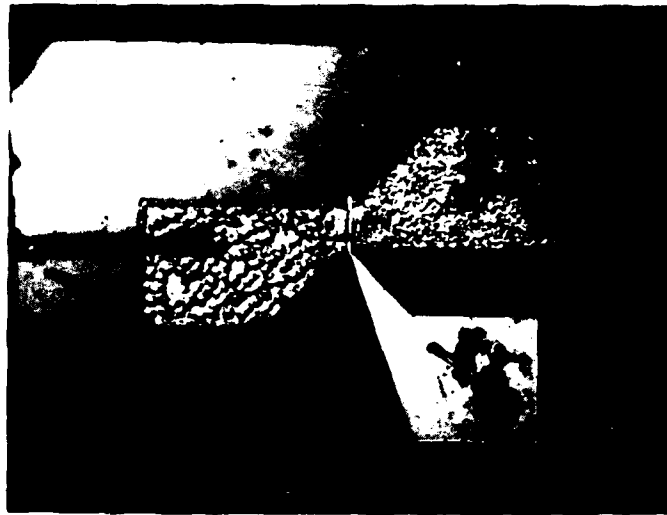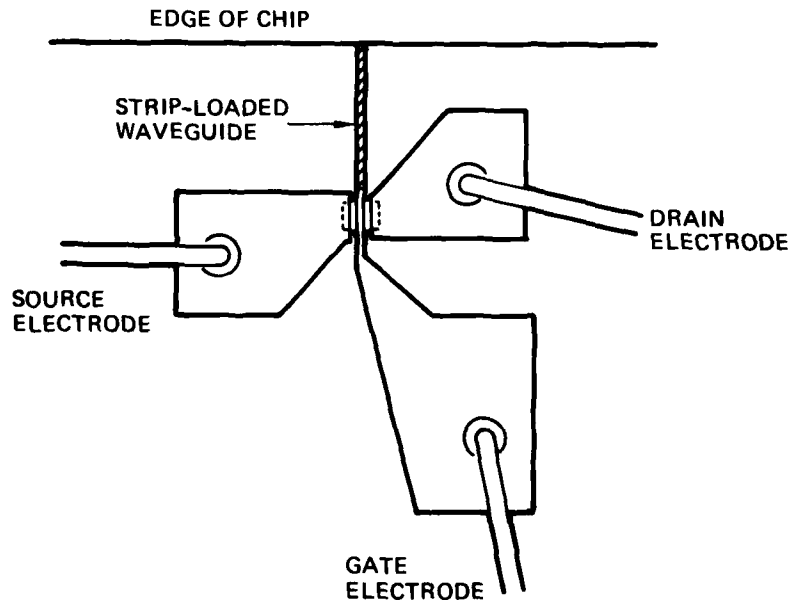
GATE
ELECTRODE

Figure 49.   Top view of the waveguide FET detector.
The dimensions of the MESFET are: width
is 50 μm, length is 50 μm, source-drain
spacing is 10-15 μm, gate length is 5 μm.

108
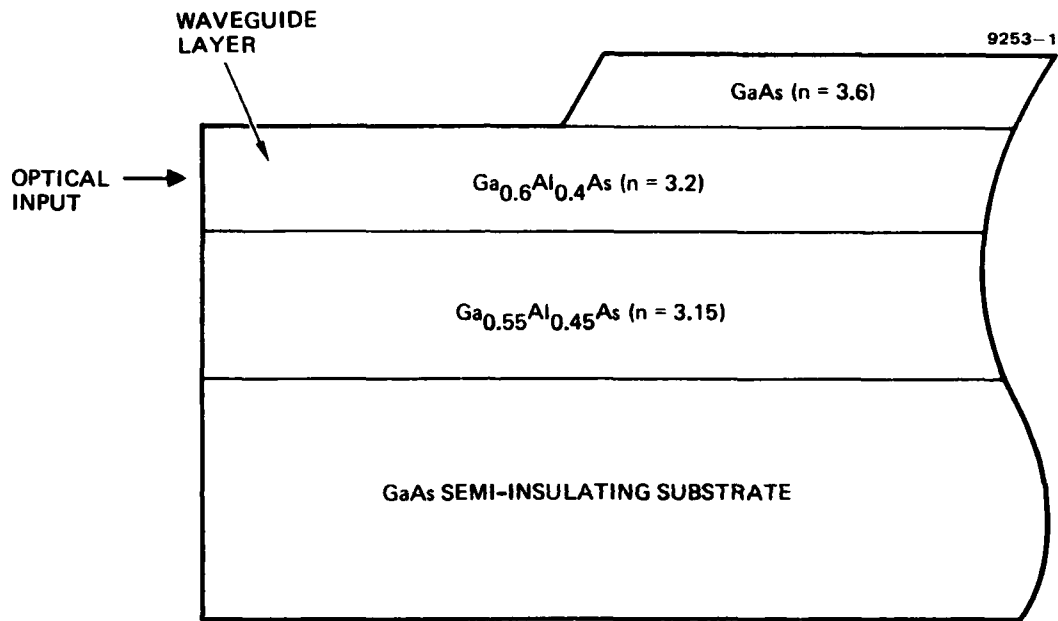
Figure 50. Cross section of the waveguide FET detector.

differences between the Waveguide MESFET and other types of detectors are (1) the generation of carriers occurs along the length of the device. Thus, by reducing the transverse and lateral dimensions the speed of the device can be increased without sacrificing quantum efficiency. (2) The structure can be easily integrated with integrated optic devices such as switches and modulators, and could serve as part of a feedback loop in hybrid-optical logic-type devices. Finally, the device can be integrated with other MESFET devices to form more complex opto-electronics devices.

The fabrication of the detector consists of growing a $Ga_{0.55}Al_{0.45}As$ buffer layer, a $Ga_{0.6}Al_{0.4}As$ waveguide layer, and a GaAs active region. The waveguide is made into a strip-loaded channel waveguide and serves as the input port for the optical signal.[49]

Typical I versus V characteristics are shown in Figure 51. Typical g_m is ~ 1 ms. This value is comparable to commercial MESFETs when one considers the different geometry used here (i.e., very narrow gate width, rather long drain-source spacing, and gate length).

We have also measured the frequency response of the detector and found it to be essentially flat up to and probably beyond 4 GHz. Measurements of the detected drain-source current versus gate voltage and drain source voltage are similar to that observed in commercial GaAs MESFETs. Furthermore, many of the results can be qualitatively explained using the photoconductive model described in the previous subsection. However, because of the poor coupling efficiency in the waveguide and the unoptimized geometry, the detector sensitivity is very low. Typical values are 10 to 20 dB lower than the commercial GaAs MESFETs. We believe this number can be improved by reducing the drain-source and gate length dimensions, and by increasing the waveguide dimensions.

One severe problem — aligning the waveguide with the high electric field region underneath the gate — still exists. Because of the complexity of this task, we feel we should reconsider the concept of a waveguide MESFET. However, this should not preclude the possibility of using an optical waveguide with a more conventional detector, such as P-I-N, or APDs. In those detectors the electric field is uniform, both in the transverse and lateral directions.

110
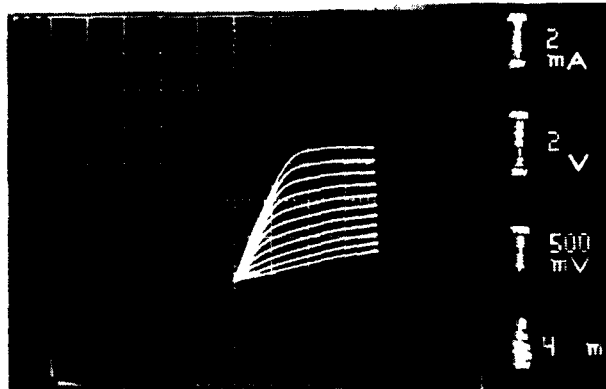
TYPICAL
CHARACTERISTIC
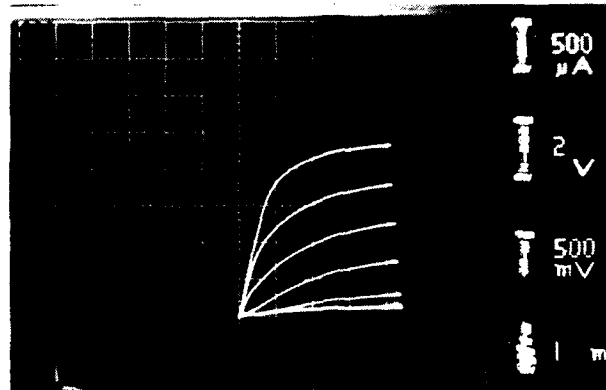
BEST DEVICES

Figure 51. Drain-source current versus drain-source
voltage.

E. GaAs/GaAlAs WAVEGUIDE GUNN DIODES

During this program we attempted to fabricate and characterize GaAs/
GaAlAs heterostructure Gunn Diodes. Our goals were to fabricate the Gunn
Diodes and use them in our microwave-optical interactions study. We devised
a new modulation scheme using a traveling high-electric-field Gunn domain,
where modulation occurs when the optical beam interacts with the high-field
domain and produces an electro-absorption effect. The concept was described
in Ref. 50. In this subsection we describe some of our results on the fabri-
cation and characterization of the Gunn diodes. Unfortunately, because of
severe heating problems, we could not make any measurements on the microwave-
optical interaction effects. However, we believe it is important to include
this section because other workers[51] have recently obtained high-modulation
rates using an electro-absorption modulator. Thus, some of the concepts
established in this program could be useful for future devices.

Figures 52 and 53 show the cross section and a photograph of the top
view, respectively, of the Gunn diodes fabricated. Figure 54 shows typical
I versus V characteristics. Note the negative resistance region. Typical
current dropback is ∿20 to 30% and is comparable to the values obtained by
other workers. In Figure 55 we show typical rf output of a Gunn Diode when
mounted on an appropriate Microstrip Line Circuit. In some of the diodes we
observed transit time operation while others oscillated at much higher
frequencies. The highest frequency of oscillation was ∿9 GHz with an output
power of ∿ -20 dBm.

In conclusion, we have fabricated and made preliminary characterization
on heterostructure Gunn diodes. These devices, when properly heat sunk, can
be useful electro-absorption modulators.

F. NOVEL HIGH SPEED PHOTO DETECTORS

In this last subsection we described high speed photodetectors developed
at Rockwell Science Center and at the Hughes Research Laboratories. These
detectors can be used to detect mode-locked pulses.

The high speed detector developed at the Rockwell Science Center is
fabricated using LPE techniques and it involves forming a heterostructure
APD[52] whereby the top (GaAl)As layer acts as a window layer. The pulse

112

ANODE   CATHODE

GaAs   N ~ 10^{16}/CM^3 ~ 2 μm

Ga$_{0.6}$Al$_{0.4}$As N ~ 3 x 10^{15}/CM^3~ 2 μm

SEMI-INSULATING GaAs SUBSTRATE
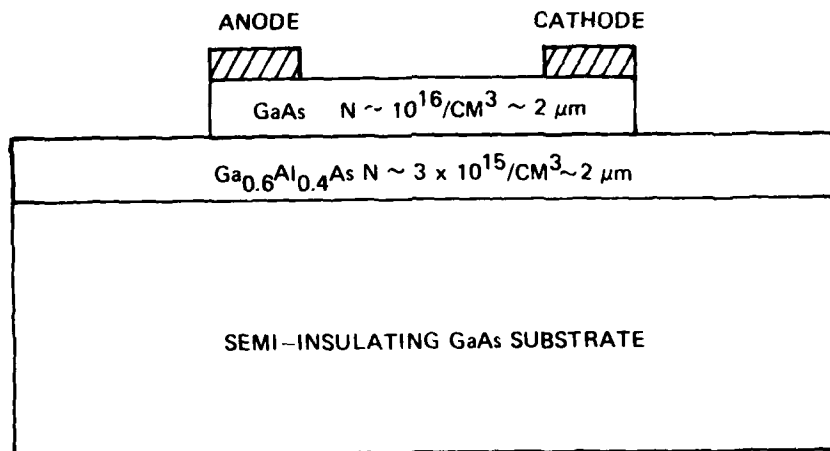
Figure 52. Cross section of a Gunn diode with
optical waveguiding structure.

113
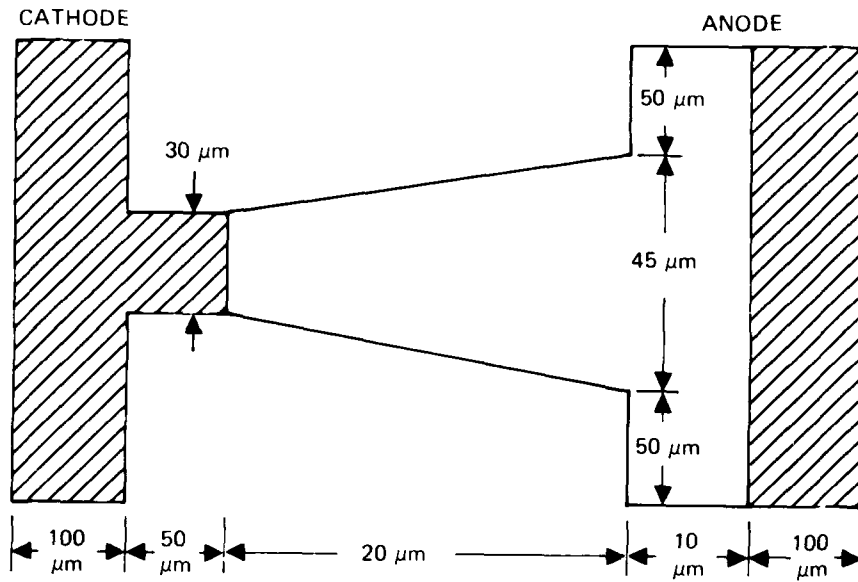
(a) Mask pattern.
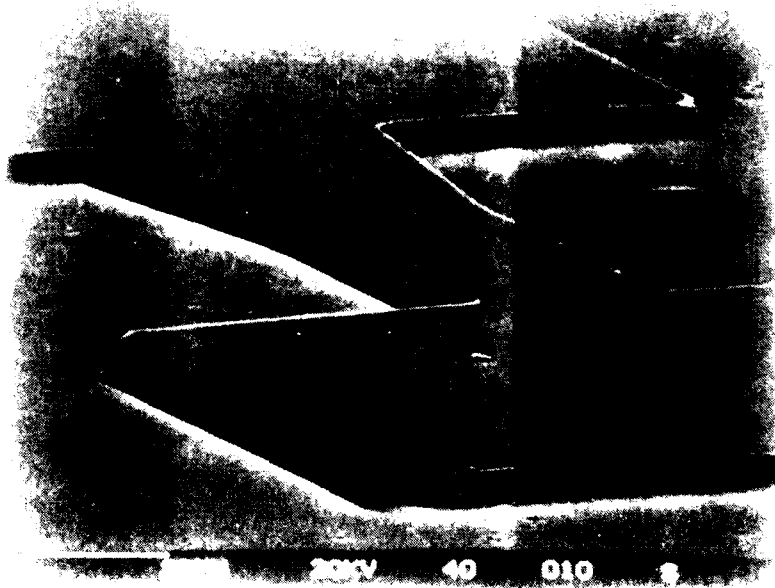
(b) Etched GaAs mesa.

Figure 53. Gunn diode active region pattern.

114

(a) L = 60 µm
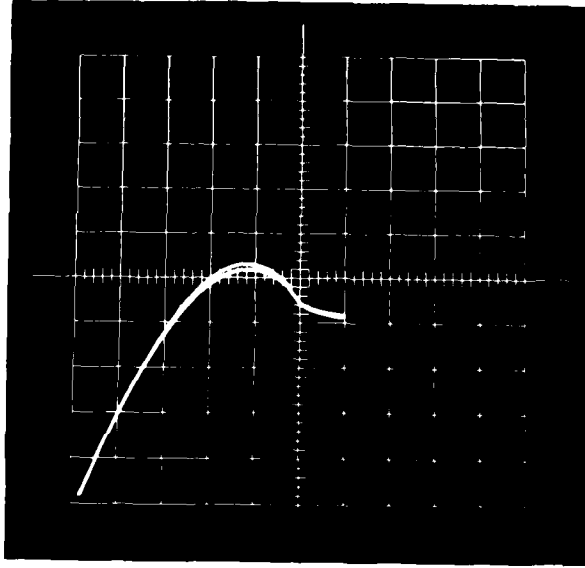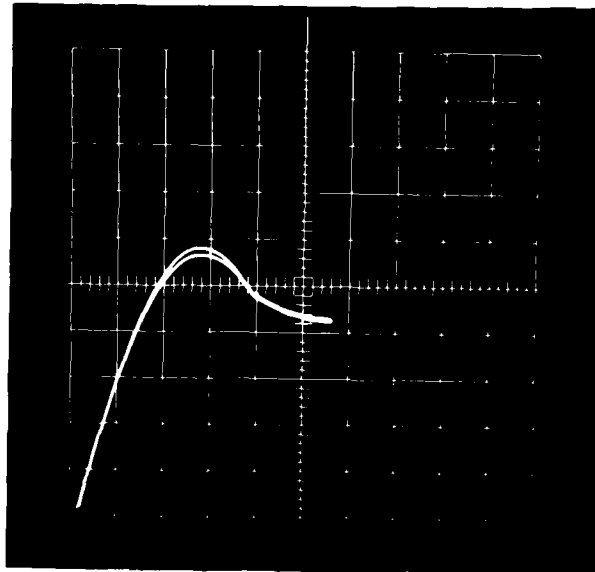
(b) L = 30 µm

Figure 54. I versus V characteristics of
(GaAl)As/GaAs Gunn diodes.

10668-4

2.804 GHz
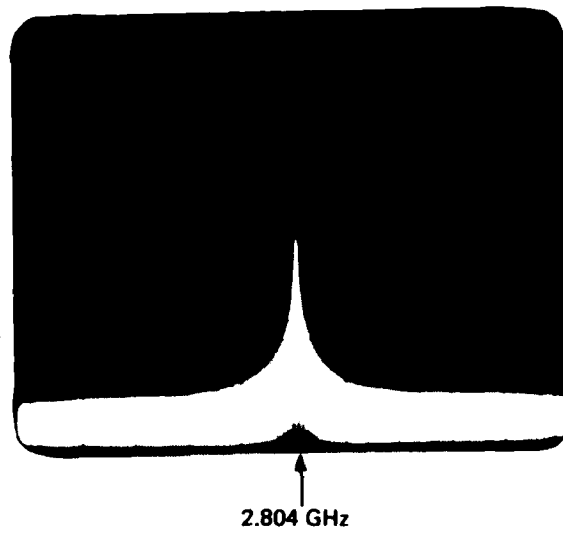
Figure 55.   Rf output spectrum of a Gunn
diode.   The frequency corresponds
to the transit time.

116

response of the detector is shown in Figure 57c. The rise time is $\sim$ 50 ps and the fall time is 80-100 ps. The high speed sensitivity is $\sim$ 0.15 mA/mW at a gain of 1.

The detector developed at the Hughes Research Laboratories (IDPC) involves placing an interdigital metal electrode[53-55] structure on top of a semi-insulating (SI) substrate or on tope of epitaxial layers which have been grown on the SI substrate. The basic operation of the device is to create back-to-back Schottky diodes such that the device is always reverse biased. Light detection is accomplished by the generation of carriers caused by an incident optical beam. For high speed operation, the incident optical beam must be absorbed in a distance shorter than the depletion layer thickness of the Schottky barriers. The optical pulse response is shown in Figure 57a. The device exhibits 50 to 60 psec rise and fall times and a sensitivity $\sim$ 0.1 - 0.8 mA/mW. The results obtained are either comparable (speed) or better (sensitivity) than the best valves obtained using state of the art detectors (Figure 57b) and other experimental detectors (Figures 57c, d). Furthermore, the alignment of the detector with the optical beam is much easier to perform with the IDPC detector.

We believe the interdigital photoconductive detector has many advantages over existing detectors. First, the device structure is planar and quite easy to implement. Second, the simplicity and design of the device makes it an attractive candidate for monolithic integration with conventional solid-state microwave devices. Third, by reducing the dimensions and slightly modifying the device structure, we believe the device can respond to 10 to 20 psec optical pulses; lastly, the speed and sensitivity are greater-than other experimental high speed detectors like the detector developed at the Rockwell Science Center.

200 μm

160 μm
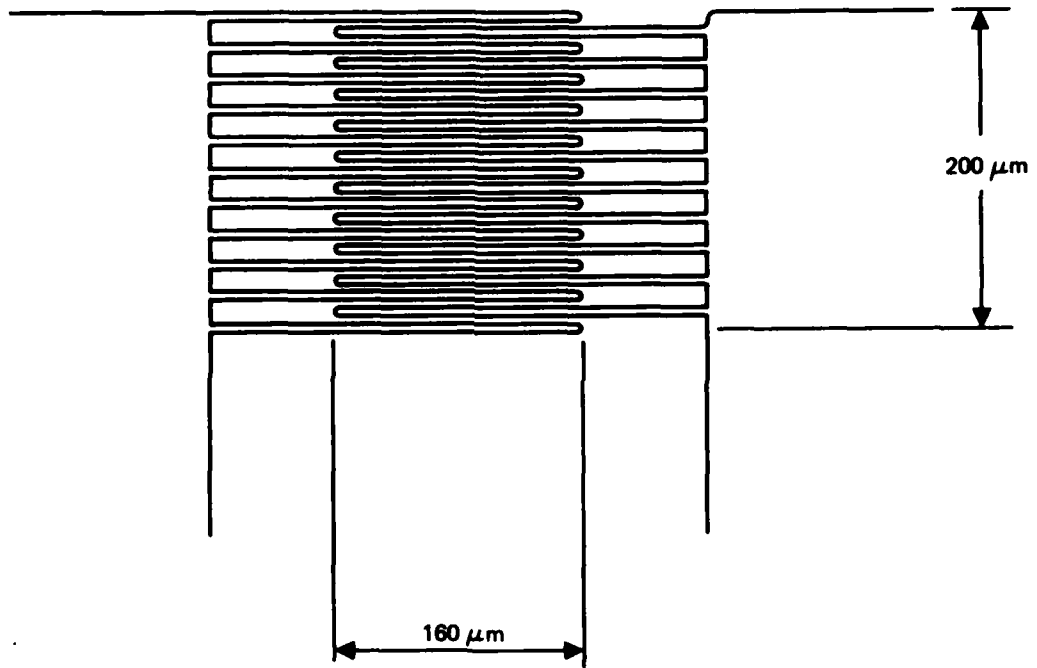
Figure 56.   Top view of interdigital electrode pattern on semi-insulating
             GaAs.
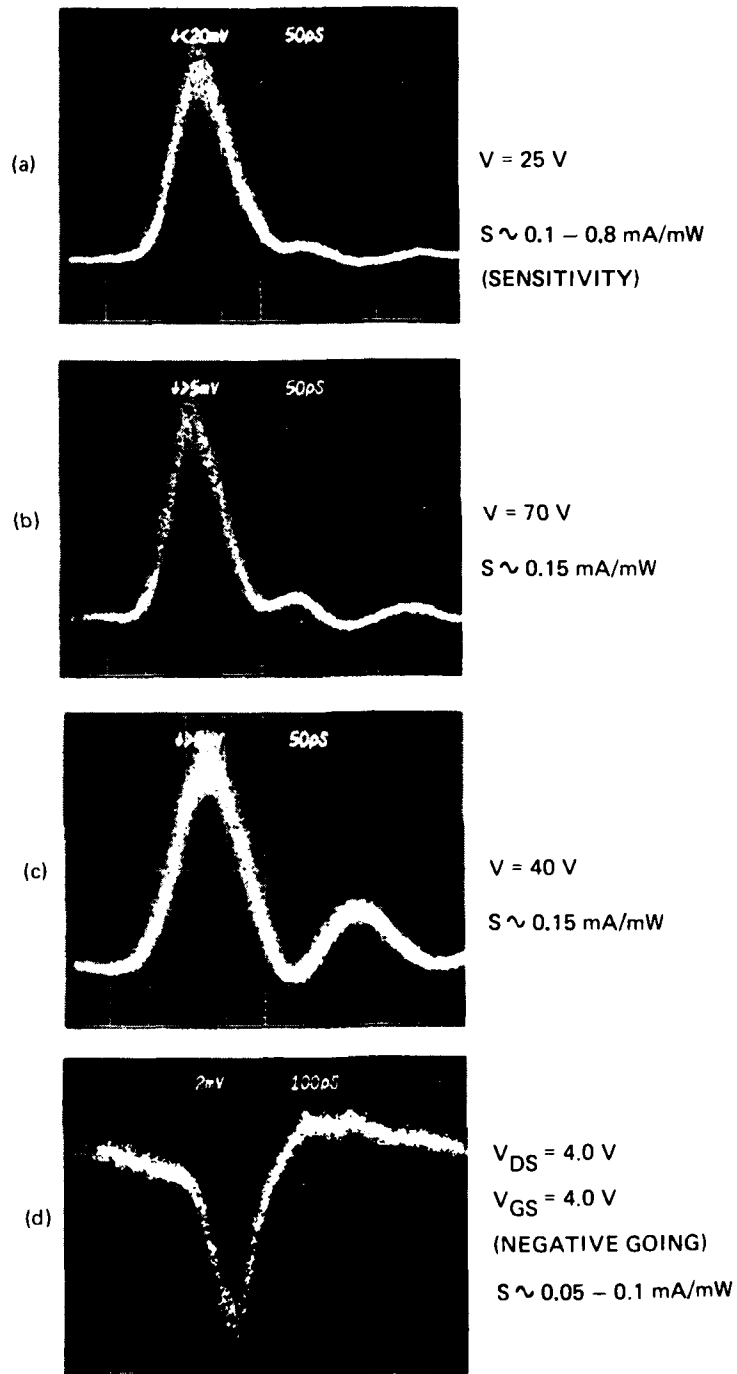
Figure 57. Optical pulse response of the "fastest" detectors tested. (a) Optimized IDPC detector, (b) Spectra Physics 403B, (c) GaAs/GaAlAs APD, (d) GaAs MESFET. The measurements were made using a mode-locked (GaAl)As injection laser.

119

G.   CONCLUSIONS

The encouraging results obtained with the GaAs MESFETs and the IDPC
detectors indicate that a photoconductive detector can provide a very large
frequency bandwidth (potentially greater than 10 GHz) with reasonable sensi-
tivities.   To increase, the sensitivity we must increase the input coupling
efficiency by optimizing either a waveguide structure or an IDPC detector.
The device speed can be increased by reducing the transit time and RC time
constant of the detector.   However, there is a tradeoff between sensitivity
and device speed in the IDPC detectors.   The ultimate speeds can be obtained
using a waveguide-type detector.

SECTION 6

CONCLUSIONS AND RECOMMENDATIONS FOR FUTURE WORK

This report has discussed our studies of optical injection locking in
IMPATT diodes, the high frequency characteristics of (GaAl)As injection lasers,
mode-locking of (GaAl)As injection lasers, high-speed optical detectors, and
novel microwave-optical devices. To our knowledge, this study represents
the first extensive characterization and documentation of these device
properties, which are of utmost importance in microwave-optical signal-
processing systems. Our results are summarized in Section 1.

We found that optical injection locking of IMPATT oscillators was
feasible at millimeter waves. However, two serious problems remain to be
solved. First, the interaction between the optically injected carriers and
the high-electric-field region must be increased. This could be accomplished
by using an optical waveguide structure. Second, the laser source must be
efficiently modulated at frequencies in excess of 10 GHz; this could be
accomplished by modifying the laser geometry.

The high-frequency modulation capabilities of injection lasers were found
to be limited by the relaxation oscillation resonance, junction parasitics and
self-pulsations. We believe that a significant improvement in the modulation
performance of injection lasers can be obtained by reducing the laser cavity
length, and lowering the ambient temperature to 77°K. Our calculations
indicate that efficient laser modulation in excess of 10 GHz can be obtained.

Mode-locking of (GaAl)As injection lasers has been correlated to the
common phemomenom of self-pulsations. Future studies should be directed
toward controlling the "self-pulsing" aspects of the laser. A possible
approach is to introduce saturable absorbing centers within the laser cavity.
We believe the repetition rate of the pulse-train can be increased by using
shorter diode cavities. The use of a fiber resonator could lead to a
stable, rugged, and high-repetition rate pulse generator. Future studies
should concentrate on single-mode fibers and the effect of the fiber on the
laser noise.

121

In the area of high-speed detectors and novel microwave-optical devices, we have demonstrated the limitations of existing devices and have fabricated novel optical detectors and heterostructure Gunn diodes. The waveguide high-speed detector needs further study. However, we should abandon the FET configuration since the alignment tolerances are too critical. Integration of waveguide detectors with other high-speed microwave devices should be pursued. Heterostructure Gunn diodes have the potential for making electro-absorption modulators. However, further work must be done on the thermal stability of the devices before any useful modulators can be fabricated.

Our demonstration of an interdigital photoconductive detector provides the first positive step in achieving an X-band optical detector. Further research should emphasize novel interdigital geometries, epitaxial layer geometries, and new material systems.

Our work has led to providing a solid cornerstone and useful insight on the implementation and limitations of microwave-optical devices. Future work should be directed toward extending the technology and the demonstration of practical devices.

REFERENCES

1. K. Kurokawa, Proc. IEEE 61, 1386 (1973).

2. H.W. Yen and M.K. Barnoski, Appl. Phys. Lett. 32, 182 (1978).

3. H.W. Yen and M.K. Barnoski, Quarterly Report 2, Contract N00173-77-C-0156, 1978 (unpublished).

4. J.R. Forrest and A.J. Seeds, Solid-State Electron. Devices 3, 161 (1978).

5. H.W. Yen, CLEA Tech. Digest 9 (1979).

6. H.W. Yen, Appl. Phys. Lett 36, 680 (1980).

7. A.C. Sanderson and A.G. Jordan, Solid-State Electron. 15, 140 (1972).

8. H.W. Yen and L. Figueroa, Quarterly Report 2, Contract N00173-77-C-0156, 1979 (unpublished).

9. W.T. Read, Jr., Bell Syst. Tech. J. 37, 401 (1958).

10. J. Carroll, Hot-Electron Microwave Generators (Arnold, 1970).

11. H. Kressel and J.K. Butler, Semiconductor Lasers and Heterojunctions (Academic Press, 1978).

12. E. Mohn, Symposium on GaAs, paper 17 (1968).

13. L. Figueroa, K. Lau, H.W. Yen, and A. Yariv, J. Appl. Phys. 51, 3062 (1980).

14. R.P. Salathe, Appl. Phys. Lett. 20, 1 (1979).

15. R.F. Broom, E. Mohn, C. Risch, and R. Salathe, IEEE J. Quantum Electron. QE-6, 328 (1970).

16. T.L. Paoli and J.E. Ripper, IEEE J. Quantum Election. QE-6, 335 (1970).

17. T.L. Paoli, J.E. Ripper, A.C. Moresini, and N.B. Patel, IEEE J. Quantum Electron. QE-11, 525 (1975).

18. P.T. Ho, L.A. Glasser, E.P. Ippen, and H.A. Haus, Appl. Phys. Lett. 33, 241 (1978).

19. L.A. Glasser, Electron. Lett. 14, 725 (1978).

20. P.T. Ho, Electron. Lett. 15, 527 (1979).

21. E.P. Ippen, D.J. Eilenberger, and R.W. Dixon, Appl. Phys. Lett. 37, 267 (1980).

22. M.B. Holbrook, W.E. Sleat, and D.J. Bradley, Appl. Phys. Lett. 37, 59 (1980).

23. J.P. Van der Ziel and R.M. Mikulyak, J. Appl. Phys. 51, 3033 (1980).

24. H. Ito, H. Yokoyama, and H. Inaha, Electron. Lett. 16, 620 (1980).

25. N.G. Basov, IEEE J. Quantum Electron, QE-4, 855 (1968).

26. T.P. Lee and R.H.R. Roldan, IEEE J. Quantum Electron. QE-6, 339 (1970).

27. D. Kato, Appl. Phys. Lett. 31, 588 (1977).

28. J.A. Copeland, Electron. Lett. 14, 809 (1978).

29. R.W. Dixon and W.B. Joyce, IEEE J. Quantum Electron. QE-15, 470 (1979).

30. J.P. Van der Ziel, J.L. Merz, and T.L. Paoli, J. Appl. Phys. 50, 4620 (1979).

31. B.W. Hakki, J. Appl. Phys. 50, 5630 (1979).

32. T.L. Paoli and J.E. Ripper, Phys. Rev. Lett. 22, 1088 (1969).

33. L.W. Casperson, IEEE J. Quantum Electron. QE-14, 756 (1978).

34. R.L. Hartman, R.A. Logan, L.A. Koszi, and W.T. Tsang, J. Appl. Phys. 40, 4616 (1979).

35. F.R. Nash, R.L. Hartman, T.L. Paoli, and R.W. Dixon, presented at the Int. Devices Meeting, Washington D.C., paper 5.4 (1979).

36. K. Mitsuishi, N. Chinone, H. Sato, and K. Aiki, IEEE J. Quantum Electron. QE-16, 728 (1980).

37. L. Figueroa, K. Lau, and A. Yariv, Appl Phys. Lett. 36, 248 (1980).

38. K. Lau, L. Figueroa, and A. Yariv, IEEE J. Quantum Electron. QE-16, 1329 (1980).

39. L. Figueroa, IEEE J. Quantum Electron., to be published, June 1981.

40. G.H.C. New, IEEE J. Quantum Electron. $\underline{QE-10}$, 115 (1975).

41. H. Haus, IEEE J. Quantum Electron. $\underline{QE-11}$, 736 (1975).

42. B.W. Hakki, J. Appl. Phys. $\underline{51}$, 68 (1980).

43. H.W. Yen, and M.K. Barnoski, "Optical Microwave Interactions in Semi-conductors," Hughes Technical Report, Contract N00173-77-C-0156 (1978).

44. T.L. Paoli, IEEE J. Quantum Electron. $\underline{QE-13}$, 314 (1977).

45. G. Arnold and K. Peterman, Appl. Phys. Lett. $\underline{10}$, 311 (1978).

46. J.C. Gammel and J.M. Ballantyne, IEDM Tech. Digest, 120 (1978).

47. K. Jarasiumus, C. Hoffman, H. Gerritsen, and A. Nurmikku, in $\underline{Picosecond}$ $\underline{Phenomena}$, C.V. Shank et al., $\underline{Eds}$. (1978), p. 327.

48. S. Wang, $\underline{Solid\ State\ Electronics}$ (McGraw Hill, 1966).

49. L. Figueroa, C.W. Slayman, and H.W. Yen, Quarterly Report No. 5, Contract N00173-78-C-0192 (1980) (Unpublished).

50. L. Figueroa, C.W. Slayman, and H.W. Yen, Quarterly Report No. 4, Contract N00173-78-C-0192 (1979).

51. D.Z. Tsang, J.M. Walpole, S.H. Groves, J.J. Hsieh, J.P. Donnelly, Paper 269-18, SPIE Proc., Hollywood, California (1981).

52. H.D. Law, K. Nakano, and L.R. Tomasetta, IEEE J. Quant. Elect. QE-10, 549 (1979).

53. T. Sugeta and T. Urisu, IEEE Trans. Electron. Devices $\underline{26}$, 1855 (1979).

54. C.W. Slayman and L. Figueroa, to be presented at the IOOC Meeting, San Francisco, California (1981).

55. L. Figueroa and C.W. Slayman, Unpublished experiments and calculations.

APPENDIX

OPTICAL-MICROWAVE INTERACTIONS
IN SEMICONDUCTOR DEVICES

(Final Report for period 17 June 1977 through 16 June 1978)

127

OPTICAL-MICROWAVE INTERACTIONS IN SEMICONDUCTOR DEVICES

Huan-Wun Yen and Michael K. Barnoski

Hughes Research Laboratories
3011 Malibu Canyon Road
Malibu, CA 90265

July 1978

Approved for public release; distribution unlimited.

Prepared for
NAVAL RESEARCH LABORATORY
4555 Overlook Avenue, S.W.
Washington, DC 20375

Sponsored by
ADVANCED RESEARCH PROJECTS AGENCY (DoD)
1400 Wilson Boulevard
Arlington, VA 22209

The views and conclusions contained in this document are those of the authors and should not be interpreted as necessarily representing the official policies, either expressed or implied, of the Defense Advanced Research Projects Agency or the U.S. Government.

REPORT DOCUMENTATION PAGE		READ INSTRUCTIONS BEFORE COMPLETING FORM
1. REPORT NUMBER	2. GOVT ACCESSION NO.	3. RECIPIENT'S CATALOG NUMBER
4. TITLE (and Subtitle) OPTICAL-MICROWAVE INTERACTIONS IN SEMICONDUCTOR DEVICES		5. TYPE OF REPORT & PERIOD COVERED Final Report 17 June 1977-16 June 1978
		6. PERFORMING ORG. REPORT NUMBER
7. AUTHOR(s) Huan-Wun Yen and Michael K. Barnoski		8. CONTRACT OR GRANT NUMBER(s) N00173-77-C-0156
9. PERFORMING ORGANIZATION NAME AND ADDRESS Hughes Research Laboratories 3011 Malibu Canyon Road Malibu, CA 90265		10. PROGRAM ELEMENT, PROJECT, TASK AREA & WORK UNIT NUMBERS
11. CONTROLLING OFFICE NAME AND ADDRESS Naval Research Laboratory 4555 Overlook Ave., S.W. Washington, DC 20375		12. REPORT DATE July 1978
		13. NUMBER OF PAGES 69
14. MONITORING AGENCY NAME & ADDRESS(if different from Controlling Office)		15. SECURITY CLASS. (of this report) UNCLASSIFIED
		15a. DECLASSIFICATION DOWNGRADING SCHEDULE

16. DISTRIBUTION STATEMENT (of this Report)

Approved for public release; distribution unlimited.

17. DISTRIBUTION STATEMENT (of the abstract entered in Block 20, if different from Report)

18. SUPPLEMENTARY NOTES

19. KEY WORDS (Continue on reverse side if necessary and identify by block number)

Injection laser modulation, Optical injection locking, Optical-microwave interactions, Optical switching of IMPATT oscillators, GaAs FET amplifier, Microwave mixing, Small-signal analysis

20. ABSTRACT (Continue on reverse side if necessary and identify by block number)

Theoretical and experimental studies of direct-current modulation of semiconductor injection lasers were carried out. The small-signal modulation frequency response of a single-mode laser was measured and found to agree well with the calculation result. Direct modulation of a single-mode laser up to 6 GHz was achieved.

DD FORM 1473 EDITION OF 1 NOV 65 IS OBSOLETE
1 JAN 73

Experiments on optical injection locking of a transistor oscillator were carried out. Injection locking was achieved not only at fundamental frequencies but also at various subharmonics with less tolerance in frequency deviation. It is also possible to perform simultaneous switching and phase locking in these oscillators. We have also succeeded in phase locking a GaAs FET oscillator at 7 GHz with an injected optical signal modulated at 3.5 GHz.

A novel scheme of carrying out microwave mixing in GaAs FET amplifiers was demonstrated in which one of the signals is fed into the input port of the amplifier while the local oscillator signal is introduced through optical injection and the mixed signal is taken from the output port of the amplifier.

Experimental results on the optical switching of GaAs IMPATT diode oscillators is presented. The IMPATT microwave output power can be either enhanced or reduced depending on the bias condition and the microwave cavity tuning. A small-signal analysis was carried out to model the IMPATT diode under optical illumination. It was found that illumination enhanced the reverse saturation current of the diode and was responsible for the change in devices characteristics, which qualitatively accounted for the observed phenomena.

TABLE OF CONTENTS

LIST OF ILLUSTRATIONS

5

6

7

SECTION 1

INTRODUCTION AND SUMMARY

Optical photons with energies higher than the bandgap energy of a semiconductor can excite electron-hole pairs in that material. Since the characteristics of almost all semiconductor devices depend heavily on the number of charge carriers available, strong interactions between the performance of the device and the illuminating optical signal can be expected. The program "Optical-Microwave Interactions in Semiconductor Devices" is intended to study such interactions as manifested in the modification of characteristics of semiconductor microwave devices by optical illumination. Through an understanding of these interaction processes, we can explore some potential applications, such as optical switching and optical injection locking of solid-state oscillators, phase jitter and frequency drift reduction of oscillators by optical illumination, and optically injected microwave mixing in solid-state amplifiers.

During the past year, our efforts were concentrated in the following areas: direct modulation of semiconductor injection lasers, optical injection locking of transistor oscillators, optically injected microwave mixing in GaAs FET amplifiers, and optical switching of GaAs IMPATT diode oscillators.

Direct current modulation of GaAs cw injection lasers was investigated both theoretically and experimentally. By using simple rate equations and small-signal analysis, we determined that the practical high-frequency limit of direct modulation of injection lasers is less than 10 GHz. Experimentally, we have obtained frequency-response curves of injection lasers and identified the small-signal resonance-like peaks. The location of the peak and its dependence on the laser driving current are found to agree with the calculated result qualitatively. With large-signal modulation, a computer program was used to calculate the shape of optical waveforms from the laser with sinusoidal variation in driving current, and the experimental results agreed well with the calculated optical waveforms.

9

Both single-mode and multimode lasers were used in the experiment. The general behavior of these two types of laser was quite similar except that the single-mode laser seems to possess a higher modulation speed. In fact, we were able to detect the output of a single-mode laser modulated at 6 GHz.

The feasibility of optical injection locking of oscillators was first demonstrated using silicon bipolar transistor oscillators. The metal caps of the transistors were partially removed so that the chips were accessible for illumination, and the optical clocking signal was generated by direct current modulation of a cw GaAlAs laser. For a transistor in the oscillator circuit, the operating point was determined by the bias voltages. However, optical illumination generated equivalent base current and modified the base resistance and collector barrier capacitance. Thus, a transistor oscillator under optical illumination experienced variation in both its output voltage amplitude and its frequency.

The injection-locking phenomenon was examined using both an oscilloscope and a spectrum analyzer. Optical injection locking was observed in oscillators with frequencies ranging from below 1 kHz up to 1.85 GHz. As with conventional injection locking, optical injection locking took place at the fundamental frequencies and at various subharmonics. For example, a 1.85-GHz oscillator was locked to a 97.5-MHz master oscillator by illuminating the transistor with a laser beam modulated at only 97.5 MHz. It was also possible to adjust the transistor bias so that the oscillator would oscillate only under optical illumination. This allowed us to control a transistor oscillator, turning it on and off, and simultaneously phase-lock its output.

We also carried out the design and fabrication of a GaAs FET oscillator. The oscillator had a stable oscillation frequency of about 7 GHz and was successfully phase locked to a 3.5 GHz signal generator through optical injection. The locking range in this case was very small, probably because of a combination of poor optical coupling and the fact that subharmonic locking was used.

10

A somewhat different approach to achieving optical injection locking of transistor oscillators was taken in which a single-stage GaAs FET amplifier was connected to the oscillator under study. The optical locking signal was focused onto the GaAs chip in the amplifier instead of directly onto the oscillator. With this arrangement, we were able to phase lock the oscillator output as before. This method might have certain merits, especially where the active element in the oscillator circuit is not light sensitive or is not easily accessible for illumination.

An experiment designed to test the feasibility of using a GaAs FET amplifier as a microwave mixer was also carried out. The incoming microwave signal was fed to the input port of the amplifier, and the local oscillator signal was carried by a laser beam and optically injected into the FET circuit. The mixed i.f. signal was taken from the output port of the amplifier. With this scheme, we were able to mix two signals at 12.4 GHz (FET amplifier input) and 3.51 GHz (optically injected) to obtain i.f. signals at 8.89 GHz and 5.38 GHz. The efficiency of this process was low, however, due to the poor optical reception of the device. In the future, some dedicated devices with specially designed structures will be fabricated to increase the conversion efficiency and to lower the noise figure.

The microwave oscillation characteristics of GaAs IMPATT diodes under external optical illumination was first studied experimentally. We found that, depending on the diode's bias condition and frequency of oscillation and also on the intensity of illumination, the IMPATT microwave output power can be either enhanced or reduced.

A theoretical study of this experiment showed that the most significant contribution of optical illumination in an IMPATT diode is the drastic increase in its reverse saturation current I_s. Under normal operating conditions, I_s results from thermally generated carriers and is negligible compared with the avalanche current. However, with intense optical illumination, I_s must be included in the dynamic equations that govern the operation of the device. Using a small-signal approximation, the impedance of the diode can be solved for as a

11

function of frequency. We have shown that these impedance versus frequency curves shift with the illuminating optical intensity. As a result, the IMPATT output microwave frequency and power vary with optical intensity, and the experimental observations can be understood qualitatively.

During the follow-on contract, we plan to continue all the activities reported here with variations in approaches and goals. For instance, we will try to extend the optical injection-locking and mixing technique to include millimeter-wave oscillators and amplifiers. In addition, we will study the modulation of semiconductor injection lasers through active mode locking and design and fabricate semiconductor devices such that the optical-microwave interaction process in these devices can be optimized.

SECTION 2

DIRECT MODULATION OF SEMICONDUCTOR INJECTION LASERS

The simplest way to modulate the optical output of an injection laser
is by changing the laser current. For example, one can operate the
injection laser in the pulsed mode by sending current pulses into the
laser. However, if a step current of amplitude I is applied to an
injection laser, there will be a turn-on delay time associated with
the corresponding optical signal output given by[1]

$$t_d = \tau_s \, \ln[I/(I - I_{th})] \; ,$$

where τ_s is the spontaneous electron lifetime, and I_{th} is the laser
threshold current.

For GaAs lasers, τ_s is typically a few nanoseconds. Thus, the
turn-on delay for a pulsed laser is $\sim$ 1 nsec. This means the maximum
repetition rate of a pulsed laser is limited to below 1 GHz. The
physical reason for the existence of turn-on delay is that it takes a
finite time for the laser to accumulate enough electrons to reach the
state of population inversion and hence lasing.

Obviously, it should be possible to eliminate t_d by prebiasing the
laser up to I_{th} of even higher and superimposing the modulation current
onto the bias to accomplish high-frequency modulation. For a single-
mode laser, the equations that describe the time behavior of the elec-
tron and photon density in the active region of the laser can be written
as:

$$\frac{dn}{dt} = \frac{I}{eV} - \frac{n}{\tau_s} - Gns \qquad (1)$$

$$\frac{ds}{dt} = Gns - \frac{s}{\tau_p} \; , \qquad (2)$$

where n and s are electron density and photon density, respectively; τ_p is the photon lifetime in the optical cavity; e is the electronic charge; V is the volume of the active region; and G is a constant.

To find the steady-state values of n and s, let

$$\frac{dn}{dt} = \frac{ds}{dt} = 0$$

and obtain

$$n_o = \frac{1}{G\tau_p} \tag{3}$$

$$s_o = \tau_p \left(\frac{I_o}{eV} - \frac{n_o}{\tau_s} \right). \tag{4}$$

If the diode is biased just at threshold, $I_o = I_{th}$ and $s_o \approx 0$, then

$$I_{th} = \frac{n_o eV}{\tau_s} = \frac{eV}{G\tau_p \tau_s} \quad . \tag{5}$$

By substituting Eqs. 3 and 5 into Eq. 4, s_o can be rewritten as

$$s_o = \frac{1}{G\tau_s} \left(\frac{I_o}{I_{th}} - 1 \right) .$$

For a small-signal modulation, substitute

$$s = s_o + \Delta s$$

$$I = I_o + \Delta I$$

$$n = n_o + \Delta n$$

into Eqs. 1 and 2 to give a set of second-order differential equations of the form

14

$$\frac{d^2}{dt^2}\begin{Bmatrix}\Delta n \\ \Delta s\end{Bmatrix} + \gamma \frac{d}{dt}\begin{Bmatrix}\Delta n \\ \Delta s\end{Bmatrix} + \omega_o^2 \begin{Bmatrix}\Delta n \\ \Delta s\end{Bmatrix} = \begin{Bmatrix}\dfrac{1}{eV}\dfrac{d\Delta I}{dt} \\[2mm] \tau_p \omega_o^2 \dfrac{\Delta I}{eV}\end{Bmatrix} \quad , \qquad \begin{matrix}(6)\\[6mm](7)\end{matrix}$$

where

$$\gamma = \frac{1}{\tau_s}\left[1 + (I_o/I_{th} - 1)\right] = \frac{1}{\tau_s} + \tau_p \omega_o^2$$

$$\omega_o^2 = \frac{1}{\tau_p \tau_s}\left(\frac{I_o}{I_{th}} - 1\right) \quad . \qquad (8)$$

Since the optical output of the laser is proportional to the photon density inside the cavity, solving Eq. 7 for Δs will yield the laser output small-signal modulation amplitude. Specifically, since we are interested in sinusoidal modulation, set

$$I = I_o + \Delta I = I_o + I'e^{i\omega t}$$

$$\Delta s = s'e^{i\omega t} \quad ,$$

where ω is the frequency of the applied modulation signal. Solving for s' yields

$$s' = \frac{\dfrac{I'}{\tau_p eV}}{(\omega_o^2 - \omega^2) + i\gamma\omega} \quad .$$

A modulation depth function $F(\omega)$ is defined as

$$F(\omega) = \frac{s'(\omega)}{s_o} \quad .$$

Also, a normalized modulation depth $f(\omega)$ is defined as

$$f(\omega) = \frac{F(\omega)}{F(0)} = \frac{\omega_o^2}{[(\omega_o^2 - \omega^2)^2 + \gamma^2\omega^2]^{1/2}} \quad . \tag{9}$$

A plot of Eq. 9 is shown in Figure 1. Here $\tau_p = 1$ psec and $\tau_s = 1$ nsec, with I/I_{th} as a parameter. It is clear from the plots that there is a resonance peak in the modulation depth curve; it occurs at

$$\omega = \omega_{max} = \left(\omega_o^2 - \frac{\gamma^2}{2}\right)^{1/2} , \tag{10}$$

and the modulation depth at this frequency can be more than 10 times as large as that at low frequencies. We will arbitrarily define the maximum usable frequency of modulation to be the frequency at which $f(\omega) = 1$. This corresponds to

$$\omega_u^2 = 2\left(\omega_o^2 - \frac{\gamma^2}{2}\right)$$

or

$$\omega_u = \sqrt{2}\,\omega_{max} \quad . \tag{11}$$

For example, in Figure 1 when $I/I_{th} = 2.0$ we have $\omega_{max} \approx 5$ GHz and $\omega_u = 7.1$ GHz. Returning to the expression for the small-signal resonance frequency of the laser

$$\omega_o^2 = \frac{1}{\tau_p\tau_s}\left(\frac{I}{I_{th}} - 1\right) , \tag{8}$$

since ω_o is directly related to the maximum usable modulation frequency, we should try to make ω_o as large as possible. In Eq. (8), τ_s is the spontaneous electron lifetime in the active region of the laser, which is somewhat governed by the material property. It appears at

16
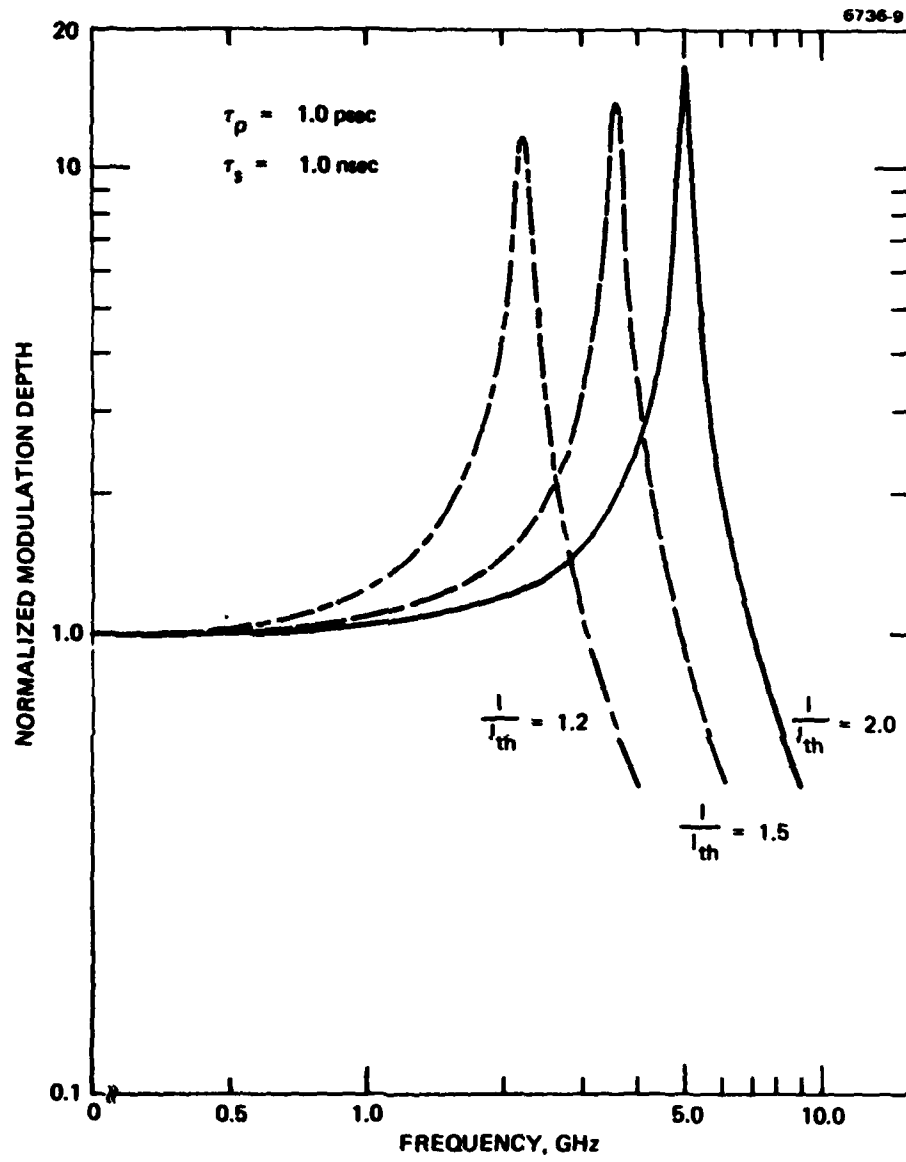
Figure 1. Frequency dependence of the normalized modulation depth of an injection laser.

17

first that we might be able to shorten τ_p, the photon lifetime, which is given by

$$\tau_p = \frac{L}{c} \frac{1}{(\alpha L - \ln R)} = \frac{1}{c\left(\alpha - \frac{1}{L}\ln R\right)} \quad ,$$

where L is the laser cavity length, c is the speed of light in the laser medium, α is the optical loss per unit length in the laser, and R is the reflectivity of the mirrors (assuming identical mirrors, which is true in semiconductor lasers without coatings).

Unfortunately, the threshold of a semiconductor laser is directly proportional to

$$\left(\alpha - \frac{1}{L}\ln R\right)$$

and the threshold figures in the expression of resonance frequency. Shortening τ_p will increase I_{th} such that the product of τ_p and I_{th} will remain almost constant. Therefore, there is little to gain from varying the device parameter. The only thing that can be done is to drive the laser harder and make I/I_{th} as large as possible. However, for most of the lasers, especially stripe-geometry lasers, $I/I_{th} \approx 2$ is about as high as can be achieved safely. Thus, according to the curves in Figure 1, the maximum usable frequency of modulation would be limited to about 10 GHz or less.

Experimental results of the small-signal laser modulation were taken using a Hitachi channeled-substrate-planar (CSP) single-mode laser.[2] Modulation speed as high as 6 GHz was obtained with the laser biased at $I \approx 1.6\ I_{th}$. Recently, a microwave network analyzer was used to examine the small-signal frequency response of a single-mode injection laser. The experimental set-up is shown in Figure 2. The frequency-swept microwave signal was taken from port 1 of the S-parameter test set and used to modulate the injection laser. The output of the laser was focused onto a silicon avalanche photodiode, followed by a wide-band amplifier. The output of the amplifier was fed to port 2

18

7725-4
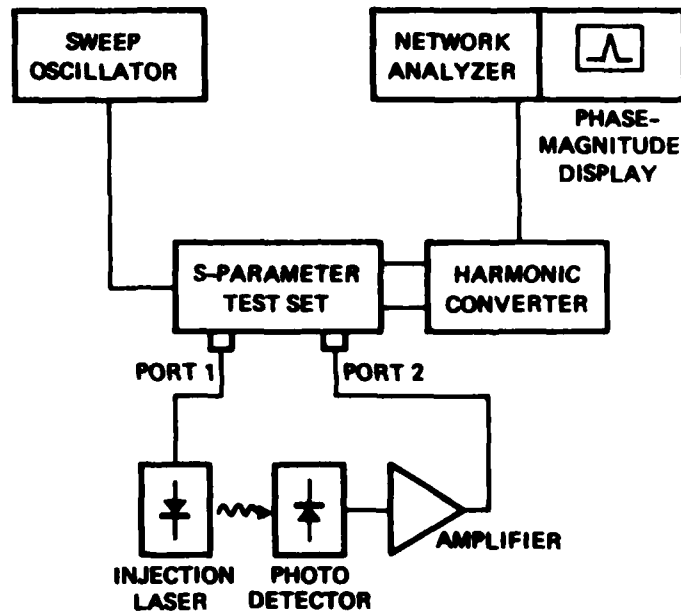
Figure 2.
Experimental set-up for measuring small-signal
frequency response of injection lasers.

of the S-parameter test set. The network analyzer compares the signal leaving port 1 with the signal coming into port 2 and displays the amplitude of this ratio as a function of frequency on the scope. Because of the experimental arrangement, we are not purely measuring the frequency response of the injection laser. The displayed result is actually the frequency response of the laser, the detector, and the amplifier combined. Figure 3 shows the result of such a measurement. The laser bias current was set at three different values: $I = 1.03 \, I_{th}$, $I = 1.21 \, I_{th}$, and $I - 1.38 \, I_{th}$. The small-signal resonance peaks are seen to differ at different pumping levels, as predicted by theory. However, the theory also predicts a flat frequency response below the resonance frequency, but the measured curve showed a significant dip between 1 and 2 GHz. The frequency response of the photodetector is assumed to be rather flat within this frequency range; the frequency response of the amplifier, which can also be measured using the same set-up, is relatively flat up to 2.5 GHz and rolls off rapidly afterwards (see Figure 4). Therefore, the dip in the curve shown in Figure 3 between 1 and 2 GHz is believed to be a result of the laser packaging and the sharp drop after 3 GHz to be a combination of the laser packaging and the detector amplifier roll off.

The resonance frequency of the small-signal laser modulation given by Eq. 8 is determined by the laser pumping current, the photon lifetime, and the electron spontaneous lifetime. We measured the resonance frequency of the laser under several bias currents and plotted a functional relation between $I/I_{th} - 1$ and ω_o^2, shown in Figure 5. The data points can be fitted to a straight line with slope 1.1×10^{-21} sec^2, which, according to Eq. 8, is equal to the product of the photon lifetime τ_p and the electron lifetime τ_s. This is a reasonable number compared with the published values for τ_p and τ_s. Thus, the rate equations used in this analysis, although somewhat simplified, still give excellent qualitative and quantitative results.

We also carried out studies on large-signal modulation of injection lasers. Since the rate equations, Eqs. 1 and 2, are coupled together, the equations for n and s alone are second-order nonlinear differential

20
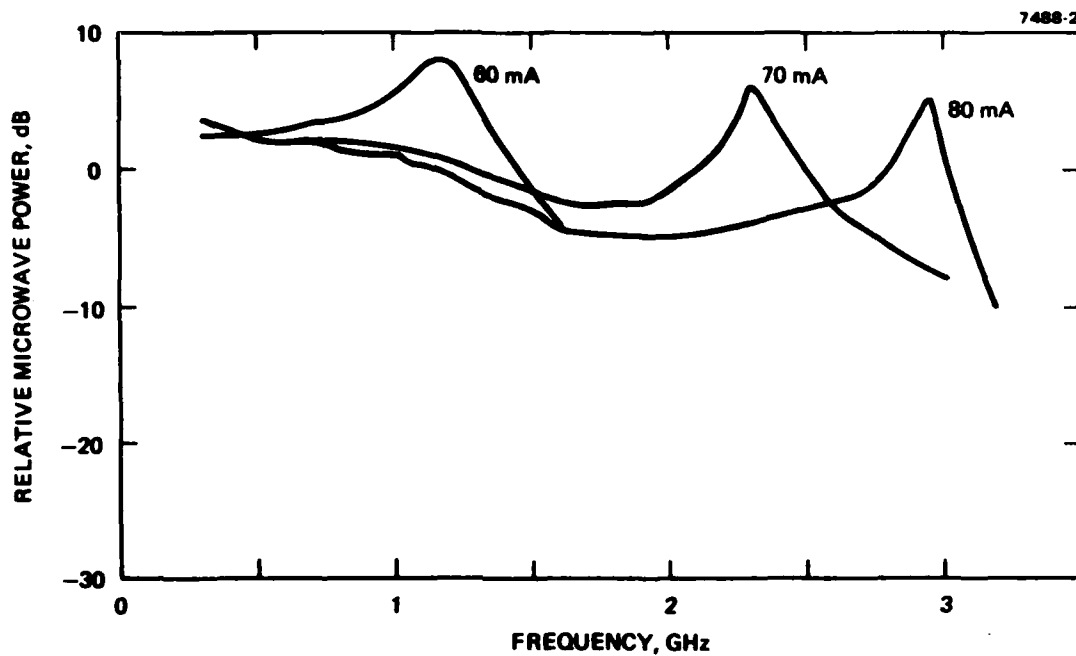
Figure 3.   Experimental small-signal frequency response of a single-mode injection laser modulation.
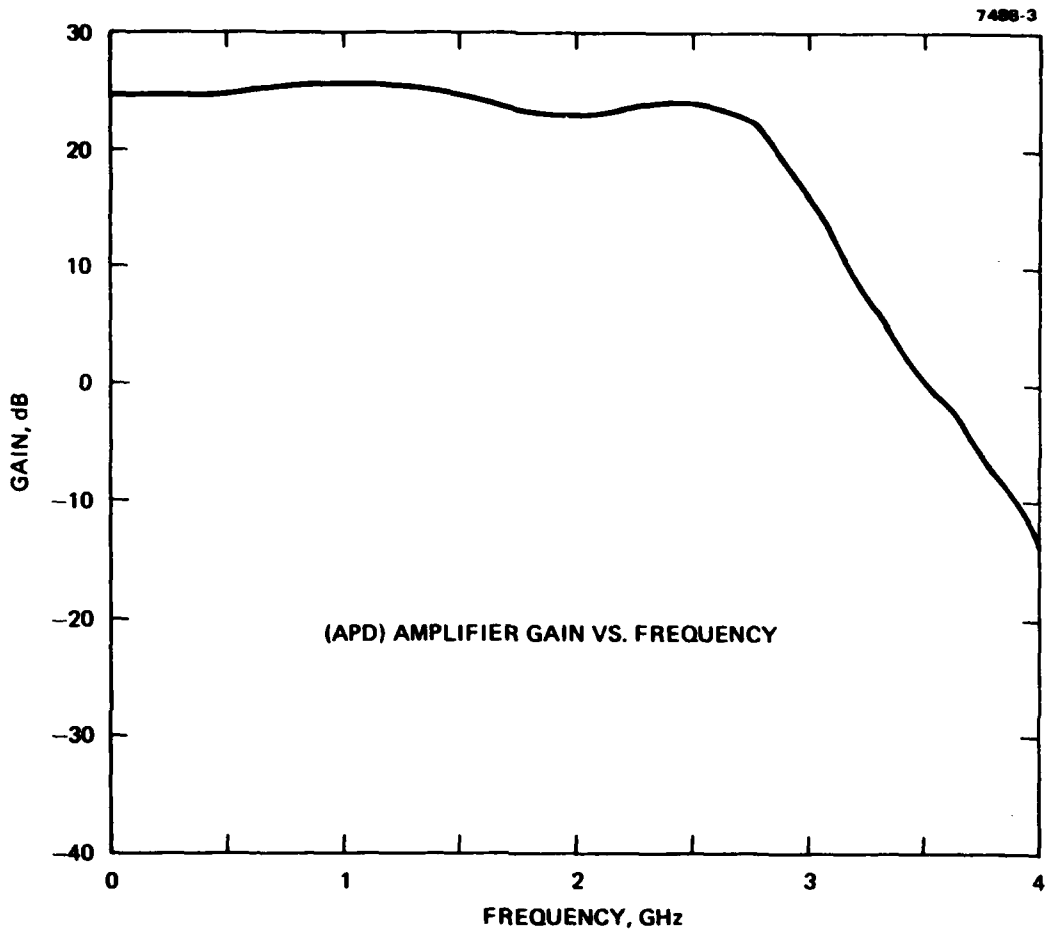
Figure 4.   Photodetector amplifier gain versus frequency plot measured using S-parameter test set.

22
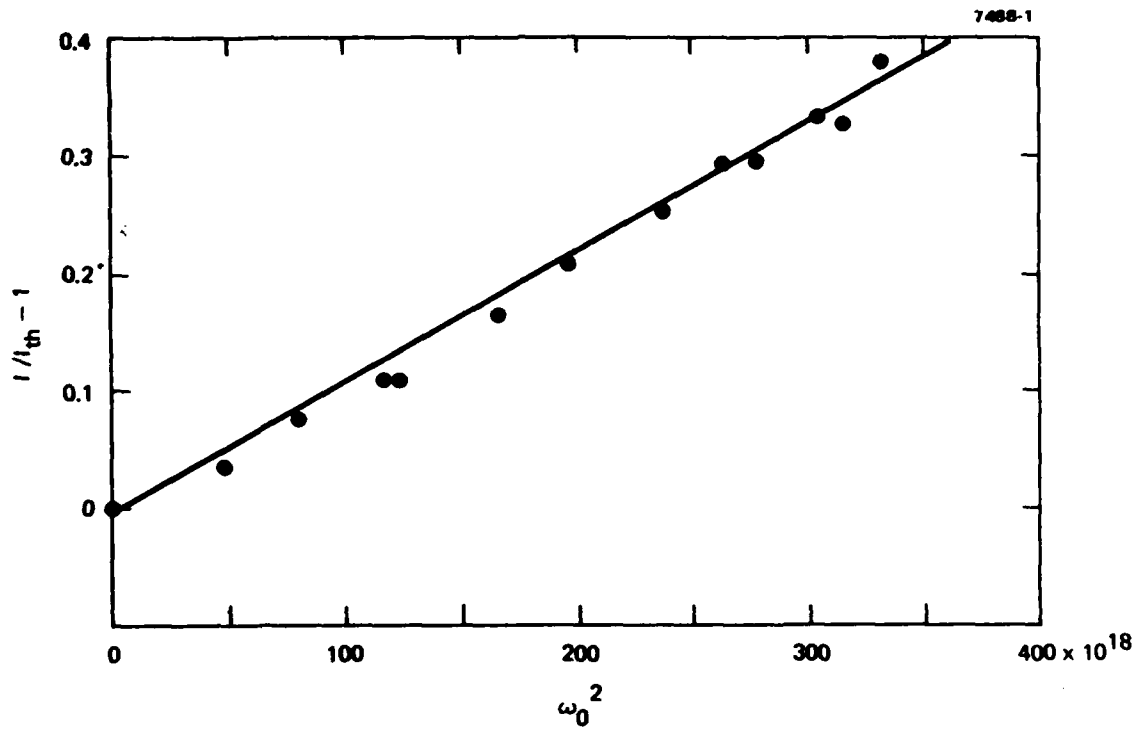
Figure 5. Measured small-signal resonance frequency as a function of laser driving current.

23

equations. Because analytical solutions for these equations could not be obtained, a computer technique was used to obtain numerical results. In the calculation, the laser current was assumed to vary sinusoidally, and the laser output optical waveforms were calculated at various frequencies. In Figure 6, the left column shows the computer-generated optical waveforms for modulation frequencies ranging from 200 MHz to 1.2 GHz. The laser parameters used in the calculation are I_{th} = 60 mA, τ_p = 1 psec, τ_s = 1 nsec, I_{bias} = 65 mA, and ΔI = 3 mA (corresponds to 60 percent current modulation). Significant distortion of the optical waveform occurs between 200 MHz and 600 MHz; from 800 MHz to 1.2 GHz, the output is almost a pulsed modulation. The experimental waveforms, displayed in the right column of Figure 6, seem to track the general features of the calculated results. However, at 1 and 1.2 GHz, the observed optical waveforms are not as sharp as those calculated, perhaps because the detection system is bandwidth limited.

The distortion generated by large-signal modulation of the injection laser is undesirable, especially in analog system applications. The amount of distortion tolerable in a given system will limit the depth of modulation that can be used. More work in this area is underway to gain a better understanding of the laser's behavior.

24

200 MHz

400 MHz

600 MHz

800 MHz

1 GHz

1.2 GHz

7725-3
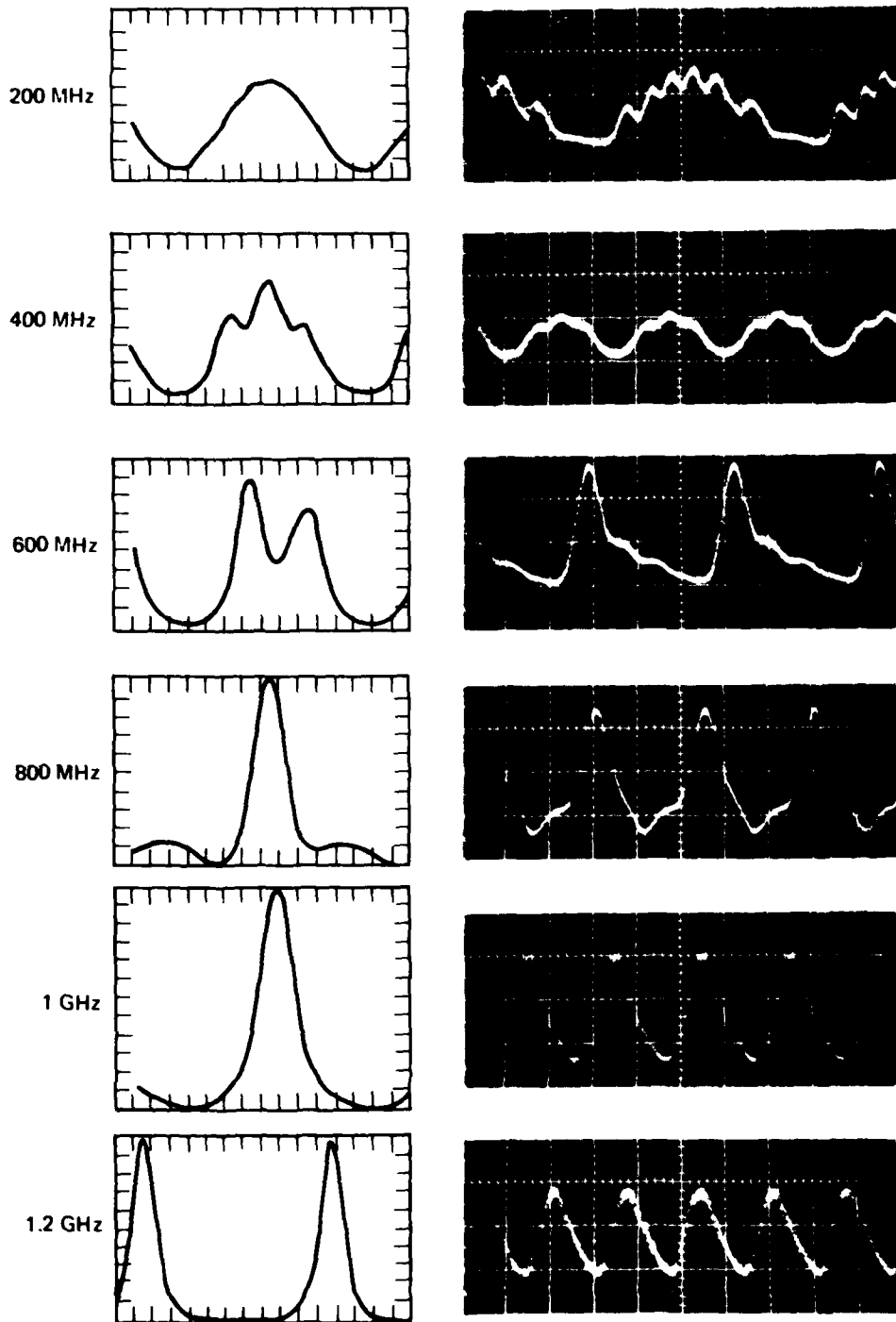
$I = 65$ mA , $\Delta I = 3$ mA, $I_{th} = 60$ mA

Figure 6. Large-signal modulation of injection lasers output optical waveforms for sinusoidal current variations.

25

SECTION 3

OPTICAL INJECTION LOCKING OF TRANSISTOR OSCILLATORS

To demonstrate the feasibility of an optical-injection-locking scheme, we carried out experiments using silicon transistor oscillators. Several oscillator circuits were constructed with both low-frequency and rf transistors. The metal cap of the transistors was partially removed so that the chips were accessible for illumination. The optical clocking signal was generated by direct current modulation of a cw GaAlAs injection laser ($\sim$8200 Å).

The effect of illumination on the characteristics of transistors was studied first. Figure 7(a) shows the collector current versus collector voltage curves of one particular transistor (2N 5108) for various base currents. There was no optical illumination in this case. In Figure 7(b), a cw optical power of $\sim$0.3 mW from a GaAlAs laser was focused onto the chip. This generated an equivalent base current of about 10 µA as evident by comparing Figures 7(a) and 7(b). For a transistor in the oscillator circuit, the operating point was determined by the biasing voltages. However, optical illumination can generate equivalent base current, hence effectively varying the operating point. Another effect of illumination is the modification of transistor base resistance and collector barrier capacitance caused by the additional carriers generated. Thus, a transistor oscillator under optical illumination will experience variation in both its output voltage amplitude and frequency.

A simple way of examining injection-locking phenomena is depicted in Figure 8. The modulated laser output is focused onto the transistor chip. The oscillator output goes to one of the vertical inputs (V_1) of an oscilloscope. A reference signal from the rf generator that modulated the laser goes to the time trigger and the second vertical input (V_2) of the same scope. Ordinarily, there is no definite phase

(a) WITHOUT ILLUMINATION   (b) WITH ILLUMINATION

| HORIZONTAL SCALE: | 1 V/div | OPTICAL POWER   0.29 mW |
| VERTICAL SCALE: | 0.2 mA/div | |
| BASE CURRENT: | 0.01 mA/STEP | |
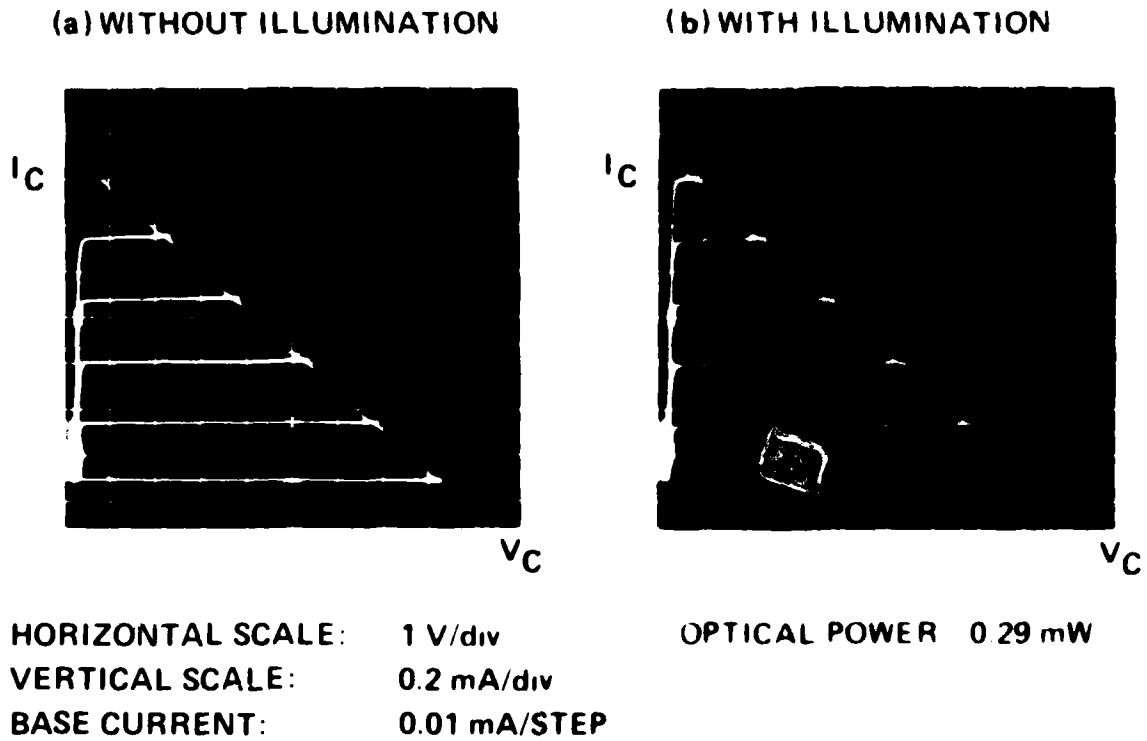
Figure 7. I_C versus V_C curves for an rf transistor (2N5108).
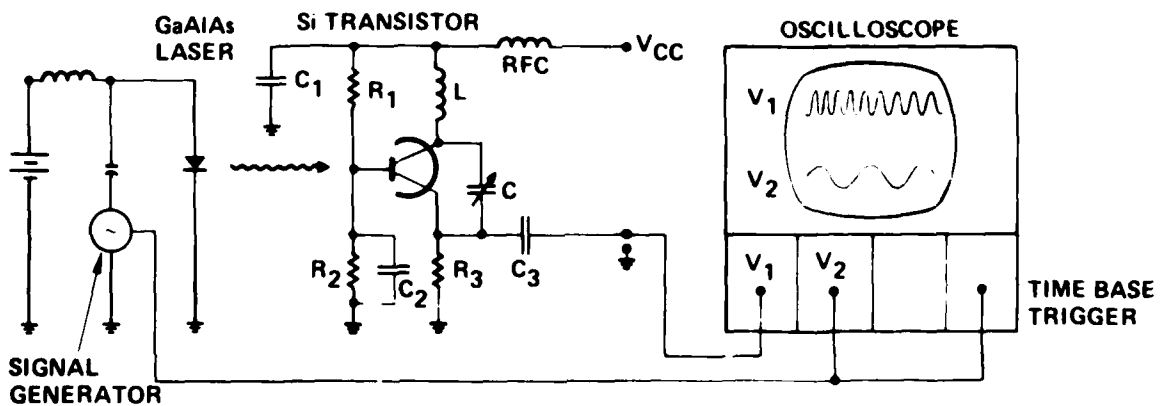
Figure 8.   The experimental setup for optical injection locking experiment.

relation between the rf generator output and the transistor oscillator output so that V_1 will not show up as a still display on the scope. However, if phase locking between the transistor oscillator and the rf generator takes place, a stationary display results.

Typical results of optical-injection locking are shown in Figure 9; the upper trace in each picture is the transistor oscillator output signal, and the lower trace is the rf generator output. Figure 9(a) is for the case when the laser beam is blocked so that no correlation exists between the two signals. In Figure 9(b), the shutter is removed; optical injection locking takes place and a still display of the oscillator was obtained. Note that the oscillator was running at 330 MHz and the rf generator put out a signal at 110 MHz. Thus, optical injection locking, as in conventional injection locking, can take place not only at the fundamental frequencies, but also at various subharmonics, and the locking range decreases as the frequency ratio increases.

Another method of examining the injection-locking process is to display the frequency content of the oscillator output on a spectrum analyzer. Figure 10 shows a sequence of pictures of the oscillator spectrum. The oscillator has an output frequency of about 440 MHz. The optical signal is being modulated at ∿439.5 MHz. The input modulating signal is increased in 10-dB steps from (a) to (d) and eventually pulls the oscillator output frequency to 439.5 MHz, as shown in (d).

With a set-up similar to that shown in Figure 2, by replacing the detector by an FET oscillator, we can also display the relative phase and magnitude between the locked oscillator output and the injecting signal. Since the injection signal frequency is being swept constantly, depending on the signal power level, there will be a certain frequency band, called the locking range, around the oscillator free running frequency such that injection locking takes place. Within the locking range, the oscillator output frequency tracks that of the injecting

29

5878-5

(b) WITH ILLUMINATION
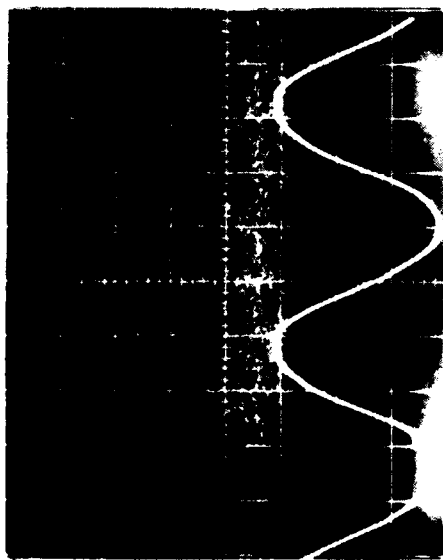
(a) WITHOUT ILLUMINATION
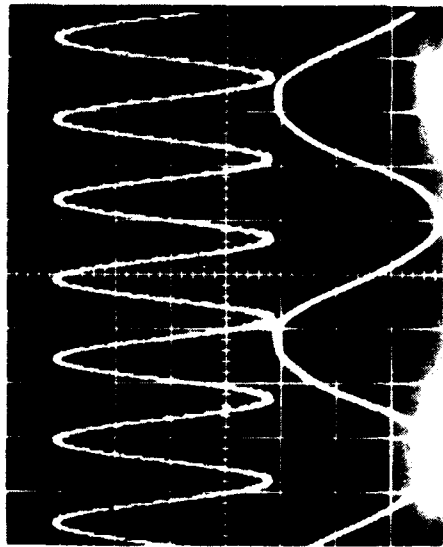
UPPER TRACE: TRANSISTOR OSCILLATOR OUTPUT (330 MHz)

LOWER TRACE: SIGNAL GENERATOR OUTPUT (110 MHz)

HORIZONTAL SCALE: 2 nsec/div

Figure 9. Scope traces of optical injection locking of silicon transistor oscillator; (a) without illumination, (b) with illumination.

30

7725-2

(a)

(b)

(c)

(d)
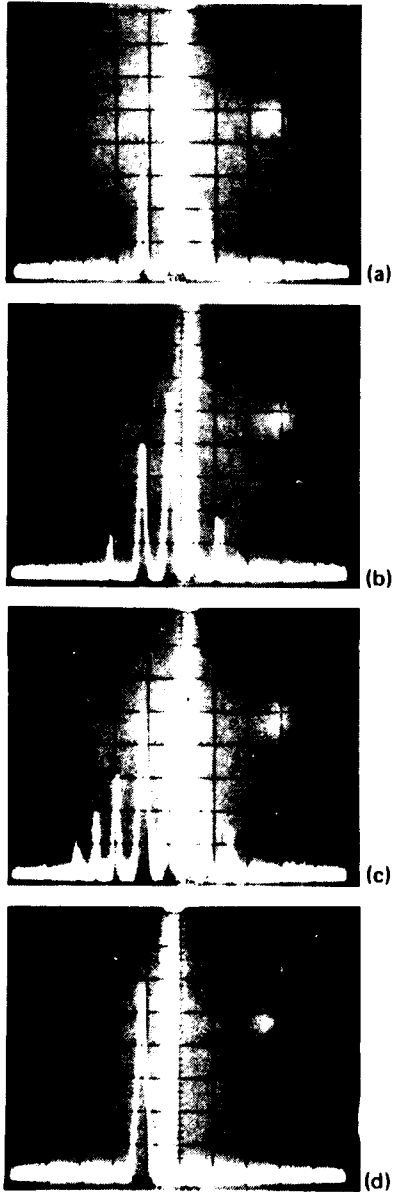
Figure 10.
Frequency spectra of an injection locked oscillator at
various injecting signal
levels (horizontal scale =
0.5 MHz/div., vertical scale
= 10 dB/div.)

31

signal, and the oscillator output power remains constant. The lower trace in each picture of Figure 11 is the relative magnitude of the oscillator output as a function of injecting frequency. Whenever the injecting signal frequency falls within the locking range, the oscillator output frequency matches that of the injecting signal and the amplitude display is large and constant, as evident from the flat plateau in the response curve. In Figure 11, the horizontal scale is roughly 0.5 MHz/ div, and the injecting signal power increases from (a) to (d) in 10-dB steps. In (a), the locking range is about 0.1 MHz; in (b) it increases to 0.25 MHz; in (c) it is ∿0.7 MHz; and in (d) it is 1.2 MHz. Another important parameter to consider in an injection-locked system is the phase of the oscillator output. In each of the pictures in Figure 11, the upper trace represents the relative phase of the oscillator output and the injecting signal. Regardless of the width of the locking range, the relative phase goes through a 180° change from one end of the locking range to the other, as can be predicted through a theoretical consideration.

The measured locking range and locking gain for our transistor oscillators are relatively low, for two reasons: (1) inefficient laser modulation and (2) nonoptimal device structure. At low frequencies, the transistors are designed so that the chip area is large and the spacing between emitter and base electrodes is large. Thus, sufficient light can be absorbed by the semiconductor. However, for rf transistors, an interdigital type of electrode is used; this leaves little area for absorbing optical energy. We believe that one can design a device that is optimized to interact with the optical signal and obtain a much better result.

As described above, dc optical illumination is equivalent to having additional base bias current. It is conceivable that the transistor bias voltage can be adjusted so that the circuit is slightly below the

7725-1

(a)

(b)

(c)

(d)
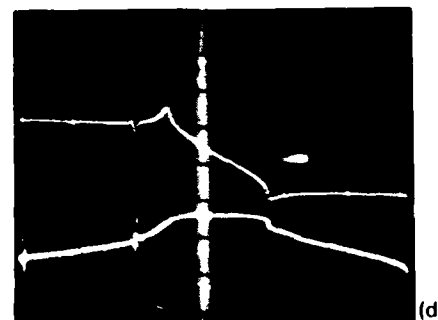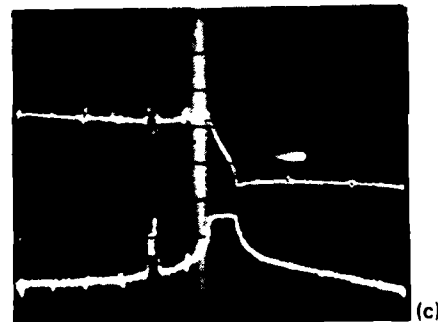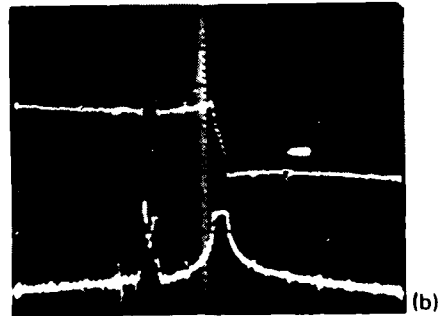
Figure 11.
Scope display of the locking
range and phase variation of a
locked oscillator. (Vertical
scale: upper trace 90°/div.
Lower trace, 10 dB/div. Hori-
zontal scale: 0.5 MHz/div.

33

threshold of oscillation and will oscillate only when there is illumination. This is possible in our setup because there is always a dc component in the modulated laser output. Thus, we can control a transistor to turn it on and off and simultaneously phase lock its output. An example of such action is shown in Figure 12. Here a transistor oscillator of frequency 1.85 GHz was switched on and phase locked by a laser output modulated at only 98 MHz.

As part of the optical injection locking experiment, we also designed and fabricated a GaAs FET oscillator.

The basic FET oscillator circuit was chosen to be the common source configuration with a series feedback element. The common source S parameters of the FET chips had to be measured. The FETs were mounted in a micro-strip carrier for ease of handling and measurement. A Hewlett-Packard network analyzer was used over the 4- to 12-GHz frequency range to characterize the chips in terms of S parameters. This measurement was then repeated using a microstrip through line in place of the chip carrier. The results from these two measurements were fed into a computer, where a computer program separated the S parameter of the FET chip from that of the carrier.

Once the S parameters are known, it is easy to design the rest of the circuit. A schematic of the completed GaAs FET oscillator circuit is shown in Figure 13.

Although the oscillator was originally designed to operate at 10 GHz, the circuit barely oscillated at this frequency. However, it oscillated quite stably at 7 GHz when biased at $V_D = + 4$ V and $V_S = + 1$ V. The main reason for this discrepancy was that the FET chip S parameters varied from chip to chip even though the chips had been diced from the same wafer. A secondary reason was that, because stray inductance and capacitance had been introduced during circuit construction, the circuit probably was too lossy at 10 GHz to sustain a stable oscillation. As a

(a) WITHOUT ILLUMINATION
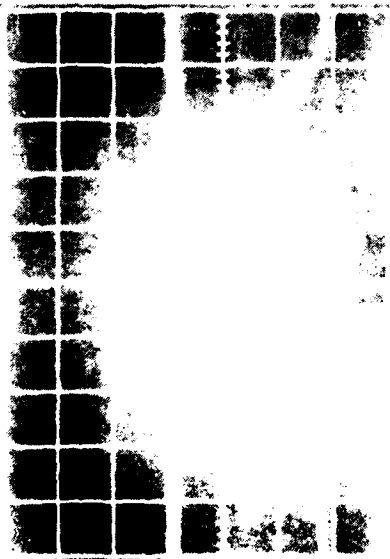
(b) WITH ILLUMINATION
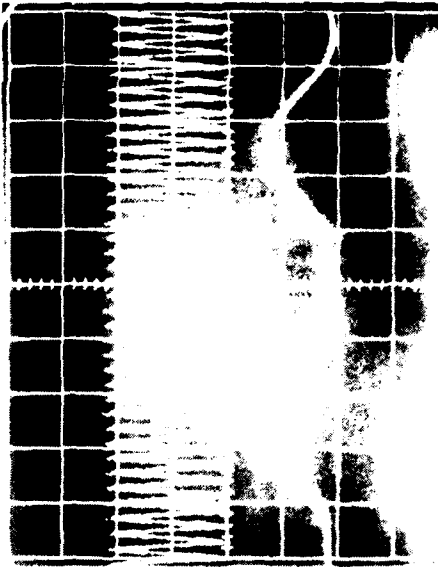
UPPER TRACE: TRANSISTOR OSCILLATOR OUTPUT (1.85 GHz)

LOWER TRACE: SIGNAL GENERATOR OUTPUT (98 MHz)

HORIZONTAL SCALE: 2 nsec/div

Figure 12.
Scope traces of simultaneous optical switching and injection locking of transistor oscillator; (a) without illumination, zero oscillator output; (b) with illumination, oscillator switched on and phase locked.
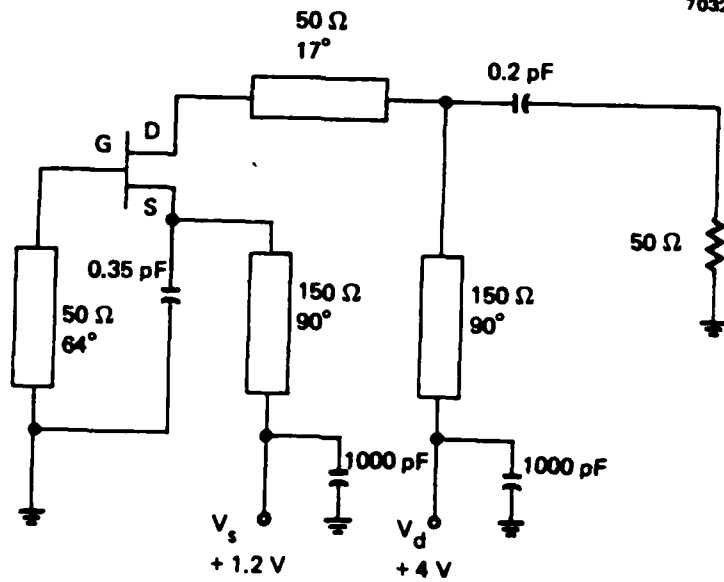
Figure 13.
Schematic of the designed GaAs FET oscillator.

matter of fact, the oscillation at 10 GHz was so unstable that, when the
FET was illuminated by the laser beam, the oscillation frequency jumped
to 7 GHz and remained at this frequency even though the laser beam was
blocked.

The output frequency of the oscillator was voltage tunable over a
limited range. The output power at 7 GHz was about 1 mW. Under certain
bias conditions, the output frequency of the oscillator was not very
stable; a frequency drift as large as 1.6 MHz was observed. DC optical
illumination was able to reduce this frequency drift to less than
0.2 MHz. The reason for this improvement is not clear at this time and
will be investigated in more detail. Since we were not able to modulate
our injection laser at 7 GHz, to check the optical injection locking of
our oscillator we had to use subharmonics of 7 GHz as our locking signal.
Therefore, we modulated the laser at 3.5 GHz and focused its output onto
the FET in the oscillator circuit and achieved optical injection locking
of the 7-GHz oscillator. The locking range in this case was very small,
which we believe was caused by a combination of poor optical coupling
and the use of subharmonic locking.

A somewhat different approach to achieving optical injection lock-
ing of transistor oscillators was also investigated. A schematic of the
experimental arrangement is shown in Figure 14(a). A transistor oscil-
lator at 440 MHz was connected to a single-stage GaAs FET amplifier with
a gain of about 14 dB at this frequency. A sweep oscillator was used to
modulate a GaAlAs laser. The output of the laser was focused onto the
GaAs chip in the amplifier. With this arrangement, we were able to
achieve phase locking of the 440-MHz transistor oscillator with a lock-
ing range of about 600 kHz (0.14 percent of 440 MHz).

For comparison, the original optical injection locking scheme is
depicted in Figure 14(b), which shows the modulated laser light focused
directly onto the oscillator. Using an amplifier might yield the follow-
ing advantages:

37

(a)

TRANSISTOR
OSCILLATOR

GaAs
FET
AMPLIFIER

SWEEP
OSCILLATOR

INJECTION
LASER

SYNCHRONIZED

(b)

TRANSISTOR
OSCILLATOR

SYNCHRONIZED

SWEEP
OSCILLATOR
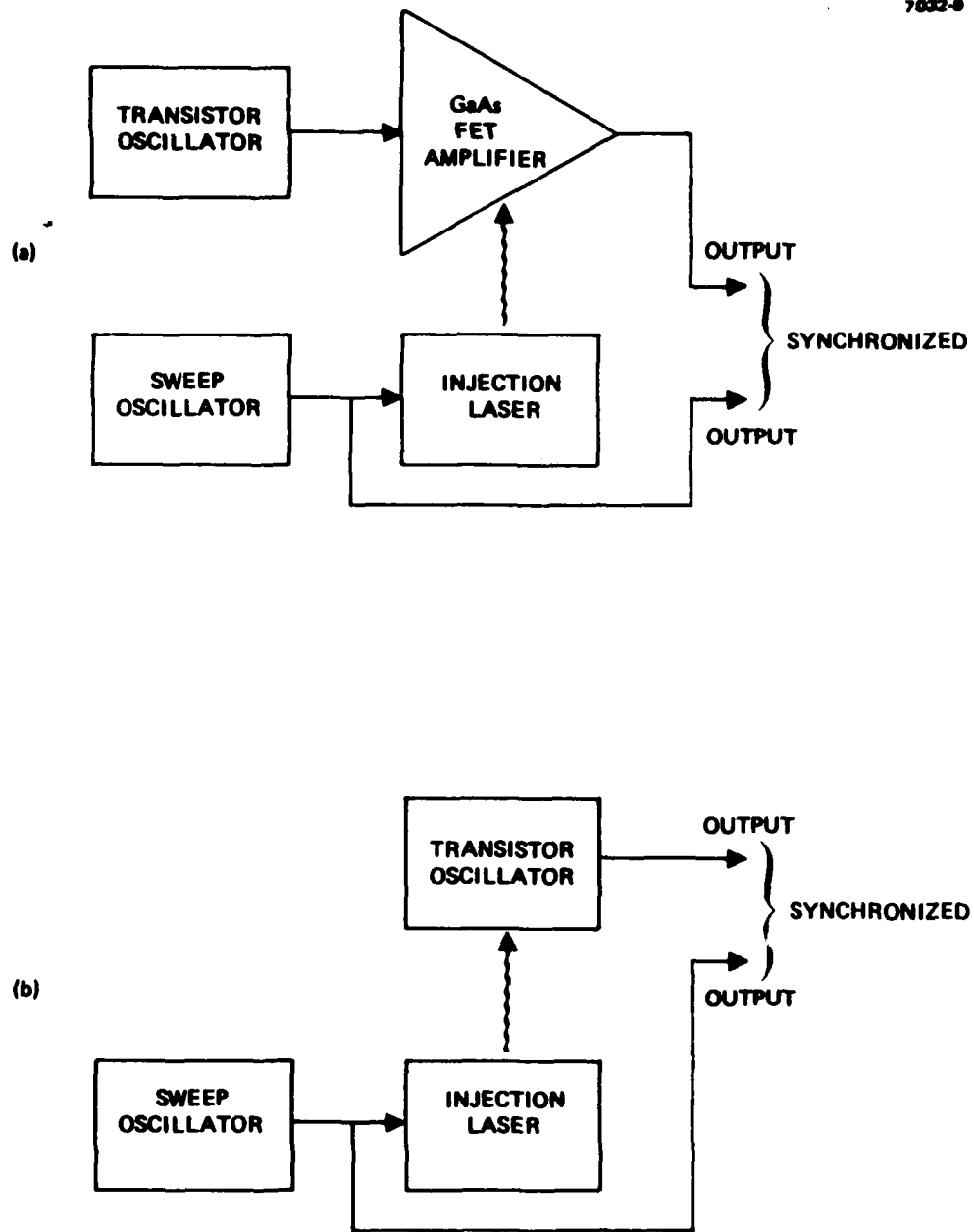
INJECTION
LASER

Figure 14.   Schematics of two optical injection locking schemes.

38

- Less frequency shift caused by optical illumination. In the
  original arrangement, the laser beam is focused onto the tran-
  sistor in the oscillator circuit, which changes the transistor
  characteristics and thus the oscillation frequency. In the
  new arrangement, the amplifier acts as part of the load of the
  oscillator; therefore, its variation due to optical illumination
  should have a smaller effect on the oscillation frequency shift.

- If the active element in the oscillator circuit is packaged so
  that it is not easily accessible for illumination or if the
  active element is not very light sensitive, the new arrange-
  ment will be particularly attractive.

- For IMPATT diode oscillators, it is difficult to achieve uni-
  form optical illumination because of the specific structure
  of the device. This may generate additional noise in the
  oscillator output. If a high-frequency FET amplifier is
  available, we might be able to solve this problem.

- Because of the amplifier gain, the total locking gain of the
  system is enhanced.

A possible drawback is that the locking range might be reduced because
it is more difficult to pull the oscillator frequency. Further study
is needed to verify these points.

39

SECTION 4

OPTICALLY INJECTED MICROWAVE MIXING IN GaAs FET AMPLIFIERS

To test the feasibility of using a GaAs FET amplifier as a micro-
wave mixer, the experiment illustrated in Figure 15 was carried out. By
feeding a 12.4-GHz microwave signal into a GaAs FET amplifier while
simultaneously illuminating the FET with a laser beam modulated at
3.51 GHz, we were able to obtain, at the output port of the amplifier, a
signal that contained frequency components of 12.4 GHz, 8.89 GHz, and
5.38 GHz. Note that

$$8.89 \text{ GHz} = 12.4 \text{ GHz} - (1 \times 3.51) \text{ GHz}$$

and

$$5.38 \text{ GHz} = 12.4 \text{ GHz} - (2 \times 3.51) \text{ GHz} .$$

This result showed that mixing can take place with the arrangement
described above. Here the amplifier input represents the incoming
microwave signal; the signal carried by the laser beam acts as the local
oscillator output; and the i.f. signal is taken from the output port of
the amplifier.

The amplifier used in the experiment was a single-stage GaAs FET
chip amplifier. The gain versus frequency plot of this device is shown
in Figure 16. At 12.4 GHz, the amplifier has a gain of about 7.6 dB.
A sweep oscillator was used to generate the 12.4-GHz input signal. The
output of the amplifier was connected to a spectrum analyzer.
Figure 17(a) shows a spectrum analyzer display of the amplified
12.4-GHz straight-through signal when the FET was not illuminated.
Figure 17(b) shows the spectrum of the amplifier output when the FET
was illuminated by a laser beam modulated at 3.51 GHz. Besides the
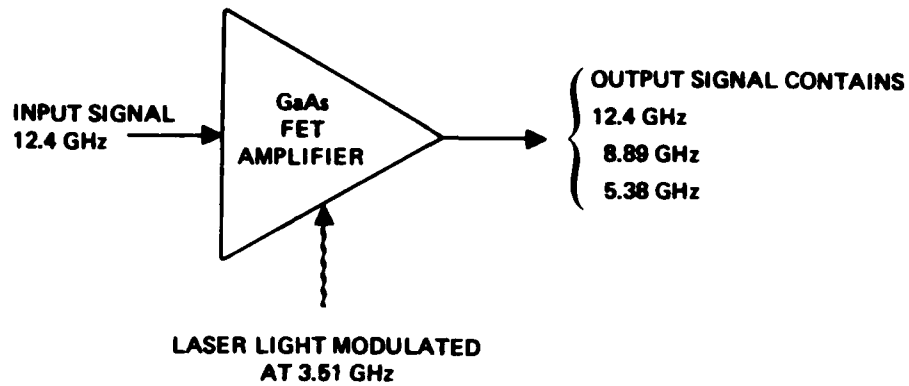
Figure 15.   Schematic of the optically injected microwave mixing experiment.
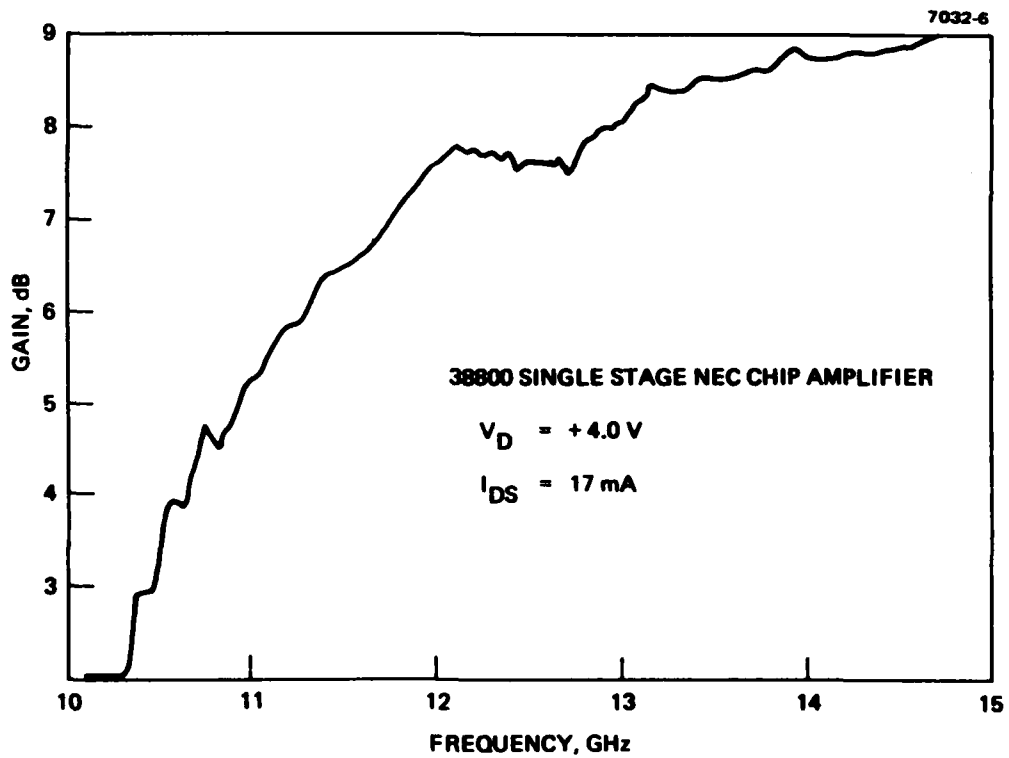

Figure 16.   Gain versus frequency plot of a single-stage GaAs FET amplifier.

42
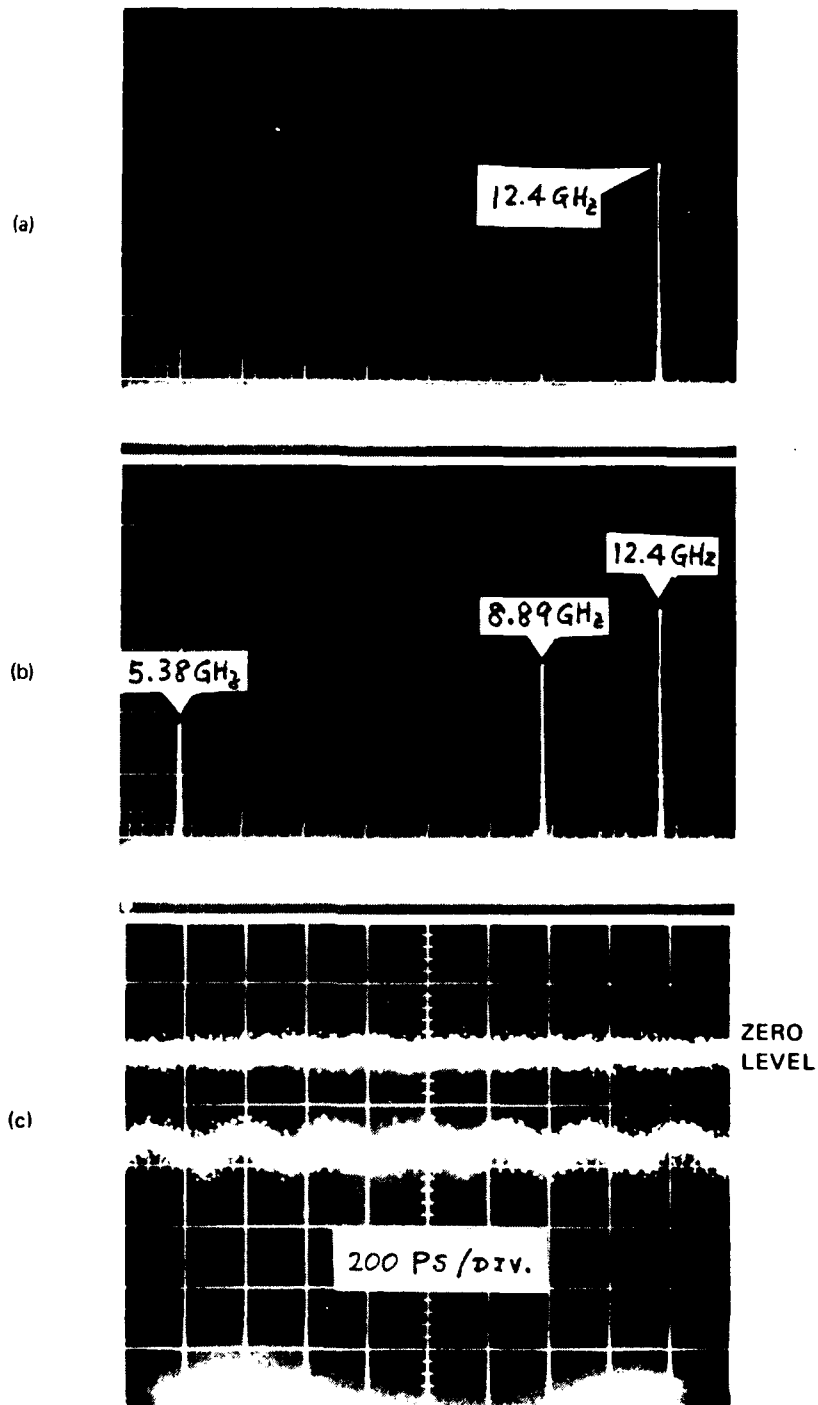
Figure 17. (a) and (b): Spectrum analyzer display of the
GaAs FET amplifier output. (c) oscilloscope dis-
play of the modulated laser output at 3.51 GHz.

original 12.4-GHz signal, two new frequency components were generated (at 8.89 GHz and 5.38 GHz). Figure 17(c) is an oscilloscope trace of the injection laser output modulated at 3.51 GHz. The optical zero-power level is as indicated in the picture. Thus, the modulation index of the laser output is ~12 percent.

A simplified analysis of this mixing process is illustrated in Figure 18. Assume that a signal of the form

$$E_o \sin \omega_o t,$$

where E_o is the amplitude of the signal, and ω_o is its angular frequency, is fed to an amplifier with voltage gain A. Then the amplifier output is

$$AE_o \sin \omega_o t.$$

Now assume that dc optical illumination causes the amplifier gain to vary and the amount of change is proportional to the light intensity. This is illustrated in Figure 18(b), where a dc optical illumination of intensity I on the amplifier changes the output to

$$A\beta E_o \sin \omega_o t.$$

If the light is intensity modulated sinusoidally at frequency ω (i.e., the light intensity is of the form $I(1 + m \sin \omega t)$, where I is the average intensity, and m is the modulation index), then the amplifier output will be

$$A\beta E_o (1 + m \sin \omega t) \sin \omega_o t.$$

It is easy to show that

$$A\beta E_o (1 + m \sin \omega t) \sin \omega_o t = A\beta E_o \sin \omega_o t + \frac{mA\beta E_o}{2} \cos (\omega_o - \omega)t$$

$$- \frac{mA\beta E_o}{2} \cos (\omega_o + \omega)t.$$

44

174

(a) $E_0 \sin \omega_0 t$ →→→ A →→→ $AE_0 \sin \omega_0 t$

(b) $E_0 \sin \omega_0 t$ →→→ A →→→ (ASSUMPTION) $A\beta E_0 \sin \omega_0 t$

I (DC OPTICAL ILLUMINATION)

(c) $E_0 \sin \omega_0 t$ →→→ A →→→ $A\beta E_0 (1 + m \sin \omega t) \sin \omega_0 t$

I $(1 + m \sin \omega t)$
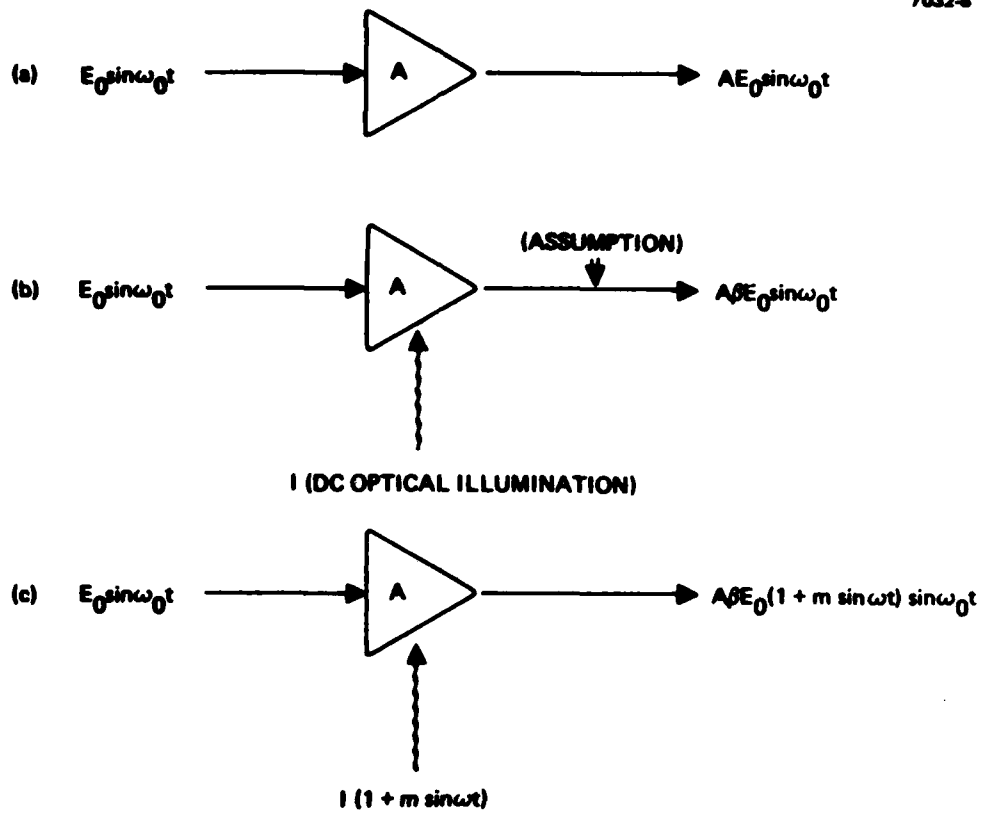
Figure 18. Simplified analysis of the mixing process.

Therefore, the output signal will have frequency components at ω_o, $\omega_o - \omega$, and $\omega_o + \omega$. The ratio of the amplitudes of these components is

$$1 : \frac{m}{2} : \frac{m}{2} .$$

Since the modulation index of the laser (as shown in Figure 17(c)) is 0.12 and since the output power carried by the component $\omega_o - \omega$ is $(m/2)^2$ times that carried by the ω_o component, it is approximately 24 dB down in this case. However, Figure 17(b) shows that the power at 8.89 GHz is only about 11 dB down from the 12.4 GHz signal. Our explanation is that the attenuation caused by the coaxial cable and the various connectors along the signal path is much larger for the 12.4-GHz signal than for the 8.89-GHz signal. The higher frequency component $\omega_o + \omega$ (15.91 GHz) does not appear in Figure 17(b) because of the band limit of the spectrum analyzer (4 to 12.4 GHz).

If the light modulation is sinusoidal but is of the form

$$I(1 + m_1 \sin \omega t + m_2 \sin 2\omega t),$$

then the signal at the amplifier output will be

$$A\beta E_o (1 + m_1 \sin \omega t + m_2 \sin 2\omega t) \sin \omega_o t,$$

which contains the following frequency components:

$$A\beta E_o \sin \omega_o t, \quad \frac{m_1 A\beta E_o}{2} \sin (\omega_o \pm \omega)t, \quad \text{and} \quad \frac{m_2 A\beta E_o}{2} \sin (\omega_o \pm 2\omega)t .$$

Thus, a nonsinusoidal light modulation generates higher order mixing terms. Higher order mixing can also occur if the amplifier gain does not vary linearly with the light intensity. In our experiment, the modulation of the laser output was typically less than 20 percent, and the amplifier gain was found to be linearly proportional to the small variations in the light intensity. Therefore, the higher order mixing term was generated by the nonsinusoidal light modulation.

46

In summary, the basic principle of this mixing approach is different from that of the conventional mixer diodes, where the nonlinear admittance of the device is responsible for the mixing. In our scheme, the modulation of the amplifier gain is the key. We attempted to measure the noise figure of a GaAs FET amplifier used as a mixer. However, the effort was not successful because the amplifier used was not an efficient mixer. Therefore, the total loss of the mixing process is out of the sensitivity range of the noise-figure meter. We believe that to increase the mixing efficiency will require modifying our present device by incorporating some waveguiding structure into the device. Work along this line will be pursued during the follow-on contract.

47

SECTION 5

STUDY OF OPTICAL SWITCHING OF GaAs IMPATT DIODE OSCILLATORS

The basic principles and characteristics of IMPATT diodes have been described extensively in the literature.[3-5] The structure of these diodes can be regarded as consisting of two main sections, the avalanche region and the drift region. Under normal operation, the diodes are reverse biased into avalanche breakdown so that electron-hole pairs are generated in the avalanche region by impact ionization. The electrons then move across the drift region under the influence of the external electric field. Because of the time delay in the avalanche multiplication process and the drifting process, the device exhibits negative resistance at microwave frequencies. Electron-hole pairs can also be generated in a semiconductor by illumination with an optical beam of sufficient photon energy. Since carrier generation is the key to the operation of IMPATT diodes, a strong interaction between the optical beam and microwave output of the IMPATT diode is expected.

This section describes an experimental study of the effect of optical illumination on the IMPATT diode oscillation characteristics, then presents small-signal analysis results to explain the observed results. The IMPATT diodes used in this experiment are GaAs Schottky-barrier junction diodes operating at about 16 GHz. The thickness of the active layer is ~ 2.8 μm, and the doping level is $N_d \sim 2 \times 10^{16}$ cm^{-3}. The diodes were mounted in a tuned microwave cavity with a feedthrough that allows an optical fiber to be butt-coupled to the active region of the diode, as sketched in Figure 19. A sliding short waveguide section was connected to one side of the cavity to increase the frequency range of tuning. On the other side, a coupling probe and crystal detector were attached for the detection of microwave output. A cw GaAlAs laser and a pulsed GaAs laser were used as light sources. The output of the laser was coupled into the fiber and guided down to the IMPATT diode.

Figure 20 shows the reverse bias I-V characteristic of one of the IMPATT diodes. With no illumination, the diode had a reverse breakdown voltage of ~ 30 V and a small leakage current. Illumination with 8200 Å

5733-1

CRYSTAL
DETECTOR

OPTICAL
FIBER

GaAs
LASER

WAVEGUIDE
TUNING
SHORT

GaAs IMPATT
DIODE
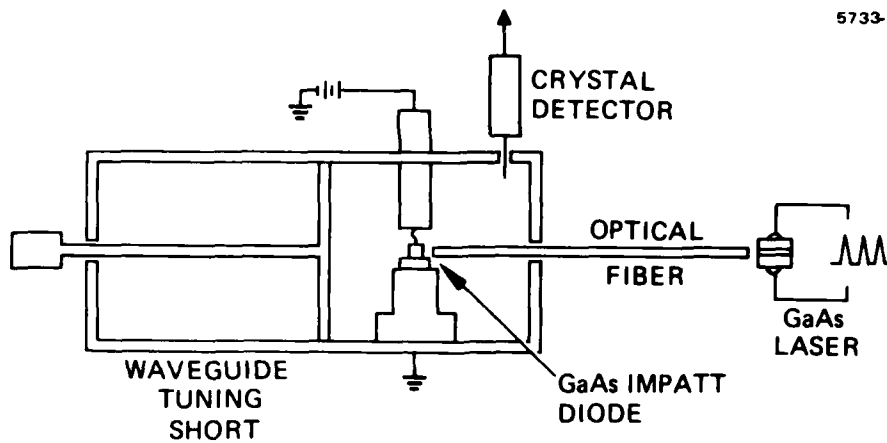
Figure 19.   Experimental setup for optical switching of
            IMPATT oscillators.

5733-2
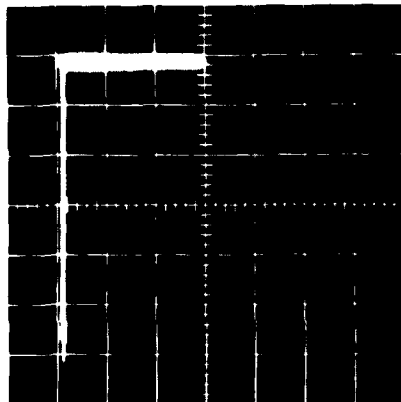
(a)   Without laser light   (b)   With laser light
   illumination.   illumination.

Figure 20.   IMPATT diode I-V characteristics. (Horizontal scale
            10 V/div., vertical scale 50 µA/div.)

50

light from a GaAlAs cw laser through a fiber produced a photocurrent, as shown in Figure 20(b). At voltages $<< V_{breakdown}$, the photocurrent was approximately 75 μA for this diode; however, at 28 V, avalanche multiplication resulted in a total photocurrent of 160 μA. Other diodes exhibited a similar photoresponse. The optical power emitted from the fiber waveguide was measured to be $\sim$7 mW.

The pulse photoresponse of the IMPATT diodes was also investigated by using a GaAs laser source emitting a 100- to 150-nsec-long pulse of $\sim$9000 Å light at a repetition rate of approximately 500 pulses/sec. Several types of response were observed depending on the illumination intensity and the "state" of the diode, which includes the bias condition and the operation frequency. Figure 21 shows the photoresponse of an IMPATT diode biased above threshold. The cavity in this case was tuned to optimize the microwave output power. The upper trace in the pictures is the light pulse from the GaAs laser, and the lower trace is the dc voltage output of the crystal detector, which is proportional to the microwave power of the IMPATT diodes. The zero level for microwave power is as indicated on the picture. Figure 21(a) shows a decrease in the microwave power output during the light pulse. The peak reduction is about 60 percent. As the light intensity was increased, as shown in Figure 21(b), the IMPATT was nearly shut off for a time interval corresponding to the light pulse duration.

If the cavity is detuned slightly so that the cavity Q favors some other frequency of oscillation that has a higher threshold, the cw microwave power will be almost zero, as shown in Figure 22(a). Illumination with a small light pulse in this case actually triggered the device into oscillation-generating pulses of microwave output. This microwave output was very sensitive to the light intensity. A 10 percent increase in light intensity gave a 75 percent enhancement of microwave output, as seen in Figure 22(b). However, a further increase in light intensity resulted in the situation shown in Figures 22(c) and 22(d). The microwave output enhancement was seen near the beginning of the light pulse but was quickly shut-off for as long as the light intensity was above a certain critical level. As the light intensity fell below this level, microwave output enhancement resumed.

51
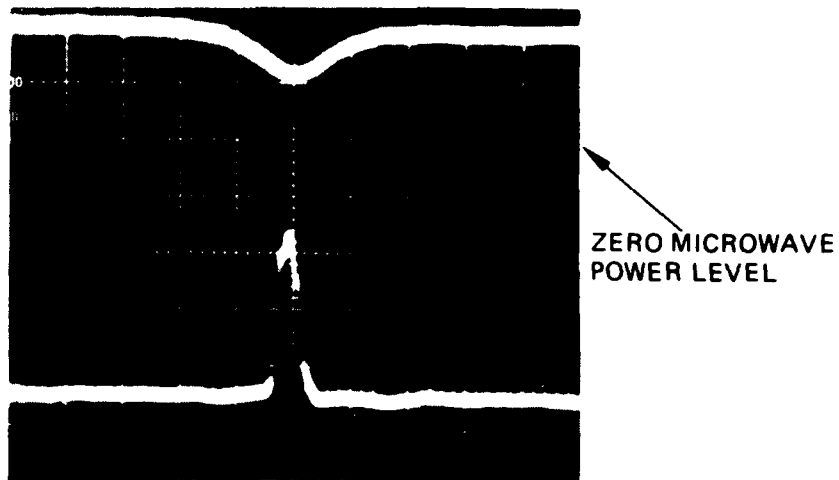
(a) At low light intensity.
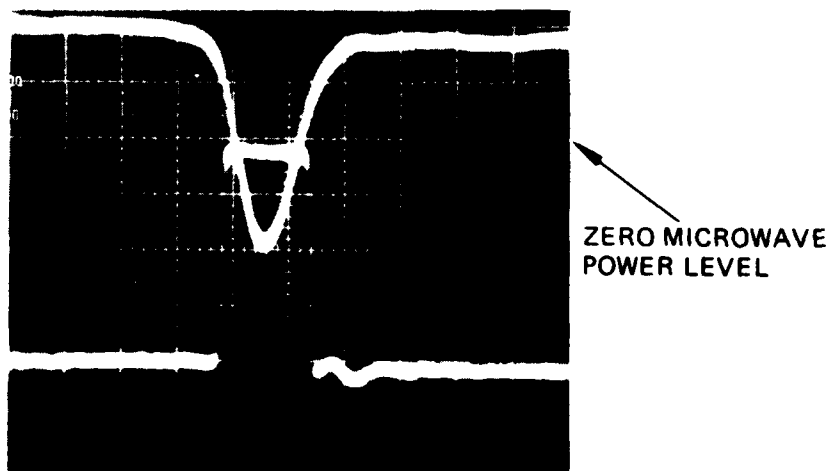
(b) At higher intensity.

Figure 11.
Pulse photoresponse of GaAs IMPATT diode biased above
threshold. The upper trace is the light pulse, the
lower trace is the microwave output power. (Horizontal
scale 100 nsec/div.)

5733-4

(a) ZERO MICROWAVE POWER LEVEL

(b)

(c)

(d)
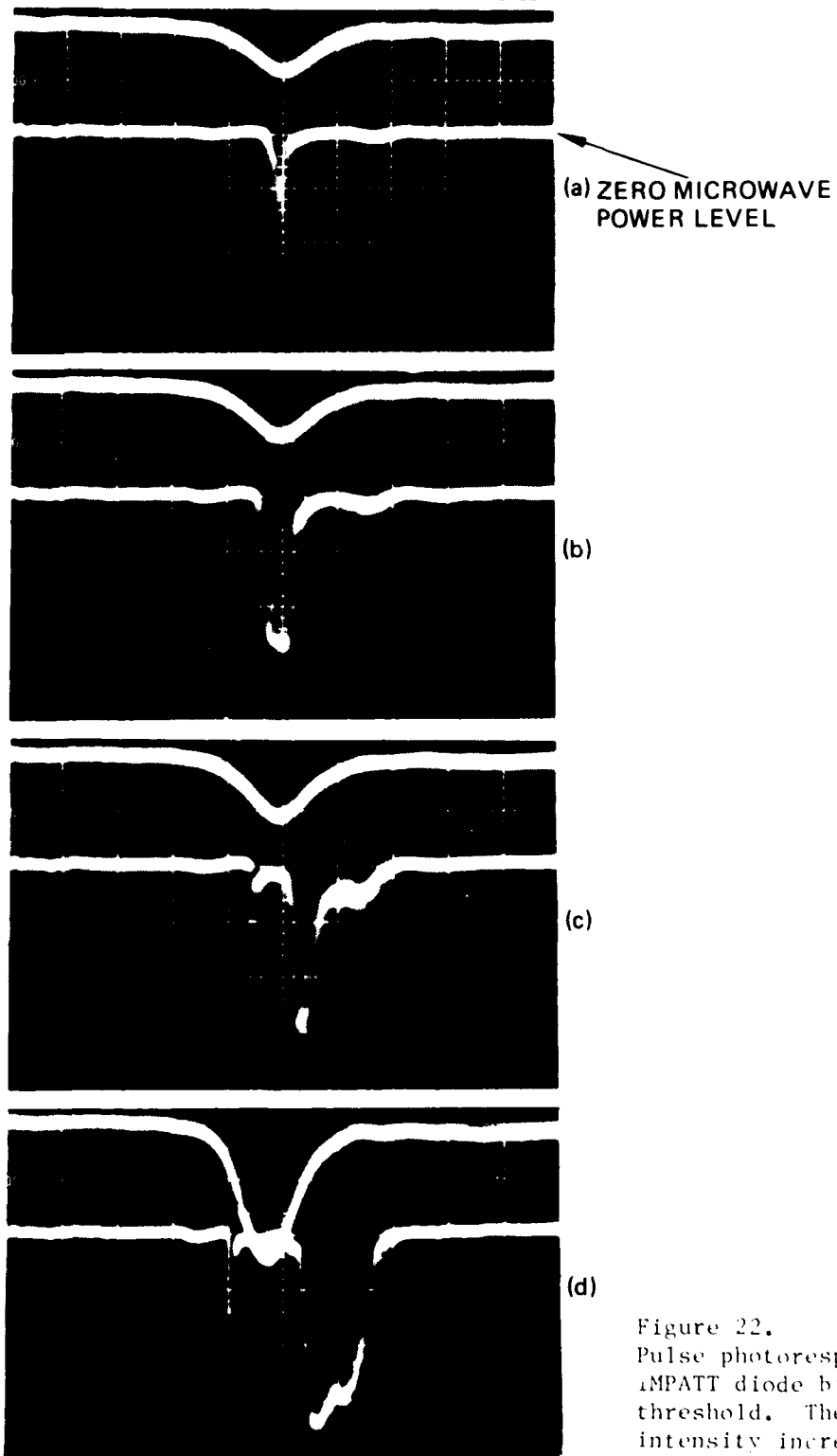
Figure 22.
Pulse photoresponse of GaAs
IMPATT diode biased below
threshold. The light
intensity increases pro-
gressively from (a) to (d).

183

If we start from the state shown in Figure 22(b) or 22(d) and increase the dc bias current, we can obtain the situation shown in Figure 21(a) or 21(b). This is because, with sufficient bias current, the device operates close to its optimum condition. Then the only effect the light pulse has is to spoil this optimum.

Thus, we have observed a strong interaction between the optical pulse and the microwave oscillation characteristics of GaAs IMPATT diodes. Both microwave power reduction and enhancement were achievable depending on the bias condition and oscillation frequency of the device. Next, a simple theory based on the small-signal analysis is presented to explain the observed phenomena.

To understand the results just described requires studying the dependence of the device impedance on the various parameters, such as the dc bias current I_o, the oscillation frequency ω, the transit angle θ, and the optically generated current I_s.[6,7] The structure that we are going to study (shown in Figure 23) is a typical abrupt p-n junction in reverse bias to breakdown. For analysis, we break the diode into two regions, the avalanche zone with length ℓ_a and the drift zone with length ℓ_d, as shown in Figure 23(a). Figure 23(b) depicts the electric field as a function of position inside the depletion zone. The electric field profile has a triangular shape, peaking near the p-n junction boundary, which corresponds to the avalanche zone.

In a typical avalanche diode, the peak electric field is estimated to be about 5×10^5 V/cm. Under this field, the carrier drift velocity V_d of both holes and electrons is nearly identical with a value of 9×10^6 cm/sec. Since the carrier drift velocity is nearly uniform throughout the depletion zone, it is treated as a constant in the following calculations.

We will use a small-signal analysis to calculate the impedance of the diode in the avalanche zone and the drift zone separately. This is done by deriving expressions for the ac voltages in terms of the ac circuit current and thereby obtain the impedance. The avalanche current of the diode can be calculated from the following equation[3]

54
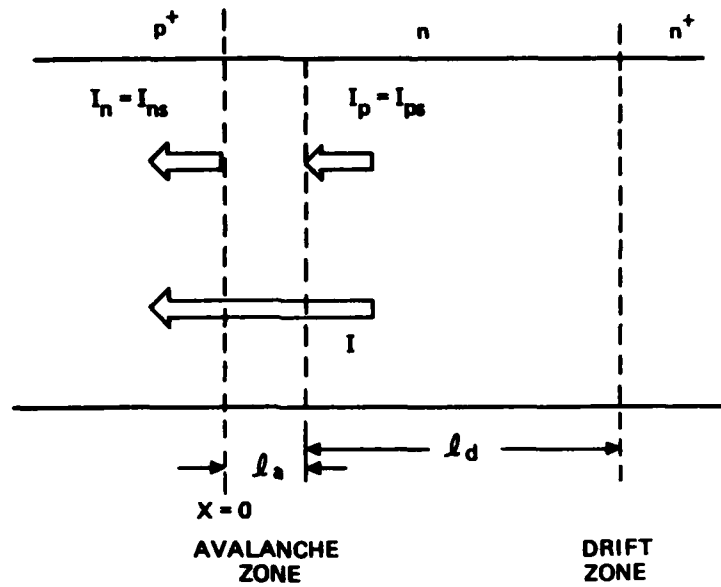
(a) Boundary conditions of the avalanche zone.
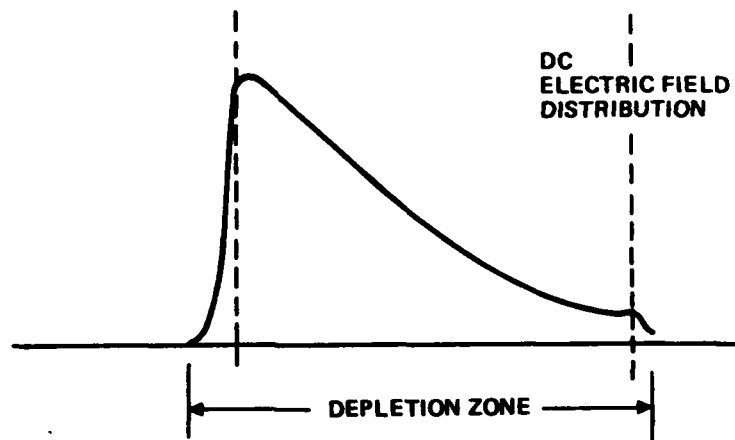
(b) Electric field distribution in
the depletion zone of the diode.

Figure 23. Structure of the IMPATT diode studied.

$$\frac{dI}{dt} = \frac{2I}{\tau_a} \left[\int_0^{\ell_a} \alpha dx - 1 \right] + \frac{2I_s}{\tau_a}, \qquad (12)$$

where α is the ionization coefficient for both holes and electrons; τ_a is the transit time across the avalanche zone, $\tau_a = \ell_a/V_d$; and $I_s = I_{ns} + I_{ps}$ is the total reverse saturation current of the diode. In an optically illuminated IMPATT diode, the reverse saturation current is greatly enhanced due to optical excitation; in an ordinary diode, I_s is caused by thermally generated carriers and is negligible.

Equation 12 can be simplified by replacing α by $\bar{\alpha}$, the average value of α in the avalanche zone:

$$\frac{dI}{dt} = \frac{2I \, (\bar{\alpha}\ell_a - 1)}{\tau_a} + \frac{2I_s}{\tau_a} . \qquad (13)$$

Next, we introduce the small-signal approximation:

$$\bar{\alpha} = \bar{\alpha}_a + \bar{\alpha}_a{}' \varepsilon_a$$

$$\bar{\alpha}\ell_a = 1 - \frac{I_s}{I_o} + \bar{\alpha}_a{}' \ell_a \varepsilon_a$$

$$I = I_o + i_a$$

$$E_a = E_o + \varepsilon_a \, ,$$

where $\bar{\alpha}_a{}'$ is the derivative of $\bar{\alpha}_a$ with respect to the electric field, E_o is the dc field, I_o is the dc current, and ε_a and i_a are small-signal quantities. Substituting these equations into Eq. 13 and neglecting products of small terms leads to

$$\frac{di_a}{dt} = \frac{2I_o \bar{\alpha}_a{}' \varepsilon_a \ell_a}{\tau_a} - \frac{2i_a I_s}{\tau_a I_o} . \qquad (14)$$

56

From Eq. 14 we can easily solve for i_a, the ac avalanche conduction current in the avalanche zone. The total current I_a in the avalanche zone is the sum of the conduction current and the displacement current. Define the factor D as

$$D = \frac{i_a}{I_a} = \frac{1}{\left(1 - \frac{\omega^2}{\omega_a^2}\right) + j\,\frac{2 I_s \omega}{\tau_a I_o \omega_a^2}} \ . \tag{15}$$

The fact that D is complex indicates that there is a phase shift between the avalanche current and the total ac current due to the optically generated reverse saturation current I_s.

The small-signal impedance of the avalance zone Z_a is

$$Z_a = \frac{V_a}{I_a} = \frac{1-D}{j\omega C_a} \ , \tag{16}$$

where $C_a = \epsilon A/\ell_a$, and A is the diode cross-sectional area. Similarly, we can obtain the small-signal impedance for the drift zone by taking the ratio of the total ac voltage across the drift region to the total ac current:

$$Z_d = \frac{V_d}{I_d} = \frac{1-D}{j\omega C_d} + \frac{D\theta}{2\omega C_d} \ , \tag{17}$$

where

$$C_d = \frac{\epsilon A}{\ell_d}$$

$$\theta = \omega \gamma_d = \omega \frac{\ell_d}{V_d} \ .$$

In deriving Eq. 17, we also assumed a small transit angle (i.e., $\theta \ll 1$).

The total ac impedance of the IMPATT diode is obtained by adding Eqs. 16 and 17:

$$Z = Z_a + Z_d = \frac{1 - D}{j\omega C_a} + \frac{1 - D}{j\omega C_d} = \frac{D\theta}{2\omega C_d}$$

$$= \frac{1 - D}{j\omega C} + \frac{D\theta}{2\omega C_d} , \qquad (18)$$

where

$$\frac{1}{C} = \frac{1}{C_a} + \frac{1}{C_d}.$$

It is instructive to first examine the frequency dependence of the IMPATT diode impedance without optical illumination. The expression of total impedance of the diode derived earlier also can be applied to the case of no illumination. From Eqs. 15 and 18, setting $I_s = 0$, we have

$$D = \frac{1}{1 - \frac{\omega^2}{\omega_a^2}}$$

$$1 - D = \frac{1}{1 - \frac{\omega_a^2}{\omega^2}}$$

$$Z = \frac{-j}{\omega C} \frac{1}{1 - \frac{\omega_a^2}{\omega^2}} + \frac{\tau_d}{2C_d} \frac{1}{1 - \frac{\omega^2}{\omega_a^2}}$$

and hence

$$R = \text{Re}(Z) = \frac{\tau_d}{2C_d} \frac{1}{1 - \frac{\omega^2}{\omega_a^2}} \qquad (19)$$

58

$$X = \text{Im}(Z) = \frac{-1}{\omega C} \cdot \frac{1}{1 - \dfrac{\omega_a^2}{\omega^2}} \quad . \tag{20}$$

A plot of $R(\omega)$ and $X(\omega)$ is shown in Figure 24. When $\omega > \omega_a$, the real part of the diode impedance is negative, and the imaginary part is capacitive; for $\omega < \omega_a$, the opposite is true. We will use a simple series inductance to illustrate the tuning and oscillation condition of the diode. The reactance of a series inductor L is ωL. We plot the negative of this quantity on the impedance versus frequency diagram of the IMPATT diode so that the intersection of this curve with the reactance curve of the diode determines the oscillation frequency ω_o. A vertical projection from the intersection to the resistance curve shows the value of negative resistance available at this frequency. This negative resistance has to be large enough to overcome the loss in the microwave cavity and in the diode itself for oscillation to sustain. For example, as illustrated in Figure 24, with inductance L_1 the available negative resistance is R_1, which is above the threshold value R_{th}, and the device will oscillate at frequency ω_o. However, if the inductance is changed to L_2, then the magnitude of the negative resistance available is only R_2, which is below R_{th}, and hence the device will not oscillate at ω_o'.

Next, we examine the frequency dependence of the IMPATT diode impedance subject to optical illumination. Again, we use Eqs. 15 and 18. With the approximation $C \approx C_d$, we can derive

$$R = \text{Re}(Z) = \frac{\tau_d}{2C_d} \omega_a^2 \frac{\omega_a^2 + \omega_s^2 - \omega^2}{\left(\omega_a^2 - \omega^2\right)^2 + \left(\dfrac{\tau_d \omega_s^2}{2}\right)^2 \omega^2} \tag{21}$$

59

Figure 24. Impedance versus frequency plot of an IMPATT diode.

$$X = \text{Im}(Z) = \frac{-1}{\omega C} \frac{\omega^2 \left[\omega^2 - \omega_a^2 \left(1 - \frac{\tau_d^2 \omega_s^2}{4}\right)^2 + \left(\frac{\tau_d \omega_s^2}{2}\right)^2 \right]}{\left(\omega_a^2 - \omega^2\right)^2 + \left(\frac{\tau_d \omega_s^2}{2}\right)^2 \omega^2} \quad , \quad (22)$$

where

$$\omega_a^2 = \frac{2\alpha'_a \ell_a I_o}{\epsilon A \tau_a}$$

$$\omega_s^2 = \frac{4 I_s}{\tau_a \tau_d I_o} \quad .$$

Without optical illumination, $\omega_s = 0$ and Eqs. 21 and 22 reduce to Eqs. 19 and 20, respectively. Equations 21 and 22 are sketched in Figures 25 and 26 for the case of

$$\frac{\tau_d}{2} = \frac{1}{\omega_a}$$

$$\omega_s^2 = \frac{\omega_a^2}{10} \ , \ \frac{\omega_a^2}{20} \ , \ \text{and} \ \frac{\omega_a^2}{30} \quad .$$

The effect of optical illumination on the negative resistance of the diode is obvious from Figure 25. Singularity at $\omega = \omega_a$ is removed, and the magnitude of the negative resistance is greatly reduced. The $R = 0$ frequency as we calculated before is larger than ω_a. The reactance of the diode, as shown in Figure 26, is also modified. For $\omega > \omega_a$, the reactance curves shift slightly toward higher frequencies as the illumination level increases. This small shift is important because it changes the oscillation frequency. A detailed drawing of the negative resistance and reactance at $\omega > \omega_a$ is shown in Figure 27 for the case of no optical illumination and for the case when

61
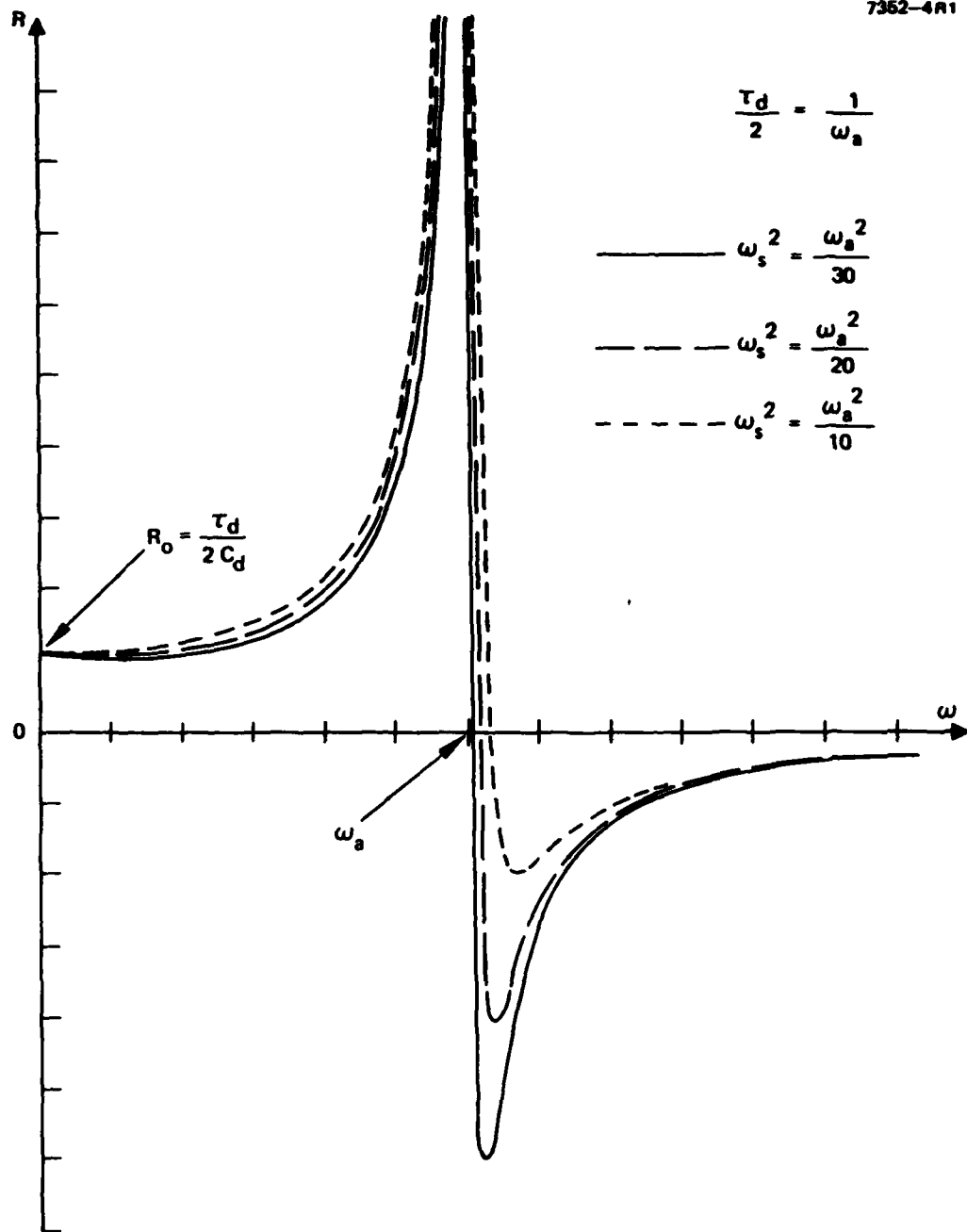
Figure 25.   Frequency dependence of the real part of the IMPATT diode
impedance subject to optical illumination.
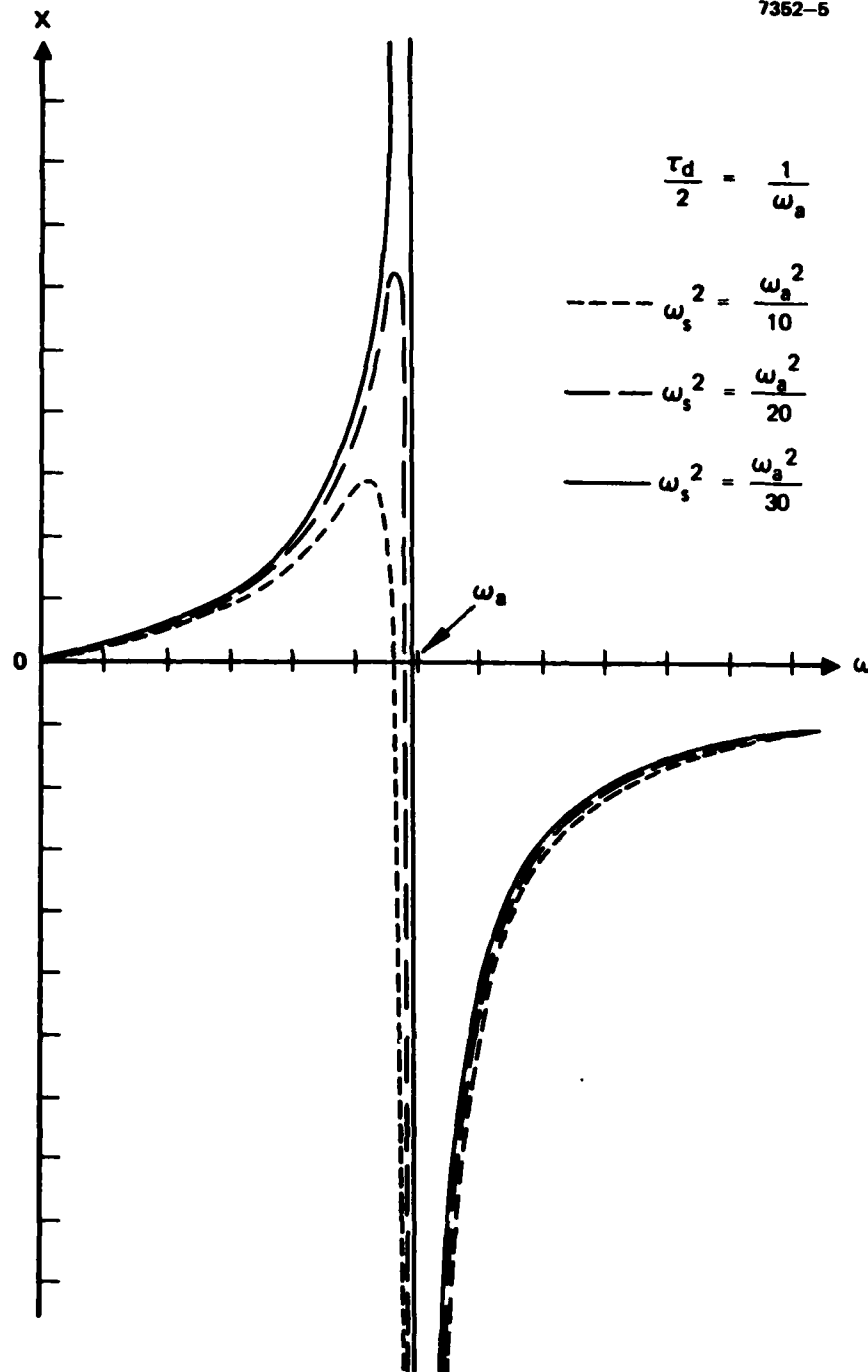
Figure 26. Frequency dependence of the imaginary part of
the IMPATT diode impedance subject to optical
illumination.

63
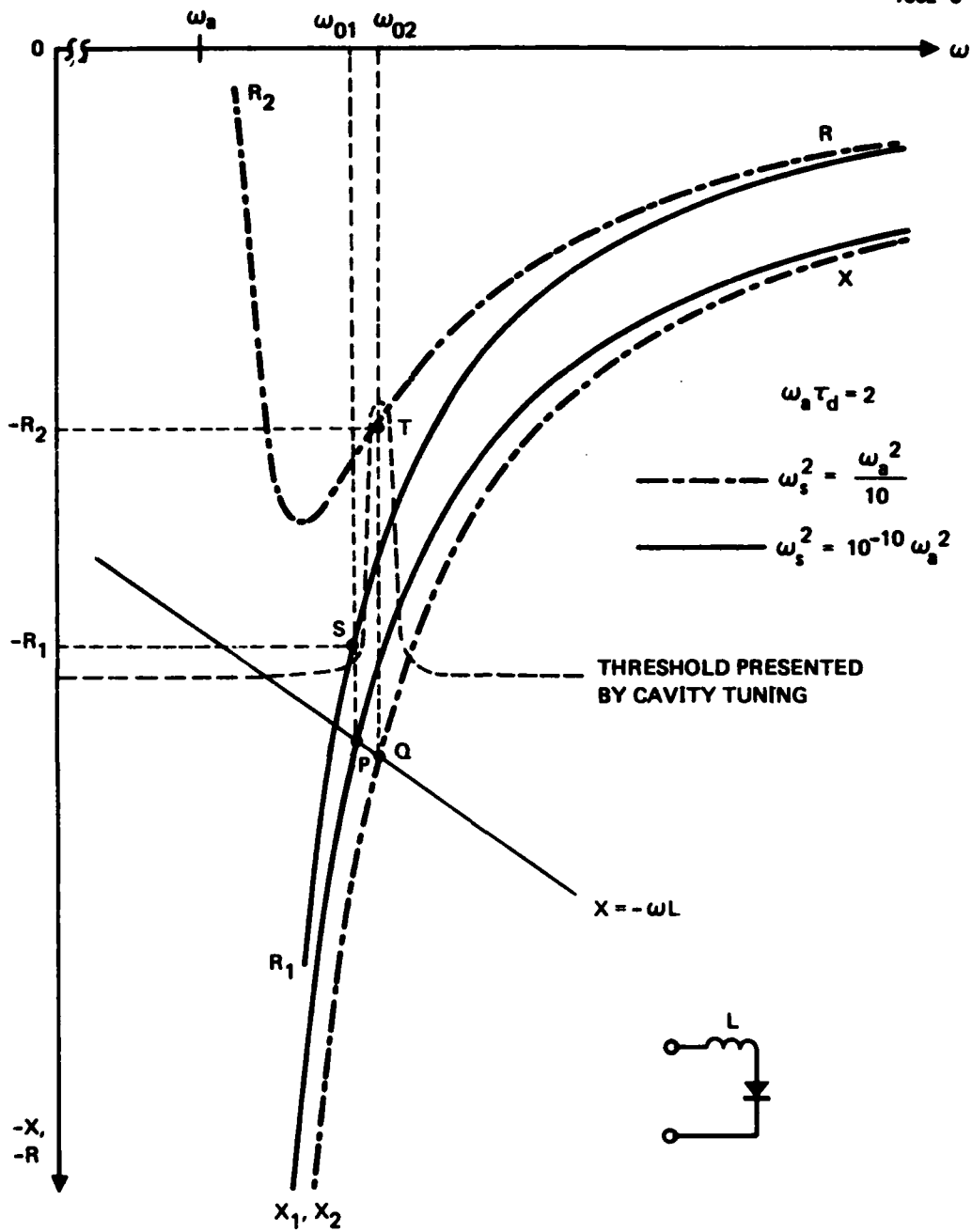
Figure 27. Determination of oscillation frequency of an IMPATT oscillator with and without illumination.

$$\omega_s^2 = \frac{\omega_a^2}{10} \, .$$

Again, the diode is in series with an inductor L to complete the circuit, and the negative of this inductance is shown by the straight line $X = -\omega L$. This line intersects the reactance curve X_1 at P, which determines the oscillation frequency ω_{01} and the magnitude of the negative resistance $-R_1$ available. If the cavity is tuned to this frequency and $-R_1$ exceeds the threshold value, then the IMPATT diode will oscillate. Now assume that an intense optical pulse is applied to the diode such that the X_1 curve is shifted to X_2 and the R_1 curve is changed to R_2. Once again, the intersection of the $X = -\omega L$ line and the X_2 curve, Q, determines the new "would be" oscillation frequency ω_{02} and the available negative resistance $-R_2$. Since $|R_1| > |R_2|$, the diode will oscillate with reduced output power if $-R_2$ is above threshold value at frequency ω_{02}, or it will cease oscillation if $-R_2$ is below threshold. This case corresponds to the experimental results shown in Figure 21. If the cavity is tuned carefully, we could have a frequency-dependent oscillation threshold, as shown by the dashed curve. With this threshold situation, the IMPATT diode will not oscillate without illumination since the negative resistance at ω_{01} is below threshold. However, if the diode is illuminated with the proper amount of light, it will oscillate at frequency ω_{02}. If the optical intensity is increased further, the "would be" oscillation frequency will be even higher, the negative resistance available will be below threshold, and therefore the oscillation will be quenched. This case corresponds to the experimental results shown in Figure 22. Thus, the experimental observations can be understood qualitatively through the calculated results and the mechanisms discussed above. However, although the output power of the IMPATT diode oscillator is being switched or modulated, there is an oscillator frequency change associated with the process.

65

SECTION 6

PLANS FOR THE FOLLOW-ON CONTRACT

The first subject to be investigated is the feasibility of optical injection locking of millimeter-wave solid-state oscillators. The approach of using subharmonic injection locking will be evaluated in detail, and a decision will be made at the end of the study as to whether further experimental work is necessary.

Millimeter-wave modulation of injection lasers through active mode locking will be pursued. Although the process is inherently narrow band, a short optical pulse train of fixed frequency still has numerous important applications.

A problem associated with the subject of laser modulation is the detection of high-speed modulated optical signals. Conventional photo-detectors have a practical bandwidth limit of a few gigahertz. Therefore, specialized detectors or detecting techniques will have to be developed together with the high-speed-modulation task.

The physics of optical illumination for phase jitter control and frequency drift stabilization of solid-state oscillators will also be investigated. Schemes will be developed to obtain stable, coherent microwave and millimeter-wave sources.

Device development, the most important task consists of two sub-tasks. The first is the design, fabrication, and evaluation of new and modified microwave devices. The design goal is to minimize the degradation of the device's microwave performance and to greatly enhance its optical interaction property. The second subtask is to design and fabricate combined injection-laser/microwave-oscillator devices such that the lasers can be modulated at speeds up to 10 GHz. Examples of such devices are injection-laser-IMPATT diode pair and injection laser-GaAs FET integrated structure.

67

REFERENCES

1. Konnerth, K. and Lanza, C., "Delay Between Current Pulse and Light Emission of a Gallium Arsenide Injection Laser," *Appl. Phys. Lett.* 4:120 (1964).

2. Aiki, K., Nakamura, M., Kuroda, T., and Umeda, J., "Channeled-Substrate Planar Structure (AlGa)As Injection Lasers," *Appl. Phys. Lett.* 30:649 (1977).

3. Read, W.T. Jr., "A Proposed High-Frequency, Negative Resistance Diode," *Bell Syst. Tech. J.*, 37:401 (1958).

4. Haddad, G.T., Greiling, P.T., and Schroeder, W.E., "Basic Principles and Properties of Avalanche Transit Time Devices," *IEEE Trans. MTT* 18:752 (1970).

5. Sze, S.M. and Ryder, R.M., "Microwave Avalanche Diodes," *Proc. IEEE* 39:1140 (1971).

6. Gilden, M. and Hines, M.E., "Electronic Tuning Effects in the Read Microwave Avalanche Diode," *IEEE Trans. Electron. Devices* ED-13:169 (1966).

7. Sanderson, A.C. and Jordan, A.G., "Electron Beam Control of IMPATT Diodes," *Solid-State Electronics* 15:140 (1972).

69